

Effects of Mitochondrial Nucleases on mtDNA Degradation

DISSERTATION

zur

Erlangung des Doktorgrades (Dr. rer. nat.)

der

Mathematisch-Naturwissenschaftlichen Fakultät

der

Rheinischen Friedrich-Wilhelms-Universität Bonn

vorgelegt von

Daniel Blei

aus

Remagen

Bonn, 2018

Angefertigt mit der Genehmigung der Mathematisch-Naturwissenschaftlichen
Fakultät der Rheinischen Friedrich-Wilhelms-Universität Bonn.

- | | |
|--------------|---------------------------|
| 1. Gutachter | Prof. Dr. Wolfram S. Kunz |
| 2. Gutachter | Prof. Dr. Dieter O. Fürst |

Tag der Promotion: 15.11.2018

Erscheinungsjahr: 2019

Table of Contents:

Acknowledgments	1
Summary	2
List of Tables	3
List of Figures	4
List of Abbreviations	6
1. Introduction	10
1.1 Morphology and function of mitochondria	10
1.2 Mitochondrial genome maintenance	12
1.3 Replication of mtDNA	14
1.3.1 Strand-displacement model.....	14
1.3.2 Strand-coupled replication model	15
1.3.3 RITOLS replication model.....	17
1.4 Members of the mtDNA replisome	18
1.4.1 Mitochondrial helicase Twinkle	21
1.4.2 Mitochondrial polymerase gamma.....	21
1.4.3 Mitochondrial single-strand binding protein (mtSSB).....	21
1.4.4 Mitochondrial RNA polymerase and primase (POLRMT) ...	22
1.4.5 Mitochondrial genome maintenance exonuclease1 (MGME1).....	22
1.5 Mitochondrial DNA damage and repair pathways.....	22
1.5.1 Base excision repair (BER).....	23
1.5.2 Nucleotide excision repair (NER).....	25
1.5.3 Mismatch repair (MMR)	25
1.5.4 Ribonucleotide excision repair (RER)	25
1.6 Mitochondrial nucleases and mtDNA degradation	25
1.7 Mitochondrial diseases.....	27
1.7.1 MtDNA maintenance disorders.....	29
1.7.2 Disease-associated mtDNA alterations	31
1.8 CRISPR-Cas9 Genome-editing and mitochondria	32
1.9 Aims	35

2. Materials & Methods	36
Chemicals.....	36
Antibodies.....	37
Enzymes.....	37
Cell medium.....	38
Solutions.....	38
Kits.....	39
Equipment.....	39
Software.....	40
Oligonucleotides.....	40
Primer.....	41
2.1 Cellular model.....	42
2.2 Cell culture.....	42
2.3 Subculturing cells.....	42
2.4 Cell pellets.....	43
2.5 Cryopreservation of cells.....	43
2.6 Mitochondrial genome linearization by mitoEagI.....	44
2.7 Mitochondrial DNA depletion.....	44
2.8 Isolation of total DNA.....	44
2.9 SgRNA design with synthetic oligonucleotides.....	44
2.10 CRISRP/Cas9 sgRNA plasmid construction.....	45
2.11 CRISRP/Cas9 transfection.....	46
2.12 Single cell cloning.....	46
2.13 CRISRP/Cas9 clone screening.....	47
2.14 PCR detection.....	47
2.15 Agarose gel electrophoresis.....	48
2.16 Polyacrylamide gel electrophoresis (PAGE).....	48
2.17 Sanger sequencing.....	48
2.18 Quantitative PCR (Real-time).....	49
2.19 Protein purification.....	50
2.20 Glycine SDS-PAGE.....	50
2.21 Western blot.....	50
2.22 Nucleic acid quantitation by optical density.....	51
2.23 DNA quantitation using PicoGreen®.....	52
2.24 Southern blot.....	52

2.25 Southern blot quantification.....	53
3. Results.....	54
3.1 Effects of mitochondrial nuclease activity on linear mtDNA.....	54
3.1.1 Monitoring degradation of linearized mtDNA in human cells	54
3.2 Generation of CRISPR/Cas9-edited knockout and knockin cell lines, with targeted mitochondrial exonucleases.....	55
3.3 Effects of mitochondrial exonuclease activity on linear mtDNA in induced CRISPR/Cas9-modified human cells	61
3.3.1 Rapid degradation of linear mtDNA fragments is absent in POLG knockin and MGME1 knockout clones during the first 24 hours.....	62
3.3.2 EXOG and APEX2 knockouts show no degradation deficiencies on linear mtDNA.....	66
3.3.3 Long term effects of linear mtDNA degradation in mitochondrial nuclease-deficient mitoEagI HEK clones.....	68
3.4 Depletion effect of mitochondrial DNA by ddC on mitochondrial nuclease-deficient POLG and MGME1 clones	70
4. Discussion	72
4.1 CRISPR/Cas9-editing creates stable human cell lines with altered mitochondrial nucleases.....	72
4.2 POLG and MGME1 perform linear mtDNA degradation	75
4.3 No additional mitochondrial nucleases, besides MGME1, influence rapid linear mtDNA degradation	79
4.4 Linearized mtDNA fragments show signs of degradation in POLG and MGME1 mutants after the first 24 hours.....	80
4.5 TWNK, POLG and MGME1 compose the mitochondrial 'degradosome'	82
References.....	85
Bibliography	96
List of Publications	96
Declaration.....	97

Acknowledgements

I am very grateful and sad at the same time to finish my PhD thesis, which had become an amazing journey in my life and would not have been possible without the support from so many different people, whom I would like to give my thanks.

First and foremost, I want to thank Professor Dr. Wolfram S. Kunz for being a great supervisor and giving me the chance to do my PhD thesis in his lab. His kind and open-minded manner made it a wonderful time working in the lab. It never ceased to amaze me how dedicated and excited he talked about so many different topics, belonging to the field of mitochondrial research and beyond – I will definitely cherish our personal discussions. Working in Professor Kunz' lab also gave me the opportunity to join the international community dedicated on mitochondrial research and disease and it was an honour for me, to be able to meet the greatest researchers from this field during international conferences and talks.

Second, I wish to thank Dr. Gábor Zsurka for being a great mentor and giving me all the support, I needed for my work in the lab. He is always dedicated to our research projects and he possesses the vision of intertwining all the small puzzle piece into a greater picture. Thank you for all our discussions and the advice you gave me to push forward. This thesis would not have been possible without your guidance.

Next, Dr. Viktoriya Peeva, I am grateful beyond words to become the PhD student under your BONFOR-program. Thank you from the bottom of my heart for being yet another kind, cheerful and jolly supervisor and friend. Working with you was never unpleasant or cumbrous, always nice and enjoyable. Your guidance, especially in the routine, was always very helpful to me and your vast knowledge on the field of mitochondrial research is inspiring to me.

I dedicate very special thanks to Thomas S. Ebert and his Professor Veit Hornung for providing me with the CRISPR/Cas9-technique and vector. Without your help, my work would not have been possible! I wish to express my thanks also to all the members of Professor Kunz' group. Thanks to Dr. Alexey Kudin for helping me with the proteomics. Thanks to Susanne Beyer, the technical assistant and backbone of the lab, who assisted me with technical problems during my PhD. Thanks to Kerstin Hallmann for introducing me into the field of RNA isolation and for our office talks. Also, thanks to Phuong Tran and Dr. Bálint Szalontai, who helped me keeping the cell culture running!

Last but not least I wish to thank my family for their aid during my time as a PhD student. Thanks mom and dad, for everything. I am deeply grateful for the support from my grandparents, Sigrid and Kurt Hentzschel for being there whenever I needed them. Finally, special love and thanks to my wife Dorothee who endured and supported me during all this time and to my brother Sebastian, for helping me throughout these difficult times. I love you all.

Summary

Mitochondria are unique to have a multicopy genome, resulting in a substantially different fate of damaged DNA molecules in comparison to nuclear DNA. Damaged DNA usually represents only a small fraction of total mitochondrial DNA (mtDNA) in a cell, which can be removed, through DNA degradation, without severe consequences and get replaced by replication of intact mtDNA. This idea of a “disposable genome” plays an essential role for modern gene therapy of mitochondrial diseases, which aim to eliminate pathogenic mtDNA mutations by selectively breaking down mutated mtDNA. Introducing mtDNA double-strand breaks (DSB), elimination of paternal mtDNA or virus-induced mtDNA depletion are described phenomena of eliminating mtDNA. The molecular machinery performing mtDNA degradation is still unknown. This work used the CRISPR/Cas9 technique to create stable knockout and knockin cell lines of selected mitochondrial nucleases in a cellular model to study degradation of linear mtDNA. An induced expression of restriction endonuclease mitoEagI introduced DSB into the mitochondrial genome of living cells, linearizing it in the process. Inactivation of the mitochondrial 5'–3' exonuclease MGME1 and the 3'–5' exonuclease activity of POLG (a subunit of the mitochondrial DNA polymerase gamma), through introducing the p.D274A point mutation severely impaired rapid linear mtDNA degradation. Additional knockout cell lines of other mitochondrial nucleases (APEX2, EXOG) showed no deficiencies on linear mtDNA degradation. Along with recent findings, that the mitochondrial DNA helicase Twinkle is also involved in linear mtDNA degradation (Peeva and Blei *et al.*, 2018), this altogether proposes novel, additional roles for the mtDNA replication machinery.

List of Tables:

Table 1: Mitochondrial DNases	25
Table 1.1: Genes and phenotypes in altered mtDNA maintenance	31
Table 2: Chemicals	35
Table 3: Antibodies	36
Table 4: Enzymes	36
Table 5: Cell medium	37
Table 6: Solutions	37
Table 7: Kits	38
Table 8: Equipment	38
Table 9: Software	39
Table 10: Oligonucleotides used in the generation of CRISPR/Cas9 vectors, showing gene specific target sites	39
Table 11: Oligonucleotides used in generating CRISPR/Cas9- mediated knockins	40
Table 12: Primers used for screening CRISPR/Cas9 clones	40
Table 13: Cloning statistics per CRISPR/Cas9-targeted gene in HEK cells	56

List of Figures:

Figure 1: The mitochondrion	10
Figure 2: Schematic representation of oxidative phosphorylation	11
Figure 3: Map of the human mitochondrial genome	13
Figure 4: Asymmetric strand-displacement model of mtDNA replication	15
Figure 5: Strand-coupled model of mtDNA replication	16
Figure 6: RITOLS model of mtDNA replication	17
Figure 7: The mtDNA replication machinery	18
Figure 8: Schematic diagram of the updated mtDNA replication machinery	19
Figure 9: MtDNA base excision repair pathways in mammalian mitochondria	23
Figure 10: Clinical representations of mitochondrial diseases	27
Figure 11: Slipped-strand model of mtDNA deletion formation	29
Figure 12: Model for the generation of mtDNA deletions during DSB Repair	30
Figure 13: Schematic representation of CRISPR/Cas9-mediated genome editing	33
Figure 14: Ligation-independent cloning (LIC) method	44
Figure 15: Inducible mitoEagI model for linearizing mtDNA	54
Figure 16: Schematic process of the generation of CRISPR/Cas9-edited HEK cell lines	55
Figure 17: CRISPR/Cas9-edited genes in mitoEagI HEK cells	57
Figure 18: Western blot analysis of mitoEagI protein expression in CRISPR/Cas9-modified mitoEagI HEK cells	58
Figure 19: Induced mitoEagI endonuclease activity on circular mtDNA in CRISPR/Cas9-edited HEK cells	59
Figure 20: Degradation of the linearized mtDNA fragment in control, POLG- and MGME1-mutant mitoEagI expressing HEK cells, showing the large digested fragment	61

Figure 21: Degradation of the linearized mtDNA fragment in control, POLG- and MGME1-mutant mitoEagI expressing HEK cells, showing the small digested fragment	63
Figure 22: Degradation of the linearized mtDNA fragment in MGME1-, EXOG- and APEX2-knockout mitoEagI expressing HEK 293 cell lines, showing the large digested fragment	65
Figure 23: Degradation of the linearized mtDNA fragment in MGME1-, EXOG- and APEX2-knockout mitoEagI expressing HEK 293 cell lines, showing the small digested fragment	66
Figure 24: Long term degradation effects on the linearized mtDNA fragment in mitoEagI expressing HEK clones, showing the large digested fragment	68
Figure 25: Depletion of mtDNA in POLG and MGME1 mutant HEK cells	70
Figure 26: Models of replication and double-strand degradation of mtDNA by the same machinery	83

List of Abbreviations:

adCPEO	autosomal dominant chronic progressive external ophthalmoplegia
ADP	Adenosine diphosphate
AFM	Atomic force microscopy
AP	apurinic/apyrimidinic
APEX	AP endonuclease
APS	Ammonium persulfate
ATP	Adenosine triphosphate
Bp	Base pair
BER	Base excision repair
Cas	CRISPR-associated protein
CoQ	Coenzyme Q10
COX	Cytochrome <i>c</i> oxidase
CRISPR	Clustered Regularly Interspaced Short Palindromic Repeats
crRNA	CRISPR RNA
CSB	Conserved sequence box
CtIP	CtBP-interacting protein
Cyt <i>b</i>	Cytochrome <i>b</i>
ddC	2',3'-dideoxycytidine
D-Loop	Displacement loop
DMEM	Dulbeco's modified eagle's medium
DMSO	Dimethyl sulfoxide
DNA	Deoxyribonucleic acid
DNA2	DNA replication helicase/nuclease 2
dNTP	Deoxyribonucleotide triphosphate
DR	Direct repeats
dRP	deoxyribose phosphate
DSB	Double-strand DNA break
DSBR	Double-strand break repair
dsDNA	Double-stranded DNA

List of Abbreviations

dTTP	Deoxythymidine triphosphate
EDTA	Ethylenediaminetetraacetic acid
ENDOG	Endonuclease G
ETC	Electron transport chain
EXOG	Exo/Endonuclease G
FCS	Fetal calf serum
FEN1	Flap structure specific endonuclease 1
HCL	Hydrochloric acid
HDR	Homologous-directed repair
HEK	Human embryonic kidney cell line
HLP	Light-strand promoter
HR	Homologous recombination
HSP	Heavy-strand promoter
H-Strand	Heavy/Leading strand on mitochondrial genome
HSV	Herpes Simplex Virus
IMM	Inner mitochondrial membrane
kb	Kilobases
LP-BER	Long-patch base excision repair
L-Strand	Light/Lagging strand on mitochondrial genome
MGME1	Mitochondrial Genome Maintenance Exonuclease1
MMEJ	Microhomology-mediated end joining
MMR	Mismatch repair
MNGIE	Mitochondrial neurogastrointestinal encephalomyopathy
MRE11	Meiotic recombination 11
MRN	Mre11–Rad50–Nbs1
mRNA	messenger RNA
mtDNA	mitochondrial DNA
mtRI	mitochondrial replication intermediate
mtSSB	mitochondrial single-stranded DNA-binding

List of Abbreviations

	protein
NADH	Nicotinamide adenine dinucleotide
NCR	Non-coding region
ND	NADH dehydrogenase
nDNA	nuclear DNA
NER	Nucleotide excision repair
NHEJ	Non-homologous end joining
OD	Optical density
O _H	See oriH
O _L	See oriL
OMM	Outer mitochondrial membrane
OR	Origin of replication
oriH	Origin of replication for H-strand
oriL	Origin of replication for L-strand
OXPHOS	Oxidative phosphorylation
PAGE	Polyacrylamide gel electrophoresis
PAM	Protospacer adjacent motifs
PBS	Phosphate buffer saline
PCR	Polymerase chain reaction
POLG / POL γ	Polymerase gamma
POLRMT	mitochondrial RNA polymerase
qPCR	Quantitative real-time PCR
RBBP8	Retinoblastoma-binding protein 8
RER	Ribonucleotide excision repair
RITOLS	Ribonucleotide incorporation throughout the lagging strand
RNA	Ribonucleic acid
RNase	Ribonuclease
rNMP	ribonucleotide 5'-monophosphate
ROS	Reactive oxygen species
rRNA	ribosomal RNA
SANDO	Sensory-ataxia neuropathy, dysarthria and

List of Abbreviations

	ophthalmoplegia
SCAE	Spinocerebellar ataxia and epilepsy
SDM	Strand-displacement model
SDS	Sodium dodecyl sulphate
SEM	Scanning electron microscope
sgRNA	single guide RNA
SN-BER	Single-nucleotide-BER
SSB	Single-strand DNA breaks
SSBR	Single-strand break repair
SSC	Saline sodium citrate
ssDNA	Single-stranded DNA
TAS	Termination-associated sequence
TE	Tris-EDTA buffer
TEMED	Tetramethylethylenediamin
TFAM	Mitochondrial transcription factor A
TFBM	Mitochondrial transcription factor B
tracrRNA	<i>trans</i> -activating CRISPR RNA
Twinkle / TWNK	T7-like mitochondrial DNA helicase
TYMP	Thymidine phosphorylase
tRNA	transfer RNA
UV	ultraviolet

1. Introduction

1.1 Morphology and function of mitochondria

A mitochondrion consists of an outer and an inner membrane, with the intermembrane space in between. Its inner membrane surrounds the lumen of the mitochondrion, called matrix (Figure 1). The outer mitochondrial membrane (OMM) is built of a phospholipid bilayer harbouring a multitude of proteins, including a diverse set of enzymes, pore forming proteins (porins) and proteins mediating mitochondrial fusion and fission (Walther and Rapaport 2009). Porins provide permeability for the OMM allowing molecules of up to 5 kDa in molecular weight to cross it in both directions (Molecular Biology of the Cell, 2011). The inner mitochondrial membrane (IMM) is a highly impermeable barrier, folded into so called cristae, which largely increase its surface area. Along the IMM aligns the electron transport chain (ETC), an assembly of protein complexes (I–IV) that reduce oxygen (O_2) to build up a proton (H^+) gradient from the matrix into the intermembrane space. The efficiency of these so called respiratory chain supercomplexes (RCS), which provide the functional roles of catalytic enhancement, substrate channelling and stabilization of complex I by complex III, is directly related to the shape and structure of the cristae, independently to changes of the mitochondrial protein synthesis or OMM permeabilization (Cogliati *et al.*, 2013).

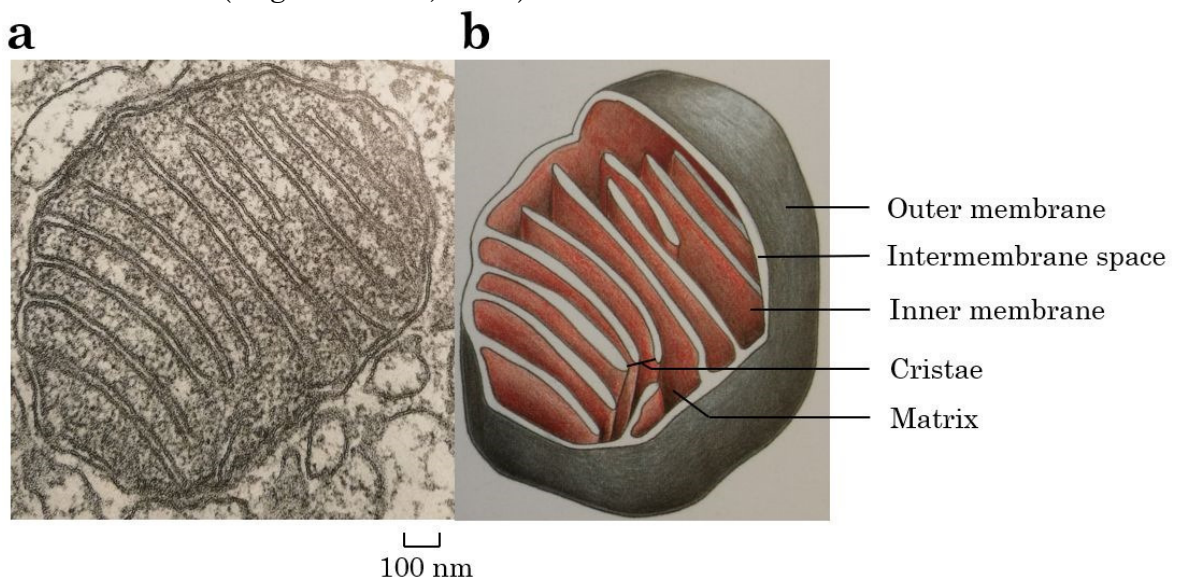


Figure 1: The mitochondrion. (a) Scanning Electron Microscope (SEM) image of a cross section through a mitochondrion. (b) Schematic drawing of the three-dimensional structure of a mitochondrion, with a part cut out (figure adapted from Molecular Biology of the Cell, Fifth Edition by Alberts *et al.*, 2011; German edition).

The reflux of protons from the intermembrane space back into the matrix occurs through the ATP synthase (complex V), incorporated at edges of the cristae. This part uses the potential energy in a reaction called oxidative phosphorylation (OXPHOS) to produce ATP from ADP and inorganic phosphate (P_i) inside the matrix (Figure 2). The matrix also contains a high concentration of proteins (2/3 of the total mitochondrion), which, among other functions, play a role in forming the citric acid cycle and aerobic respiration. Additionally, mitochondrial ribosomes, tRNAs and mitochondrial DNA (mtDNA) are present in the matrix as well (Molecular Biology of the Cell, 2011).

While the conversion of energy is the most crucial function of mitochondria, they also play vital roles in the metabolism of amino acids (Costa-Guda *et al.*, 2007), heme synthesis (major functional form of iron, Lange *et al.*, 1999), or calcium homeostasis (Vandecasteele *et al.*, 2001). Mitochondria also mediate apoptotic cell death (Fransson *et al.*, 2003), synthesize hormones (Miller *et al.*, 2013) or detoxify ammonia by conversion to urea (Norenberg 2003). Dysfunction of mitochondria and the associated diseases can directly result from mutations or damage to the mitochondrial genes or nuclear proteins, that translocate to the mitochondria, which makes the mitochondrial genome maintenance yet another crucial function (Prakash *et al.*, 2015).

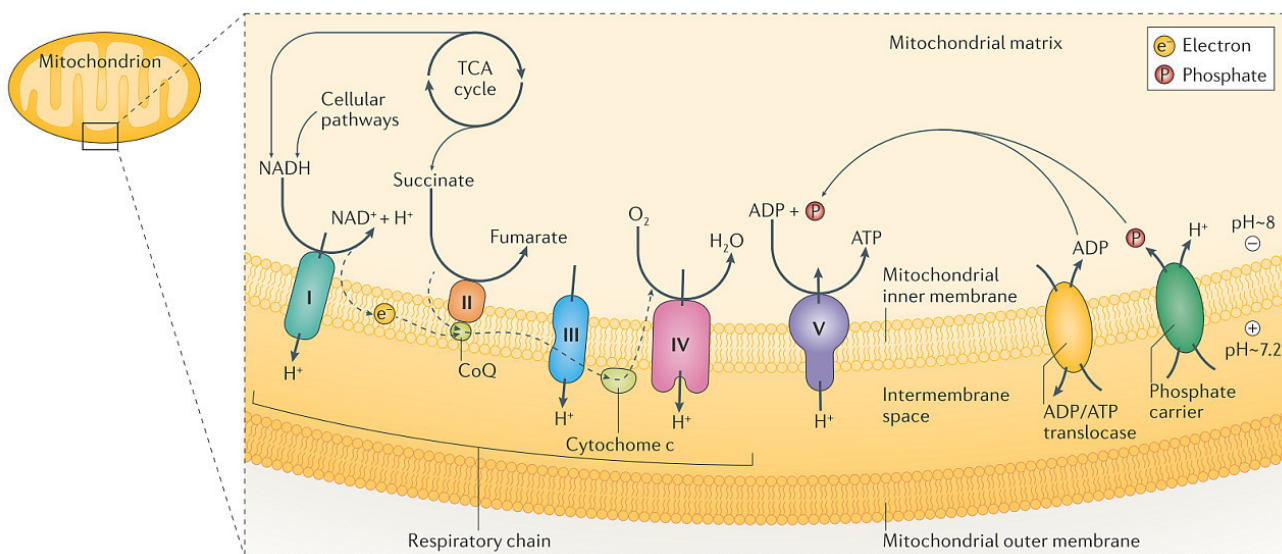


Figure 2: Schematic representation of oxidative phosphorylation. Oxidative phosphorylation is a metabolic pathway in cells to oxidize nutrients and convert energy in the form of ATP. The respiratory chain consists of complexes I–IV. Complex I (NADH coenzyme Q oxidoreductase) oxidizes NADH with the reduction of coenzyme Q10 (or CoQ) from its ubiquinone (CoQ; Q) form to ubiquinol (QH₂), generating an electrochemical gradient across the

inner mitochondrial membrane. Complex II (succinate–CoQ oxidoreductase) is linked to the Krebs cycle (or tricarboxylic acid (TCA) cycle) within the respiratory chain and oxidizes succinate with the reduction of CoQ from its ubiquinone form to ubiquinol. Complex III (ubiquinol–cytochrome *c* oxidoreductase) catalyses the reduction of cytochrome *c* by oxidation of ubiquinol, which generates an electrochemical gradient. Complex IV (cytochrome *c* oxidase) catalyses the terminal reaction of the respiratory chain by transferring electrons (e^-) to molecular oxygen, further building up the electrochemical gradient. Complex V (ATP synthase) converts the transmembrane electrochemical proton (H^+) gradient energy into mechanical energy, which catalyses ADP and phosphate (P) into ATP (figure adapted from Gorman *et al.*, 2016).

1.2 Mitochondrial genome maintenance

In 1963, Margit and Sylvan Nass discovered for the first time the presence of DNA within mitochondria through electron microscope imaging of chicken embryos (Nass and Nass, 1963). Human mtDNA forms a circular double-stranded molecule of 16,569 bp size (Figure 3). Its 37 genes encode 13 polypeptides, 22 transfer RNAs (tRNAs) and 2 ribosomal RNAs (rRNAs), necessary for proper assembly and function of the mitochondrial oxidative phosphorylation complexes (Anderson *et al.* 1981). In contrast to diploid nuclear DNA (nDNA), a cell contains several hundred to several thousand copies mtDNA (Miller *et al.*, 2003, Copeland *et al.* 2014), residing in the mitochondrial matrix. The multiple mtDNA molecules are organized together into protein-DNA complexes, called nucleoids (Bogenhagen *et al.*, 2008). These histone-free formations have a diameter of only ~ 100 nm (Gilkerson *et al.*, 2013), much smaller compared to the contour length of a completely relaxed and circular mtDNA molecule with a length of ~ 5 μ m (Zsurka *et al.*, 2018). A key protein in mtDNA nucleoid formation is the mitochondrial transcription factor A (TFAM). TFAM contains two high-mobility-group (HMG) domains, which bind to the mtDNA and unwind DNA in a non-sequence specific manner (Fisher *et al.*, 1992).

It was also proposed that the D-loop serves as a binding centre of proteins, involved in the regulation of mitochondrial nucleoids (He *et al.*, 2007).

1.3 Replication of mtDNA

In the late 60's, screening of rat liver mitochondria revealed replication circles of DNA (Leffler II *et al.*, 1970), together with a newly discovered mitochondrial DNA polymerase (Meyer and Simpson, 1968), which differs from the nuclear polymerase. This proved independent mtDNA replication within the mitochondrion. Since then, hypotheses about mtDNA replication have constantly evolved and been discussed.

1.3.1 Strand-displacement model

The strand-displacement model (SDM), or asynchronous replication model, was the first proposed model for mtDNA replication, described by Robberson *et al.* in 1972. It describes an asymmetric mechanism of mtDNA replication, starting from the oriH in clockwise direction, further expanding the D-loop and progressing towards the oriL (Figure 4). Once oriL is reached, it is exposed and H-strand replication stalls, while synthesis of the lagging strand proceeds in the opposite direction. After L-strand replication started, leading strand synthesis continues forth. By the time when replication of the H-strand is complete, L-strand synthesis has only finished two-third of its replication, spanning over the major arc from oriL to oriH with an approximate length of 11 kilobases (kb). This so called gapped circle molecule, stemming from the displaced strand, continues replication anti-clockwise until it reaches oriL and finishes L-strand replication (Clayton *et al.* 1982).

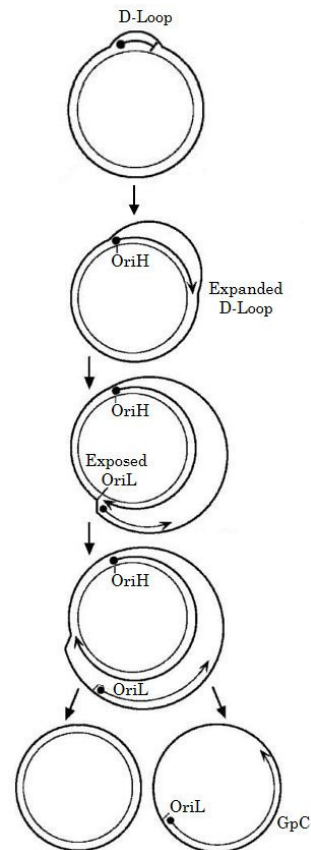


Figure 4: Asymmetric strand-displacement model of mtDNA replication. Replication of H-strand initiated at oriH, leads to further expansion and displacement of the D-loop. Once the oriL is exposed on the L-strand, the replication continues, followed by synthesis of new L-strand in the opposite direction. Intermediates of both strands are formed. The asymmetric replication creates one complete and one gapped circle (GpC) mtDNA molecule (Figure adapted from Brown *et al.*, 2005).

1.3.2 Strand-coupled replication model

In 2000, Holt and colleagues questioned the strand-displacement model, after electron microscopy of mtDNA from rat hepatocytes and HeLa cells revealed duplex replication intermediates (Koike and Wolstenholme, 1974, Crews *et al.*, 1979) and raised the hypothesis for coupled leading and lagging strand replication. The new model by Holt *et al.* described a symmetrical or strand-coupled replication of leading and lagging strand synthesis (Holt *et al.*, 2000), progressing from bidirectional replication forks (Figure 5). Followed by the experimental results by Yang *et al.* in 2002, replication would involve mostly double-stranded replication intermediates, with multiple RNA–DNA hybrids present on the light strand. These hybrids were then cleaved by RNase H1, resulting in single-stranded DNA intermediates. Replication, according to this model would create two complete daughter molecules at same pace, with no gapped circle molecule.

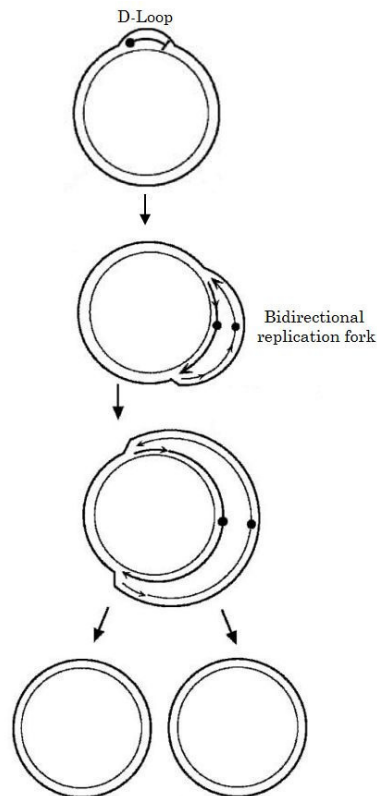


Figure 5: Strand-coupled model of mtDNA replication. Synchronous replication is initiated within a broad area beyond the simple D-loop. The double-stranded replication forks synthesize both strands bidirectionally and proceed through the length of the mtDNA, preventing the formation of oriL strand intermediates and the formation of gapped circle molecules (Figure adapted from Brown *et al.*, 2005).

In 2005, Brown *et al.* presented atomic force microscopy (AFM) results from mouse liver, that questioned the strand-coupled replication model and supported the orthodox, strand-displacement model. However, they claimed the existence of more than one light strand replication origin, which would require further modifications on the strand-displacement model, currently holding only one oriL. Together with previous findings from the literature (Robberson *et al.*, 1972; Koike and Wolstenhole, 1974; Pikó *et al.*, 1984), they all favour the asynchronous replication model.

1.3.3 RITOLS replication model

After the results from Brown *et al.* questioned the strand-coupled replication model, but also indicated missing pieces of evidence on the strand-displacement model, Yasukawa *et al.* proposed new findings one year later, regarding the properties of these replication intermediates, using two-dimensional gel electrophoresis (2D-AGE, Yasukawa *et al.*, 2006). They presented a novel

replication model, termed **ribonucleotide incorporation throughout the lagging strand (RITOLS)**. Their investigation on the presumed intermediates of strand-coupled synthesis showed the formation of duplex intermediates, created from slow-moving arcs of replication (Figure 6). These intermediates were indistinguishable from duplex DNA based on their mass and shape, however no restriction endonuclease, targeting double-stranded DNA (dsDNA) was able to cut them. Treatment with RNase H1, proved highly effective (which degrades RNA only if it is hybridized to DNA) and resulted in the formation of single-stranded DNA. Further 2D gel analysis on extracted mitochondrial replication intermediates (mtRIs) revealed L-strand RNAs of 200–600 nucleotides in length. Yasuka *et al.* therefore suggested, that RNA was incorporated throughout the lagging strand during mtDNA replication (Yasuka *et al.* 2006). The RITOLS model of replication resembles the SDM quite well: both models predict asynchronous mtDNA synthesis and mark the oriL as a major initiation site of light-strand synthesis. The NCR is also regarded as the oriH-containing region in both, however the RITOLS model proposes two origins (O_R) within the D-loop, one close to each end (Yasukawa *et al.*, 2006). To put it simple, RITOLS replication equal SDM plus lagging strand RNA incorporation (Holt and Reyes, 2012). In 2013, Holt and colleagues argued that during leading strand synthesis, pre-existing RNA is incorporated into the lagging strand via a “bootlace” strategy and not being synthesized in parallel (or symmetrical) to leading strand synthesis (Reyes *et al.*, 2013).

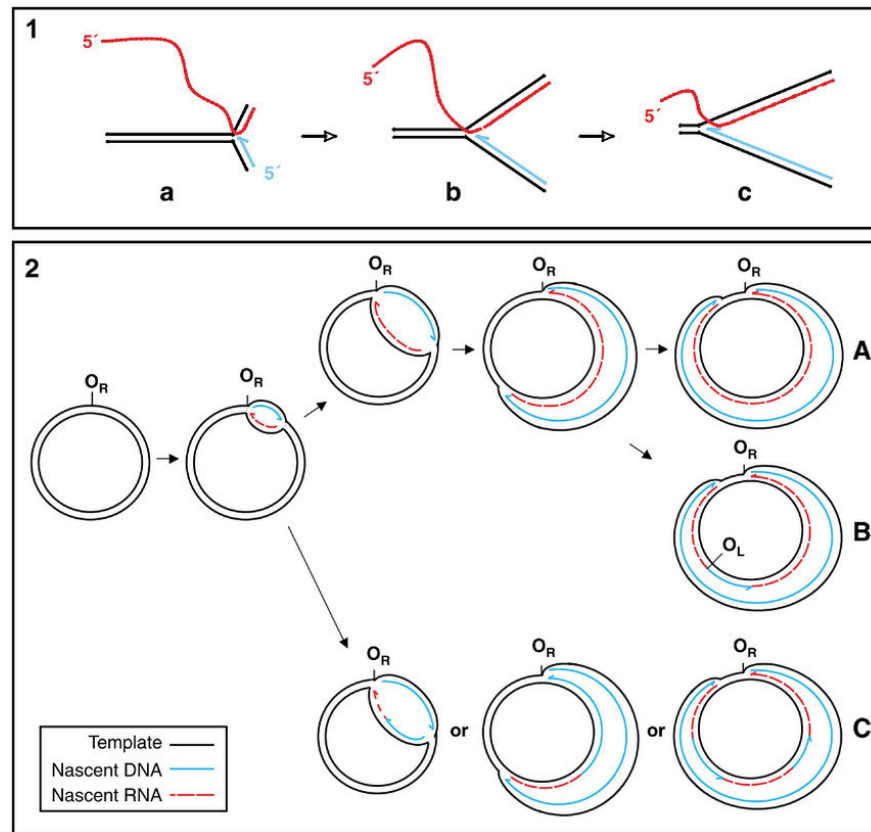


Figure 6: RITOLS model of mtDNA replication. 1) Incorporation of RNA (red) throughout the lagging strand with DNA (blue) synthesis on the leading strand. As the fork advances preformed RNA is threaded through the replication complex in 3'–5' direction, hybridized to the displaced parental strand 2) Bootlace model. Unidirectional replication initiated at one of two origin(s) of RITOLS (O_R) within the NCR. Lagging strand is initially laid down as RNA. As the replication fork advances, conversion to DNA starts a) after the entire lagging strand is fully incorporated as RNA b) at the oriL(O_L) or c) at scattered sites around the genome. (Figure adapted from Yasukawa *et al.*, 2006).

1.4 Members of the mtDNA replisome

The core members of the mitochondrial replication machinery include the mitochondrial homohexamer helicase Twinkle (TWNK), the mitochondrial DNA heterotrimer enzyme polymerase gamma (POL γ), the mitochondrial single-stranded DNA-binding protein (mtSSB) and the mitochondrial RNA polymerase (POLRMT, Figure 7). In 2004, a minimal mtDNA replisome was rebuilt *in vitro*, containing a dsDNA template and recombinant forms of the human TWNK, POL γ and mtSSB (Korhonen *et al.*, 2004).

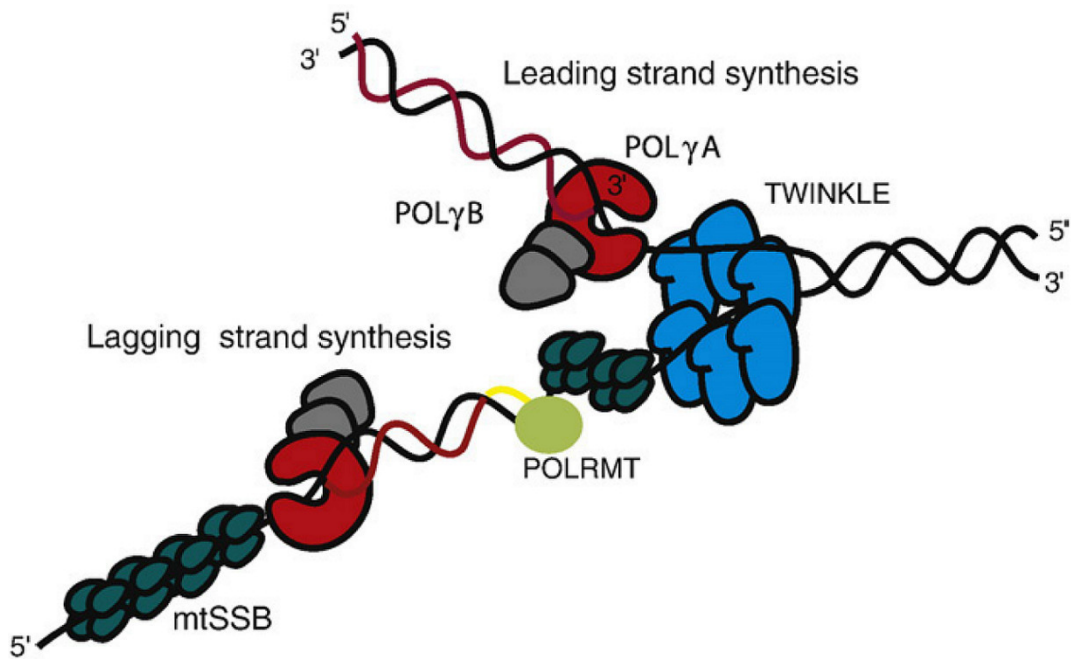


Figure 7: The mtDNA replication machinery. Replication model, showing two replication forks. Twinkle helicase (blue) unwinds dsDNA (black lines) in 5'–3' direction. mtSSB (dark green) stabilizes the ssDNA (black line) and stimulates DNA synthesis (red line) by POL γ (catalytic subunit A: red, accessory subunits B: gray). POLRMT (light green) synthesises RNA primer (yellow line) for lagging strand DNA synthesis (Figure adapted from Wanrooij and Falkenberg, 2010).

POL γ and TWNK alone were able to assemble on the dsDNA template with preformed replication forks to synthesize single-stranded DNA (ssDNA) products of ~2 kb. With the addition of mtSSB, the processivity of the replication machinery drastically increased and generated DNA products longer than 16 kb – the size of the human mitochondrial genome (Korhonen *et al.*, 2004).

Based on the reconstructed minimal replication machinery and together with recent findings, additional factors were incorporated into the hypothesis on mtDNA replication and proposed a novel replication model (Figure 8) and included additional enzymes, like the mitochondrial genome maintenance exonuclease 1 (MGME1), mitochondrial ligase III (mtLigIII) and mitochondrial transcription factor A and B2 (TFAM and TFB2M). TFAM and TFB2M both interact with POLRMT during RNA primer synthesis. MGME1 degrades ssDNA in 5'–3' direction, unwound by Twinkle and mtLigIII seals the mtDNA nicks (DeBalsi *et al.*, 2017).

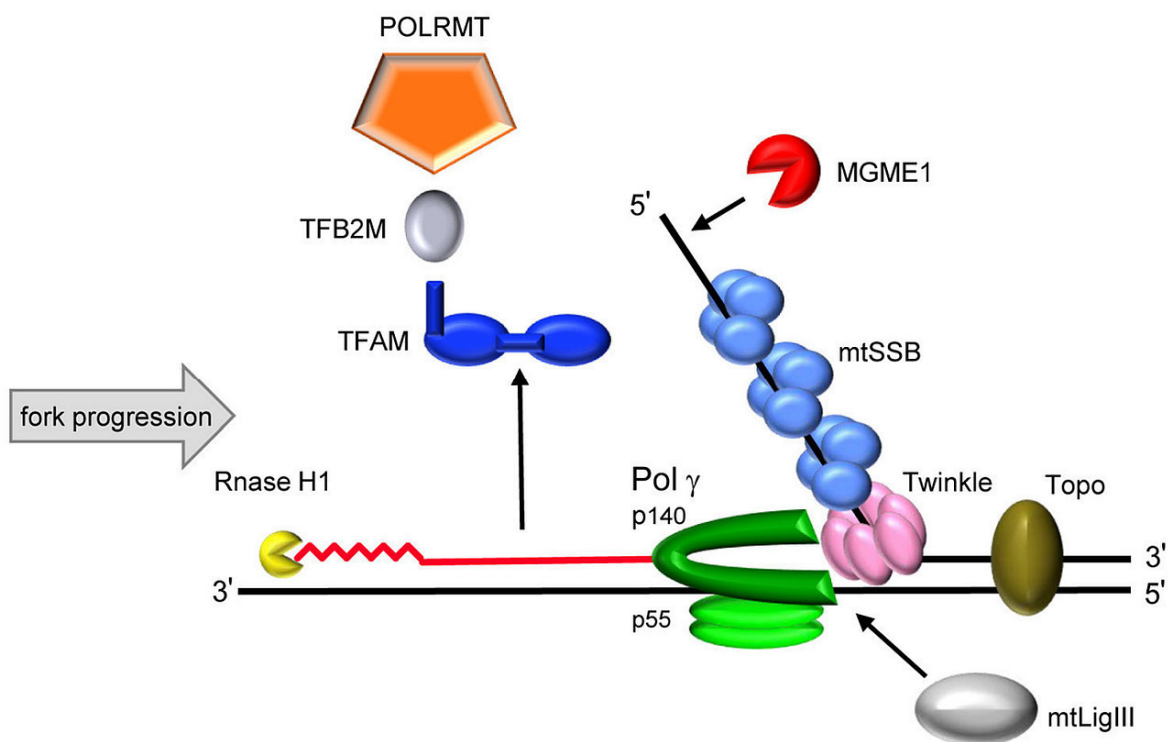


Figure 8: Schematic diagram of the updated mtDNA replication machinery. POLRMT produces RNA primer (jagged red line), required to initiate DNA replication in conjunction with TFAM (deep blue) and TFB2M (gray). After initiation, POLRMT, TFAM and TFB2M separately leave the DNA and the RNA primer is degraded by RNase H1 (yellow). In a 5'–3' direction, Twinkle helicase (pink) unwinds dsDNA at the replication fork. The ssDNA is stabilized by mtSSB (light blue), while MGME1 (red) degrades ssDNA. MtLigIII (white) seals the mtDNA nick. Nascent DNA (solid red line) is synthesized by Pol γ (green). Topoisomerases (brown) relieve the torsional tension in the DNA, caused by unwinding (Figure adapted from DeBalsi *et al.*, 2017).

1.4.1 Mitochondrial helicase Twinkle

In 2001, Spelbrink *et al.* described for the first time the mitochondrial helicase Twinkle. It showed a high similarity to the T7 bacteriophage primase/helicase (gene 4 protein, gp4), which gave rise to its name (**T7 gp4-like protein with intramitochondrial nucleoid localization**). *In vitro*, Twinkle forms multimers, with a hexameric ring helicase as the functional enzyme (Spelbrink *et al.*, 2001), that unwinds short stretches (<20 bp) of dsDNA in 5'–3' direction (Korhonen *et al.*, 2004). Within the mitochondrial replisome, Twinkle needs free DNA ends, that can be threaded through the helicase ring in order to execute its enzymatic activity.

1.4.2 Mitochondrial polymerase gamma

In humans, POL γ is the only known DNA polymerase involved in mtDNA synthesis (Ropp and Copeland, 1996). It is an asymmetric holoenzyme (or heterotrimer; 245 kDa) built of one catalytic subunit POLG (140 kDa) and two accessory subunits of POLG2 (53 kDa) (Carrodeguas *et al.*, 2001; Yakubovskaya *et al.*, 2006). The POLG subunit has a 5'–3' polymerase activity, a 3'–5' exonuclease proofreading activity and a 5'-deoxyribose phosphate (dRP) lyase activity, used for base excision repair (Foury and Vanderstraeten, 1992). Subunit POLG2 accelerates the polymerization rate by enhancing the affinity for DNA of the catalytic subunit. It prefers binding to dsDNA and could provide proper binding of POLG to the template strand behind the slower moving Twinkle helicase and helps in coordinating enzymatic activities of TWNK and POLG at the mtDNA replication fork (Wanrooij and Falkenberg, 2010).

1.4.3 Mitochondrial single-strand binding protein (mtSSB)

The mtSSB forms a tetramer (13–15 kDa) that binds ssDNA (Thömmes *et al.*, 1996), preventing it from refolding or being degraded by nucleases. The ssDNA wraps around the tetramer in electropositive channels, guided by flexible loops (Yang *et al.*, 1997). Together with TFAM, mtSSB is suggested to influence the stabilization as well as the turnover of the D-loop (Takamatsu *et al.*, 2002). MtSSB has been shown to improve primer recognition and binding by POL γ (Farr *et al.*, 1999) in the mitochondrial replisome.

1.4.4 Mitochondrial RNA polymerase and primase (POLRMT)

Mitochondrial transcription relies on a unique RNA polymerase (Greenleaf *et al.*, 1986). Transcription is initiated at the light-strand promoter (LSP) within the NCR (Falkenberg *et al.*, 2002), but POLRMT requires two additional transcription factors: TFAM and TFB2M (Asin-Cayuela *et al.*, 2007). In the mitochondrial replisome, POLRMT synthesizes RNA primers, used to initiate leading-strand mtDNA synthesis at the oriH, that can be utilized by POL γ to initiate DNA replication (Wanrooij and Falkenberg, 2010). But POLRMT also specifically synthesizes RNA primers of ~25 nucleotides at the oriL in the presence of mtSSB, for lagging strand synthesis (Fuste *et al.*, 2010).

1.4.5 Mitochondrial genome maintenance exonuclease1 (MGME1)

MGME1 is an exonuclease that localizes in mitochondria and belongs to the PD-(D/E)XK nuclease superfamily. It requires free nucleic acid ends for catalysis and processes 5'-flaps during mtDNA replication. MGME1 also possesses 3'-5' exonuclease activity on ssDNA (Kornblum *et al.*, 2013; Nicholls *et al.*, 2014) and is involved in mtDNA maintenance.

1.5 Mitochondrial DNA damage and repair pathways

Damaged mtDNA can arise, like nDNA, from DNA polymerase replication errors, DNA strand breaks, or through exposure to radiation, genotoxic chemicals or reactive oxygen species (ROS, Alexeyev *et al.*, 2013). During oxidative phosphorylation, the partial reduction of oxygen constantly challenges mtDNA to ROS exposure (Lenaz, 2001), given the natural proximity of ROS production sites and the nucleoids within the mitochondrial matrix (Wiesner *et al.*, 2006). Oxidative damage caused by ROS includes single-strand DNA breaks (SSB) and double-strand DNA breaks (DSB). Mutations of mtDNA through ROS exposure comprise base substitution, deletions and missense mutations (Cline, 2012). SSBs usually result in the loss of a single nucleotide and damaged 5' and/or 3' ends at the breakage.

1.5.1 Base excision repair (BER)

Apart from oxidative damage, SSBs can also occur during base excision repair (BER), by enzymatic cleavage of the phosphodiester backbone (Alexeyev *et al.*, 2013). Mitochondrial BER is initiated by DNA glycosylases (Prakash *et al.*, 2015), which recognize and cleave oxidized or damaged bases either by a single-nucleotide-BER (SN-BER) or long-patch-BER (LP-BER) pathway (Figure 9). Both of these single-strand break repair (SSBR) pathways leave an abasic site, that is cleaved at a 5'-end by an apurinic/apyrimidinic (AP) endonuclease (APE or APEX), generating a gap, which is filled up by POL γ to a 5'-deoxyribose phosphate (dRP) flap (or 5'-flap, Hedge *et al.*, 2012; Copeland *et al.*, 2014).

In mitochondrial SN-BER, POL γ filled in a single nucleotide to create a ligatable substrate, that requires the removal of the 5'-dRP fragment, which is performed by the catalytic subunit of POL γ (Longley *et al.*, 1998). In the LP-BER pathway, the displaced 5'-flaps must also be removed prior ligation, but is assumed to be performed by DNA replication helicase/nuclease 2 (DNA2, Masuda-Sasa *et al.*, 2006) or Flap structure-specific endonuclease 1 (FEN-1, Hiraoka *et al.*, 1995), but might also be performed by Mitochondrial Genome Maintenance Exonuclease 1 (MGME1, Kornblum *et al.*, 2013) or Exo/Endonuclease G (EXOG, Tann *et al.*, 2011) under certain circumstances. DSB either result in the formation of blunt ends or, 5' or 3' overhangs. DSB repair (DSBR) is performed by homologous recombination (HR), also known as homologous directed repair (HDR), or nonhomologous end joining (NHEJ, Alexeyev *et al.*, 2013).

In HR, a single strand of the damaged DNA invades a healthy complementary strand, leading to a D-loop formation and subsequent DNA synthesis. In order to anneal properly, long stretches of homology are required. Afterwards, the damaged strand reanneals with its own complementary strand, the gap is filled in and ligation eventually repairs the dsDNA. Standard NHEJ is supposed to be absent in mtDNA repair and is instead replaced by microhomology-mediated end-joining (MMEJ, Tadi *et al.*, 2015), as supportive studies showed that ~85 % of mtDNA deletions were flanked only by short repetitive sequences (Krishnan *et al.*, 2008).

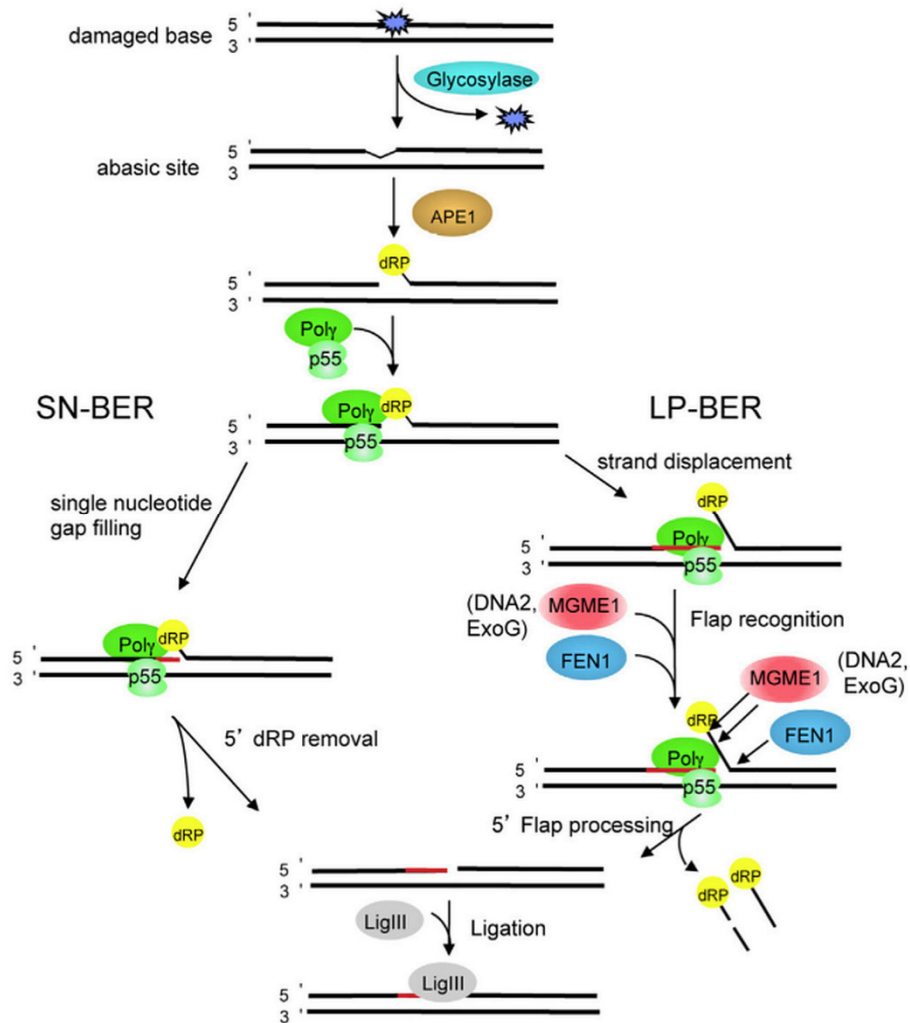


Figure 9: MtdNA base excision repair pathways in mammalian mitochondria. An oxidized base is excised by a glycosylase, leaving an abasic site. APE1 creates a SSB with a 5'-dRP flap on the downstream DNA. Single-nucleotide-BER (SN-BER) repair pathway involves POL γ filling the single nucleotide gap and removing the 5' deoxyribose phosphate (dRP) flap, creating a ligatable substrate. In LP-BER, the extended 5'-dRP flap is recognized and cleaved by MGME1 and FEN1, prior to ligation by ligase III. Alternately, the 5' end may be processed by DNA2 or EXOG to produce a ligatable substrate (figure adapted from Copeland and Longley, 2014).

Mitochondrial HR is still questioned, as various experiments showed either no recombination, even under selective environmental pressure (Gilkerson *et al.*, 2008), or only low amounts of intermolecular recombination after mtDNA depletion (D'Aurelio *et al.*, 2004) or induced DSB (Bacman *et al.*, 2009).

1.5.2 Nucleotide excision repair (NER)

In 1975, Clayton et al. demonstrated proof for the absence of a pyrimidine dimer repair mechanism for mtDNA in mice and humans. Alkylation damage to mtDNA or UV-exposure-caused mutations were also unable to be repaired by NER in mitochondria (Pascucci *et al.*, 1997; Croteau and Bohr, 1999; Copeland and Longley, 2014).

1.5.3 Mismatch repair (MMR)

The mismatch repair pathway in nuclear DNA can remove base mismatches, short insertions or deletions (Copeland *et al.*, 2014). In mitochondria, the presence of MMR pathways was reported in *Saccaromyces cerevisiae* (Alani *et al.*, 1994), but not in higher eukaryotes (Copeland *et al.*, 2014).

1.5.4 Ribonucleotide excision repair (RER)

Human cells contain two RNase H enzymes, that remove incorporated RNA (Sparks et al., 2012) during a process, called RER. RNase H1, as mentioned before, cleaves and degrades RNA from RNA–DNA hybrids, while RNase H2 removes individually incorporated ribonucleotide 5'-monophosphate (rNMP) residues in DNA (Copeland *et al.*, 2014). However, only RNase H1 is present in mitochondria (Cerritelli *et al.*, 2003). The single ribonucleotides in the template DNA can be bypassed by POL γ , which has a strong reverse transcriptase activity (Copeland *et al.*, 2014).

1.6 Mitochondrial nucleases and mtDNA degradation

Due to the multicopy nature of the mitochondrial genome, mtDNA is not constrained to “repair or die” compared to diploid nDNA. A fraction of mtDNA can be lost without damaging effects (Alexeyev *et al.*, 2013), which leads to a different handling of damaged mtDNA, that cannot be repaired—namely through degradation. This degradation of damaged mtDNA is suggested to be performed by nucleases (Bruni *et al.*, 2016), yet the complete degradation machinery, or ‘degradosome’ of mtDNA is still unknown.

Up to date, there are several identified mitochondrial DNases (Table 1) with endonuclease or strand-specific exonuclease activity (Bruni *et al.*, 2016) that might influence mtDNA degradation.

Table 1: Mitochondrial DNases (table adapted from Bruni *et al.*, 2016).

Nuclease	Mitochondrial process(es)	Cleavage activity	Substrate	
			DNA	RNA
APEX1	Base excision repair	Endonuclease	+	
APEX2	Base excision repair	Endonuclease	+	
		ssDNA 3'–5' Exonuclease		
FEN1	Base excision repair	5'–3' Exonuclease	+	+
	Flap processing	5'-flap Endonuclease		
		RNase H activity		
DNA2	Flap processing	Endonuclease	+	
MGME1	Flap processing	ssDNA 5'–3' Exonuclease	+	
	Base excision repair	ssDNA 3'–5' Exonuclease		
MRE11	DSB repair	Endonuclease	+	
		ssDNA 3'–5' Exonuclease		
RBBP8	DSB repair	Endonuclease	+	
ENDOG	Apoptosis	Endonuclease	+	+
EXO1	SSB repair	5'–3' Exonuclease	+	+
		Endonuclease		

As mentioned earlier, APEX1 generates a gap at apurinic/apyrimidinic sites during BER, that forms a 3' end with a hydroxyl group used to initiate DNA replication and a 5' phosphate residue, which must be removed to fully ligate the replicated DNA. APEX2 localizes predominantly in the nucleus, but also to some extent in mitochondria (Tsuchimoto *et al.*, 2001). It is presumed to be involved in nuclear BER; activity in mitochondria has not been demonstrated yet (Bruni *et al.*, 2016). APEX2 also possesses a 3'–5' exonuclease activity, preferentially targeting mismatched base pairs (Burkovics *et al.*, 2006), that could potentially be utilized in degradation of linear mtDNA.

Interactions between FEN1 and DNA2 have shown an increased flap processing efficiency (Zheng *et al.*, 2008), yet mitochondrial localization of FEN1 is still

questioned (Bruni *et al.*, 2016). MGME1 is involved in mtDNA maintenance and processes 5'-flaps during mtDNA replication, but also possesses 3'-5' exonuclease activity on ssDNA (Kornblum *et al.*, 2013; Nicholls *et al.*, 2014). MRE11 exerts DNA endonuclease and 3'-5' exonuclease activity and forms the MRN complex with the RAD50 homolog and NBS1 (or Nibrin), required for NHEJ (Buis *et al.*, 2008). Together with the endonuclease RBBP8 (or Retinoblastoma-binding protein 8, also known as CtBP-interacting protein, CtIP), the MRN complex can also perform DSB repair through the HR pathway (Chen *et al.*, 2008). EXOG possesses endonuclease nicking activity on supercoiled DNA and also favours ssDNA for its 5'-3' exonuclease activity during SSB repair (Cymerman *et al.*, 2008).

1.7 Mitochondrial diseases

Since mtDNA is limited by its DNA repair capacity (Young *et al.*, 2016), it is more prone to damage than nDNA with an estimated 10–20 times higher mutation rate (Richter *et al.*, 1988). Accumulated mutated mtDNA leads to phenotypic manifestations in mitochondria if a certain threshold is exceeded (Rossignol *et al.*, 2003). Since disease-associated mutations of mtDNA are often heteroplasmic (they exist simultaneously with wildtype mtDNA and do not occur in every copy of mtDNA in each cell), the proportion of wild-type vs. mutated mtDNA determines the pathological nature of mitochondrial disease, depending on the affected organ (Figure 10) and age of onset (Debrosse and Parikh, 2012).

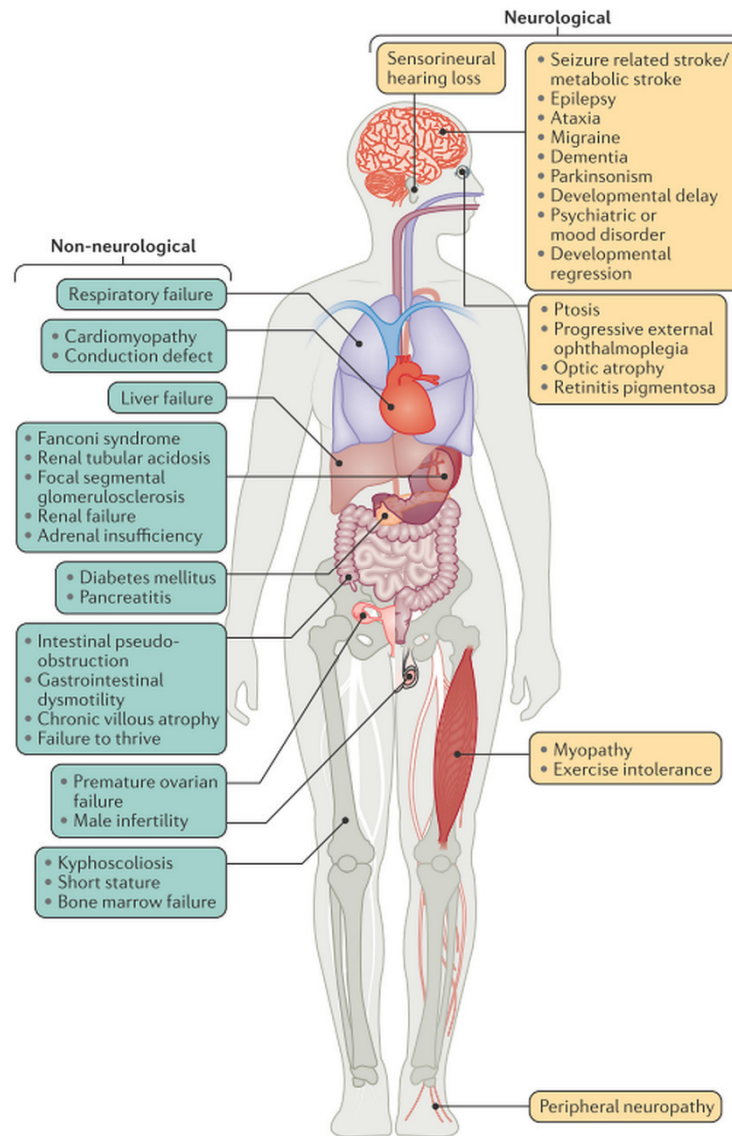


Figure 10: Clinical representations of mitochondrial diseases. Onset of mitochondrial diseases highly varies between patients and can encompass dysfunction of any organ or tissue, but can be divided in two characteristics: neurological or non-neurological (figure adapted from Gorman *et al.*, 2016).

Pathogenic mtDNA mutations affect the structural subunits of the respiratory chain (through mtDNA rearrangements/deletions) or the mitochondrial protein synthesis machinery (through mutations in mRNA, rRNA, tRNA; Gorman *et al.*, 2016). Over 200 disorders are associated with point mutations or single deletions in mtDNA (Chabi *et al.*, 2003). The largest subset includes functional mutations of the respiratory chain, occurring at least once in 5000 live births (Vafai and Mootha, 2012). Assessing the prevalence of mtDNA mutations is still difficult, because molecular screening usually restricts to detection of mtDNA deletions (plus a few common mutations, Bannwarth *et al.*, 2013). Only whole mtDNA screenings can reliably reveal rare mtDNA mutations.

1.7.1 MtDNA maintenance disorders

There are three major classes of pathological mtDNA alterations: point mutations, deletion-duplications and reduced mtDNA copy numbers. For the latter, a copy number reduction below 30% of the normal mtDNA content is defined as mtDNA depletion and usually results in lethal infancy or childhood diseases due to deficiencies in the mtDNA encoded proteins of respiratory chain complexes I, III, IV and V (Rötig and Poulton, 2009).

Errors or inaccuracies in mtDNA maintenance can also result in deletion of mtDNA. The majority of mtDNA deletions was found in close vicinity of direct repeats (DR, Bua *et al.*, 2006) but also near stem-loops (SL, Lakshmanan *et al.*, 2012). Mechanisms, that can lead to the formation of deletions between DRs include DSB repair (Krishnan *et al.*, 2008) and slip-replication (Shoffner *et al.*, 1989). The slipped-strand mechanism (Figure 11) assumes the asynchronous strand displacement model and describes misannealing of a single-stranded repeat of the H-strand during replication with a newly synthesized L-strand repeat (Pitceathly *et al.*, 2012). A loop of the single-stranded H-strand forms and it eventually gets degraded, while the free ends ligate and allow continued replication. The deleted loop however, results in a mtDNA major arc deletion (Krishnan *et al.*, 2008).

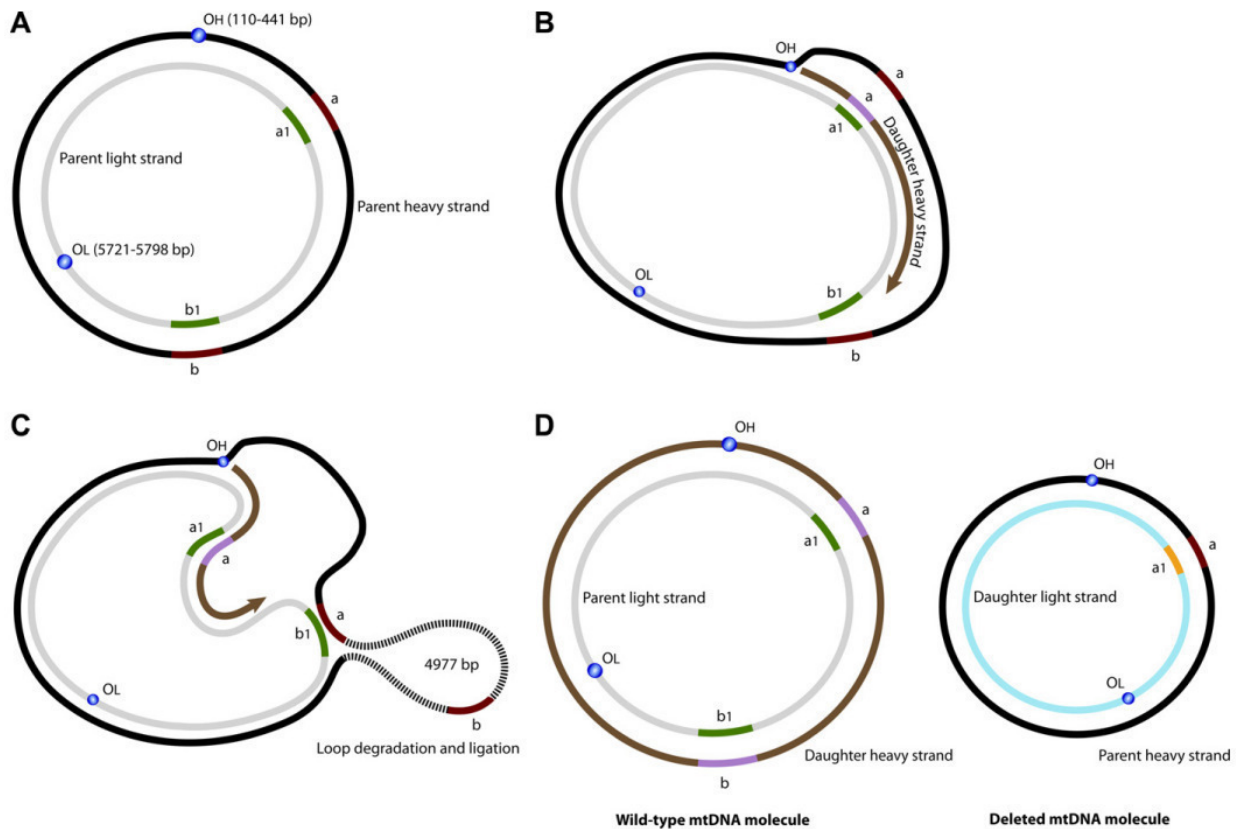


Figure 11: Slipped-strand model of mtDNA deletion formation. A) MtDNA molecule prior replication, containing two direct homologous repeats (*a/a1* and *b/b1*) with origins of replication (OH - heavy, OL - light) shown. B) MtDNA replication initiated at OH. The newly formed daughter heavy strand (brown) uses L-strand as template, thereby displacing the parental H-strand. C) Two direct homologous repeats between parental H-strand and L-strand (*a* and *b1*) misalign, forming a downstream H-strand loop. The free ends of the parental H-strand are ligated and replication of the daughter H-strand continues. D) Slipped strand replication results in the synthesis of two mtDNA molecules, one wild-type (parent L-strand plus daughter H-strand) and one deleted (parent H-strand and daughter L-strand) molecule (Figure adapted from Pitceathly *et al.*, 2012).

Krishnan *et al.* suggested that not the slipped-strand mechanism, but DSB repair is the responsible major cause for the formation of large scale deletions (Figure 12). After DSB, the free mtDNA ends are susceptible to exonuclease activity, resulting in the formation of single-strand ends. The homologous repeats within both strands misalign, in which the overhangs get degraded, resulting in the formation of a partially deleted mtDNA molecule. Besides homologous-directed end joining repair of DSB, NHEJ repair of DSB can also result in the formation of deletions, even in the absence of direct repeats (Gredilla *et al.*, 2012).

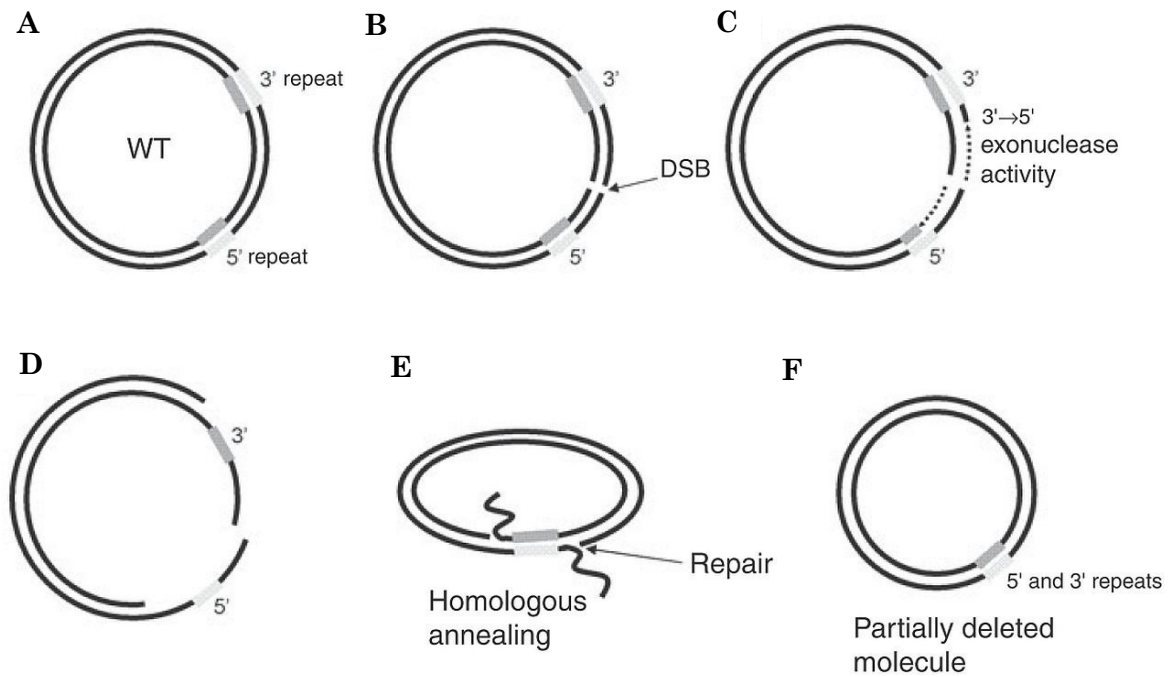


Figure 12: Model for the generation of mtDNA deletions during DSB repair. **A)** wild-type mtDNA molecule, with two indicated direct repeats (3' and 5'). **B)** Introduced DSB. **C, D)** DSB is susceptible to 3'–5' exonuclease activity, resulting in the formation of single-stranded ends. **E)** The direct repeats can misanneal, resulting to degradation of the unbound single-stranded ends and ligation of double strand. **F)** A partially deleted mtDNA molecule forms, with copies of 5' and 3' repeats. If the repeats contain mismatched bases, subsequent repair could use either strand as a template to correct the mismatch (Figure adapted from Krishnan *et al.*, 2008).

1.7.2 Disease-associated mtDNA alterations

Through aging, mtDNA maintenance disorders or neurodegenerative diseases, the heteroplasmic drift of mtDNA mutations can extend to the entire cell, through a process called clonal expansion. Clonal expansion of large-scale mtDNA deletions or mtDNA copy number reduction (depletion) can lead to prominent clinical phenotypes. The most frequent presentations (Table 1.1) include autosomal dominant chronic progressive external ophthalmoplegia (adCPEO), mitochondrial neurogastrointestinal encephalomyopathy (MNGIE), hepatopathic poliodystrophy (Alpers–Huttenlocher syndrome), sensory-ataxia neuropathy, dysarthria and ophthalmoplegia (SANDO), infantile-onset spinocerebellar ataxia (IOSCA) and spinocerebellar ataxia and epilepsy (SCAE, Viscomi and Zeviani, 2017).

Table 1.1: Genes and phenotypes in altered mtDNA maintenance (Table adapted from Viscomi and Zeviani, 2017).

Gene	mtDNA alteration	Inheritance*	Main clinical phenotype
<i>TWINK</i>	Multiple deletions	AD	adCPEO
	Multiple deletions	AR	IOSCA
	Depletion	AR	Alpers-like
<i>POLG</i>	Multiple deletions	AD	adCPEO
	Multiple deletions	AR	adCPEO
	Depletion	AR	Alpers-Huttenlocher
	Multiple deletions	AR	SANDO/SCAE
<i>POLG2</i>	Multiple deletions	AD	adCPEO
<i>MGME1</i>	Multiple deletions	AR	adCPEO
<i>DNA2</i>	Multiple deletions	AD	adCPEO
<i>TFAM</i>	Depletion	AR	Hepatocerebral syndrome
<i>TYMP</i>	Multiple deletions and depletion	AR	MNGIE

*AD = autosomal dominant; AR = autosomal recessive

1.8 CRISPR/Cas9 genome-editing and mitochondria

Studying mtDNA maintenance can be performed by various approaches, like directly modelling mtDNA damage, or by manipulating components of the mtDNA maintenance machinery. Modern gene-editing in living cells has become cost-efficient, fast and easy to handle, due to the CRISPR/Cas9 genome-editing system. Compared to restriction endonucleases, the CRISPR/Cas9 tool allows precise targeting of specific genes to introduce DSB followed either by NHEJ or, in case of a repair template, HR. Direct mitochondrial genome engineering is still elusive, as the existence of an endogenous mechanism for nucleic acid import into mammalian mitochondria, which is a prerequisite for mitochondrial CRISPR/Cas9-editing, remains controversial (Gammage *et al.*, 2017). Therefore, genetic engineering, by CRISPR/Cas9 can only be performed on nuclear genes, which encode mitochondrial proteins.

CRISPR stands for **C**lustered **R**egularly **I**nterspaced **S**hort **P**alindromic **R**epeats and was coined in 2002 by Jansen *et al.* to describe repetitive repeats in bacterial and archaeal genomes. CRISPR-associated (Cas) genes are located near a CRISPR locus and indicate functional relationship. Cas3 genes possess characteristics of helicases of the superfamily 2 and Cas4 genes show motifs of the RecB family of exonucleases, which suggests the involvement of these genes in DNA metabolism or gene expression (Jansen *et al.*, 2002). Over the next years CRISPR research identified CRISPR spacer sequences matching foreign DNA (Bolotin *et al.*, 2005) and CRISPR was characterized as a bacterial adaptive immune system (Makarova *et al.*, 2006). In 2010, the CRISPR/Cas system was identified as a bacterial and archaeal immune system, that targets and cleaves phage DNA, that can also insert new spacer sequences into the genome, making the CRISPR/Cas system an adaptive immune system (Garneau *et al.*, 2010). One year later, Cas9 from *Streptococcus pyogenes* was described to associate with two RNA molecules: CRISPR RNA (crRNA) and *trans*-activating CRISPR RNA (tracrRNA). These three components together were sufficient to protect *S. pyogenes* against phage infection (Deltcheva *et al.*, 2011). Following these discoveries, in 2012 Cas9 was described as an endonuclease, introducing DSB in DNA, allowing complementary binding of crRNA to the target DNA (Jinek *et al.*, 2012). Finally, in 2013, the CRISPR/Cas9 system was used to edit targeted genes in both human and mouse cells, using custom made crRNA sequences (Cong *et al.*, 2013). The technique was further improved in 2014, through the identification of protospacer adjacent motifs (PAM), which are required for the RNA-guided DNA recognition (Anders *et al.*, 2014) and the design of a single guide RNA (sgRNA), combining the functions of crRNA and tracrRNA (Nishimasu *et al.*, 2014; Ramakrishna *et al.*, 2014). Today CRISPR/Cas9 encoding plasmids are commercially available and can target any nuclear gene of interest, given an adjacent PAM sequence (Figure 13).

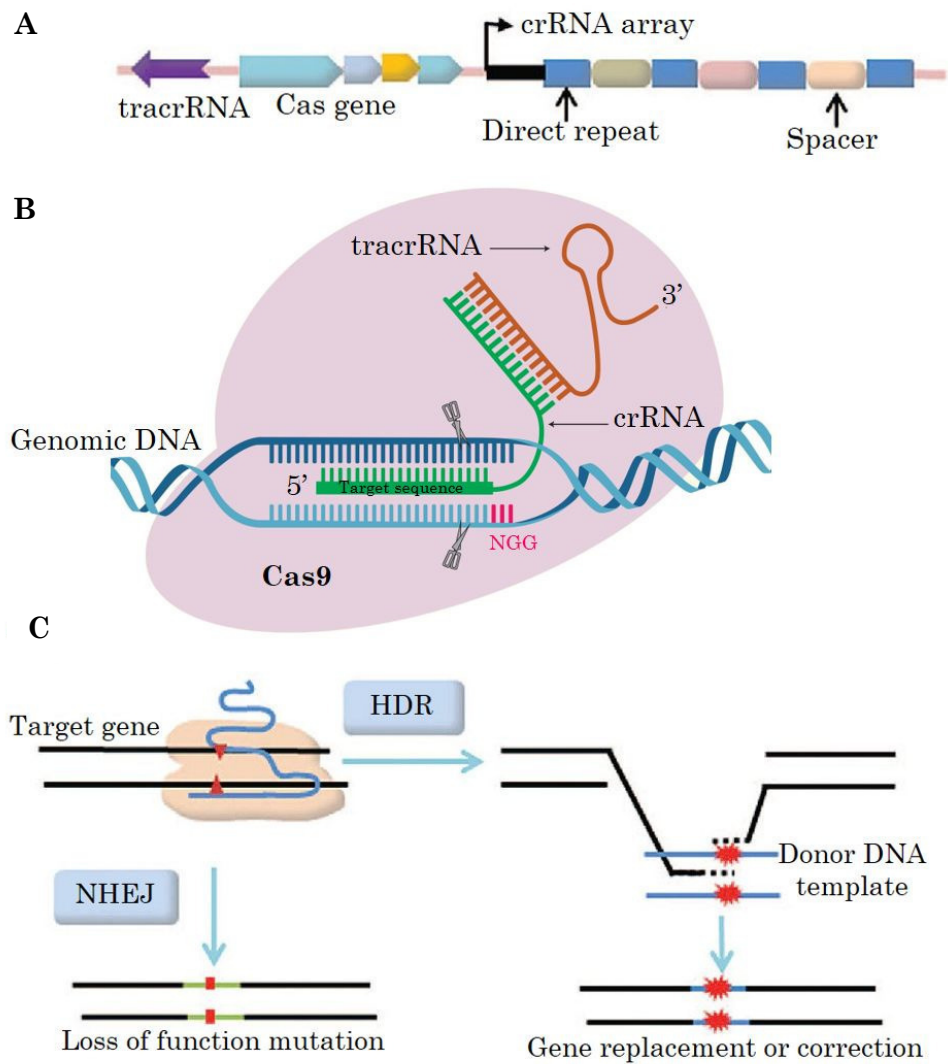


Figure 13: Schematic representation of CRISPR/Cas9-mediated genome editing. **A)** Schematic CRISPR locus (from *Streptococcus pyogenes*). **B)** Site-specific DNA cleavage by Cas9 nuclease, directed by complementary single guide RNA (sgRNA), complementary to target site, given a protospacer-adjacent motif (PAM) on the opposite strand. **C)** The resulting double-strand break (DSB) and subsequent repair, either by non-homologous end joining (NHEJ) or homology-directed repair (HDR), in presence of a donor template. NHEJ is more error prone to produce indels, whereas HDR can result in precise gene modification. (figure adapted from Dai *et al.*, 2016 (a & c); Integrated DNA technologies (eu.idtdna.com), 02.2018 (b)).

1.9 Aims

The main focus of this thesis was dedicated to the study of the role of mitochondrial nucleases in degradation of linear mtDNA, to gain insights into the still unknown mtDNA degradation machinery. For this purpose, I used the CRISPR/Cas9 genome-editing tool to alter mitochondrial nucleases in living cells. (I) In the first step, I had to design and assemble custom-built CRISPR/Cas9-vectors against gene-specific target sequences. Once applied, cloning strategies had to be established and optimized to handle the ample screening process, in order to identify positive clones, bearing the altered mitochondrial nucleases. A HEK 293 T-REx cell line was used, expressing the mitochondrial-targeted endonuclease protein EagI, as a model of mtDNA damage by introducing DSB's and linearization of mtDNA. Once the individual cell lines were identified through screening, bearing the desired mutations for the targeted genes, mitoEagI expression had to be checked for its endonuclease activity to excluded potential off-target effects by CRISPR/Cas9. (II) In the next step, I used the validated mitoEagI mutant cell lines to induce mitoEagI expression and study linear mtDNA degradation over the first twenty-four hours in two-hour intervals, which allowed me to compare time-dependent degradation effects between the mutant clones. Additionally, prolonged degradation experiments were performed, together with dideoxycytidine treatment instead of mitoEagI induction to linearize mtDNA, to study long-term effects of mutant nucleases on mtDNA degradation. Taken together, this study aimed to identify key enzymes in the mitochondrial degradation machinery and to show their function in removal of linear mtDNA, which would overall give a better understanding of mtDNA maintenance.

2. Materials & Methods

Table 2: Chemicals

Compound	Supplier
Acrylamide/Bis solution, 40%	BIO-RAD
Agarose	Sigma-Aldrich
Ammonium persulfate (APS)	Carl Roth GmbH & Co. KG
Bromophenol blue	Sigma-Aldrich
Bovine serum albumin	Sigma-Aldrich
2',3'-dideoxycytidine	Sigma-Aldrich
Coomassie Brilliant Blue R-250	BIO-RAD
CSPD	Roche
Digitonin	Serva Electrophoresis GmbH
dNTPs	Sigma-Aldrich
DIG Easy Hyb	Sigma-Aldrich
Dimethyl sulfoxide (DMSO)	Merck
Dulbeco's modified eagle's medium (DMEM), GlutaMAX	Thermo Fisher Scientific
EDTA	Sigma-Aldrich
Ethidium bromide	Sigma-Aldrich
Fetal calf serum (FCS)	PAN-Biotech
Glycerol	Sigma-Aldrich
Hydrochloric acid (HCL)	Sigma-Aldrich
Mannitol	Sigma-Aldrich
MgCl ₂	Sigma-Aldrich
Midori Green	Nippon Genetics
PBS (Phosphate buffer saline) pH 7.4	Invitrogen Corporation
PBST (PBS with Tween 20)	Thermo Fisher Scientific
Penicillin / Streptomycin	Invitrogen Corporation
PicoGreen	Thermo Fisher Scientific
Saline sodium citrate (SSC)	Thermo Fisher Scientific
Sodium chloride (NaCl)	Sigma-Aldrich
Sodium dodecyl sulphate (SDS)	Sigma-Aldrich
Sodium hydroxide (NaOH)	Sigma-Aldrich

SuperSignal West Pico Chemi-luminescent Substrate	Thermo Fisher Scientific
SYBR Green I nucleic acid gel stain	Sigma-Aldrich
Tetramethylethylenediamin (TEMED)	Sigma-Aldrich
Tris-Borat- EDTA buffer solution	Sigma-Aldrich
Trizma (TRIS)	Sigma-Aldrich
Uridine	Sigma-Aldrich
Xylene cyanol	Merck
1 kb DNA ladder	New England Biolabs
1 kb Extended DNA ladder	New England Biolabs
2-Log DNA ladder (0.1–10.0 kb)	New England Biolabs
25 bp DNA ladder	Invitrogen Corporation
DIG-labeled DNA Molecular Weight Marker II and III	Roche

Table 3: Antibodies

Antibody	Supplier
Anti-beta-Actin antibody	GeneTex
Anti-DIG fab fragments	Roche
Anti-HA antibody	Thermo Fisher Scientific
Secondary anti-rabbit IgG-peroxidase-Conjugated	Sigma-Aldrich

Table 4: Enzymes

All enzymes used the provided reaction buffers by the manufacturer.

Enzyme	Supplier
ExoSAP-IT PCR Product Cleanup	Thermo Fisher Scientific
JumpStart AccuTaq LA polymerase	Sigma-Aldrich
Mung Bean nuclease	New England Biolabs
Proteinase K	Qiagen
Restriction Endonuclease ApaI	New England Biolabs
Restriction Endonuclease BamHI	New England Biolabs
Restriction Endonuclease EcoRV	New England Biolabs

Materials & Methods

Restriction Endonuclease PstI	New England Biolabs
Restriction Endonuclease SpeI	New England Biolabs
T4 DNA ligase	New England Biolabs
T4 DNA polymerase	New England Biolabs
TaKaRa La TaqHS	TAKARA BIO INC
Trypsin	GE Healthcare

Table 5: Cell medium

Medium	Ingredients
Cell freezing medium	90% [v/v] FCS, 10% [v/v] DMSO
MitoEagI HEK 293 medium	DMEM (4.5 g/L glucose, GlutaMAX™, 1 mM sodium pyruvate), 10% [v/v] FCS, uridine (50 µg/L), penicillin & streptomycin (10 U/mL), blasticidin S hydrochloride (15 µg/mL), hygromycin B (50 µg/mL)

Table 6: Solutions

Solution	Components
Loading dye	1×TBE buffer, 30% [v/v] glycerol, 0.04% [w/v] bromphenol blue, 0.4% [w/v] xylene cyanol
Cell Lysis buffer	1 mM CaCl ₂ , 3 mM MgCl ₂ , 1 mM EDTA, 1% Triton X-100, 10 mM Tris, pH 7.5
Denaturing solution	0.5 M NaOH, 1.5 M NaCl, pH 13
Depurination solution	0.25 M HCl
Laemmli buffer	4% SDS, 10% 2-mercaptoethanol, 20% glycerol, 0.004% bromophenol blue, 0.125 M Tris HCl, pH 6.8
Neutralizing solution	0.5 M Tris-HCl, 1.5 M NaCl, pH 7
Protein Lysis buffer	20 mM Tris-HCl (pH 7.4), 150 mM NaCl, 1 mM EDTA, 1 mM EGTA, 1% Triton X-100, protease inhibitor cocktail (1 tablet/10mL, Roche).
Stripping solution	0.2 M NaOH + 0.1% SDS

Table 7: Kits

Kit	Supplier
DIG DNA labelling and detection Kit	Roche
iQ™ SYBR® Green Supermix	BIO-RAD
QIAamp DNA Mini Kit	QIAGEN N.V.
QIAquick Gel Extraction Kit	QIAGEN N.V.
QIAquick PCR Purification Kit	QIAGEN N.V.
Quant-iT PicoGreen dsDNA Kit	Thermo Fisher Scientific
PCR DIG Probe Synthesis Kit	Roche
SYBR Green RT-PCR Reagents Kit	BIO-RAD

Table 8: Equipment

Equipment	Model	Company
Analytical balance	TE214S	Sartorius
Camera	3CCD Color Model DXC-9100P	Sony Corporation
DNA quantitation	Fluorat Panorama	Lumex Instruments
Gel-electrophoresis chamber	Sub-Cell GT System	BIO-RAD
Haemocytometer	BLAUBRAND® Neubauer	BRAND GMBH
Phase contrast	Axiovert 40C	Carl Zeiss AG
PCR thermocycler	GeneAmp® Applied PCR system 9700	Biosystems
PCR thermocycler	MJ Research PTC-100	GMI, Inc.
PCR thermocycler	MJ Research	GMI, Inc.
Quantitative real time PCR (qPCR) thermocycler	iCycler iQ™ cyclers	BIO-RAD
Semidry transfer cell	Trans-blot SD	BIO-RAD
Spectrophotometer	Cary 50 scan PTC-200	Varian, Inc.
Ultrasonic processor	GEX-600	Cole-Parmer
UV-illuminator	Geldoc™XR	BIO-RAD

Table 9: Software

Software	Program	Company
DNA quantitation	Fluorometry Panorama	Lumex Instruments
Image processing and analysis	ImageJ	Wayne Rasband
Image acquisition	Quantity One 1-D	BIO-RAD
	CFX Manager	BIO-RAD
	Analysis Software	
Primer design	Primer-BLAST	NCBI, NLM
qPCR	MyiQ™	BIO-RAD
qPCR	IQ5	BIO-RAD
qPCR	Sigma plot	Systat Software Inc.
Spectrophotometry	CaryWinUV	Varian, Inc.
Sequence analysis	scftk	Dr. Zsurka inhouse

Oligonucleotides

Table 10: Oligonucleotides used in the generation of CRISPR/Cas9-vectors, showing gene specific target sites. Note that vectors for MGME1 were purchased directly.

Gene	Target site + PAM (5'-3')	Species	Oligonucleotide (5'-3')
MGME1	AGACCATTGTCAGGCAGCTCAGG	human	-
POLG	CCTTTGACCGAGCTCATATCAGG	human	GGAAAGGACGAAACACCGCTTTGACCGAG CTCATATCGTTTTAGAGCTAGAAATAGCAA GTTAAAATAAGG
EXOG	AGTATCGCTTCCCGCCTCCGGGG	human	GGAAAGGACGAAACACCGGTATCGCTTCC CGCCTCCGGTTTTAGAGCTAGAAATAGCA AGTAAAATAAGG
APEX2	GCCCTTTAAGATGTTGCGCGTGG	human	GGAAAGGACGAAACACCGCCCTTTAAGAT GTTGCGCGTTTTAGAGCTAGAAATAGCA AGTAAAATAAGG
CAS9UNIV	-	-	Phos-AACGGACTAGCCTTATTTTAACTTGC TATTTCTAGCTCTAAAAC

Table 11: Oligonucleotides used in generating CRISPR/Cas9-mediated knockins.

Underlined: Changes from wildtype sequences.

Name	Oligonucleotide (5'–3')
POLG	GTCCCTACTGGTGCCAGCAGCCCCACCCAGAGAGACTGGCAGGAGCAGTTAGTGG
HDRF	TGGGGCACAATGTTTCCTTTG <u>CC</u> CGAGCTCATATCAG <u>A</u> GAGCAGTACCTGATCCAG GTAAGGTTCTGGGGCCA <u>ACTGC</u> CGTTCTGGCATGG

Table 12: Primers used for screening CRISPR/Cas9 clones.

Name	Sequence (5'–3')	Annealing temperature (°C)*
CAS9PLF	GAGGGCCTATTTCCCATGAT	-
CAS9PLR	TTATGTAACGCGGAACTCCA	-
MGME1F	GTTCACTTTTTTCTTCCGGCCAC	62.6
MGME1R	CATCAAAGCGAAAGCTGCATCAG	62.6
POLGF	AAATGCCACAGAGACGAAGG	62.6
POLGR	CCACTCCACAACAACCACTG	62.6
EXOGF	ATCATATTCCCATCCATCG	62.0
EXOGR	TCTGACCTTTATTCTCCCGG	62.0
APEX2F	CTGAACAGGAAGCAGTTCGC	65.0
APEX2R	CAAGGGGTGGCAAATCAGGA	65.0
KIR835F	GCGCAAAGCCTCCTCATT	62.5
KIR903R	CCTTCCTGGTTTGGTGGG	62.5
MITOEAGIF	AACATCACCTCTAGCATCACCAG	54.0
MITOEAGIR	ACCCTCGTGGAGCCATTCATA	54.0
MT12602F	TCATCCCTGTAGCATTGTTTCG	55.5
MT12690R	GAAGAACTGATTAATGTTTGGGTCT	55.5
MT14558F	CCCCATAAATAGGAGAAGGCTTA	55.5
MT14695R	GGTTGTAGTCCGTGCGAGAA	55.5
18SRNAF	GTTGGTGGAGCGATTTGTCT	55.0
18SRNAR	GGCCTCACTAAACCATCCAA	55.0

* Temperature is indicated if the oligonucleotide was used for PCR

2.1 Cellular model

MitoEagI cell line was created by Minczuk and colleagues in human HEK 293 T-REx cells. It holds resistances against blasticidin S and hygromycin B and encodes for bacterial restriction endonuclease EagI. EagI was optimized for mammalian codon usage, fused with a mitochondrial targeting sequence of human COX8B at the N-terminus and a hemagglutinin tag at the C-terminus. The construct is expressed under control of a tet-on system, however, even in the uninduced state, cells express a small baseline level of mitoEagI (termed leaky expression). MitoEagI cleaves the mitochondrial genome within the minor arc at a single position (2566/2570), creating 4-nucleotide 5' overhangs.

2.2 Cell culture

MitoEagI cells were stored in liquid nitrogen (-195°C) in cryopreservation tubes. After quick thawing at 37°C , cells were put into tissue culture flasks (75 cm^2) with high-glucose Dulbecco's Modified Eagle Medium (GlutamaxTM DMEM, Gibco) containing 10% foetal calf serum (FCS, PAN Biotech), $50\text{ }\mu\text{g/mL}$ Uridine, 10 U/mL Penicillin, 10 mg/L Streptomycin (Gibco), $15\text{ }\mu\text{g/mL}$ Blastocidin S hydrochloride (Sigma) and $50\text{ }\mu\text{g/mL}$ Hygromycin B (Sigma). Approximately 4 hours later, once cells attached, medium was exchanged to remove DMSO traces from the freezing medium. Culturing conditions were maintained in a humid CO_2 incubator at 37°C with 10% CO_2 levels.

2.3 Subculturing cells

Once cells exceeded 95% confluency, they were split. Old medium was aspirated, and cells washed once with 1xPBS. To detach cells from the culture flask, a $2,5\text{ mg/mL}$ solution of Trypsin was added (2 mL for 75 cm^2 flasks; 4 mL for 175 cm^2) and cells were incubated for up to 5 min at 37°C . To confirm successful trypsinization, cells were checked under a light microscope. Fresh culture medium was added to stop the activity of Trypsin (at least 2x volume of Trypsin). Resuspended cells were collected in a total volume of 10 mL or 12 mL , respectively. Out of this, $50\text{ }\mu\text{L}$ of cell suspension was taken and diluted with $50\text{ }\mu\text{L}$ of Erythrosine B staining solution [0.1% in PBS] for live/dead cell assays.

10 μL of the mix was applied to one counting grid of a Neubauer haemocytometer and examined under a light microscope. 4 squares per counting grid were examined and concentration of cells/mL was calculated using the following formula:

$$\text{Number of cells/mL} = \text{number of counted cells} \times \text{dilution factor} / \text{number of squares} \times 10^4$$

To calculate the total amount of cells in the suspension, the concentration of cells/mL must be multiplied by the total volume of which the sample was originally taken from. Cells were then either transferred to a larger culture flask (175 cm^2) or split in volume to attain desired cell numbers and filled up with fresh culture medium. Afterwards passaging number of the cell line increased by 1.

2.4 Cell pellets

Trypsinized cells were collected in Falcon tubes (10 mL or 50 mL, filled up with 1xPBS). If DNA or proteins were to be isolated from cells, pelleting was performed at 3000 rpm for 5 min. Supernatant was aspirated, pellet resuspended in 1 mL 1xPBS and transferred to an 1,5 mL Eppendorf tube. Tubes were centrifuged for 10 min at 6000 rpm. Supernatant was again aspirated and cell pellets were frozen at -20°C or directly used for DNA isolation or protein purification. Cells for subculture were centrifuged only once, at 1000 rpm for 10 min, with supernatant aspirated and pellet resuspended in fresh culture medium afterwards.

2.5 Cryopreservation of cells

After cells were pelleted for subculturing, supernatant was aspirated and pellets resuspended in ice cold freezing medium (10% DMSO in FCS) to reach concentration of 1×10^6 cells/mL. Afterwards, 750 μL were put into each cryopreservation tube. Tubes were stored at -20°C for 12–24 hours and transferred on ice to -80°C . On the next day, cells were put into liquid nitrogen (-196°C) for long-term storage.

2.6 Mitochondrial genome linearization by mitoEagI

MitoEagI HEK cells were grown either on 6-well plates or in 75 cm² flasks until 90% confluency was reached. Linearization of mtDNA was initiated by the addition of 20 ng/mL doxycycline, a member of the tetracycline class, which induced the expression of mitoEagI. Cell samples were taken for DNA isolation every 2 hours over 18 hours, with additional 24th hour sample.

For prolonged induction experiments, doxycycline was removed after 24 hours and replaced with normal culture medium. Subsequent samples for total DNA isolation were taken after 3, 6 and 10 days.

2.7 Mitochondrial DNA depletion

As described above, mitoEagI HEK cells were grown either on 6-well plates or 75 cm² flasks until 90% confluency was reached. To start mtDNA depletion, 2',3'-dideoxycytidine (ddC) was added to the medium to a final concentration of 400 μM. Total DNA samples were taken each day over 7 days. Medium was changed every second day, also providing fresh ddC (400 μM). On day 2, all remaining samples were split to avoid reaching 100% confluency.

2.8 Isolation of total DNA

Column purification of DNA was performed according to the manufacturers protocol (QIAmp® DNA Mini Kit, QIAGEN). Each sample was eluted twice in 50–150 μL elution buffer provided with the kit and stored at 4°C.

2.9 SgRNA design with synthetic oligonucleotides

Single guide RNAs (SgRNAs) were selected either from studies in a yeast experimental model (*POLG*) or based on online recommendation tools (*EXOG* & *APEX2*) like “CHOPCHOP” (Labun *et al.*, 2016) or “Optimized CRISPR Design” [Zhang Lab, Massachusetts Institute of Technology, 2016-2017]. All oligonucleotides used in the generation of CRISPR/Cas9 plasmids were purchased by Integrated DNA Technologies (IDT). For detailed information see Table 10 and Table 11.

2.10 CRISPR/Cas9 sgRNA plasmid construction

MGME1 knockouts were created using two purchased plasmids from Origene. The first plasmid carried a single gRNA against the MGME1 gene in a CRISPR vector and the second plasmid coded for Cas9. All other sgRNA plasmids were created using the method described by Schmidt et al. (Schmidt *et al.*, 2015).

In short, a BGH-pA-CMV-gRNA-Cas9 vector was linearized by restriction endonuclease digestion (ApaI, SpeI, EcoRV), followed by agarose gel separation with purification of the cleaved product, using QIAquick® Gel Extraction Kit. Next, T4 polymerase chew-back treatment in the presence of dTTP produced long single-stranded overhangs. A short universal reverse-strand oligonucleotide was added to create the template vector mix (CAS9UNIV, AACGGACTAGCCTTATTTTAACTTGCTATTTCTAGCTCTAAAAC, PAGE purified, 5'-phosphorylated, 100 µM, IDT). Gene-specific sgRNA oligonucleotides (desalted, 100 µM, IDT) were annealed using the following conditions: temperature was gradually decreased from 75°C to 60°C over 37.5 min; 60°C for 30 min; 60°C to 25°C over 87.5 min. The annealed vector was transformed into *E. coli* without ligation. The bacterial host generates a completely repaired, circular plasmid which was isolated with the Plasmid Miniprep Kit (Pqlab) and sequenced using CAS9PLF and CAS9PLR primers to confirm the correct sequence of the desired hybrid sgRNA.

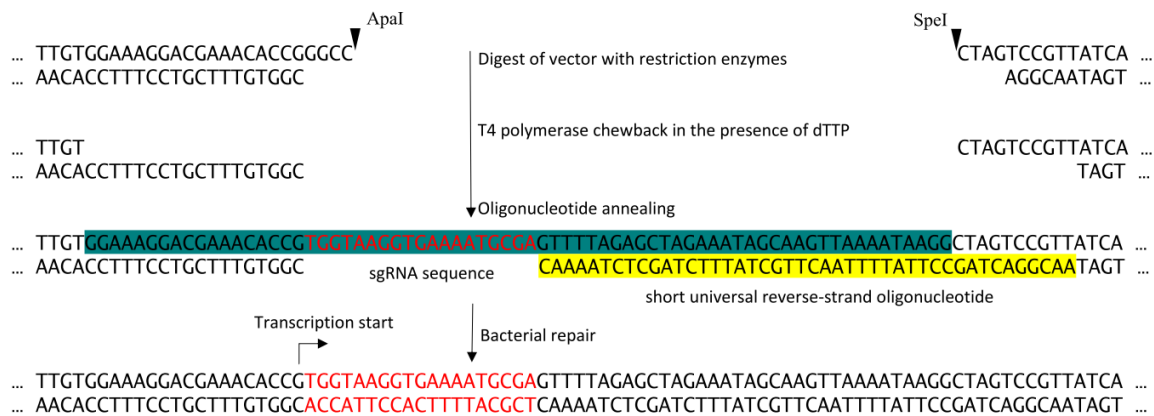


Figure 14: Ligation-independent cloning (LIC) method. Schematic view of LIC-based sgRNA cloning. A plasmid vector is linearized by restriction enzymes ApaI and SpeI. T4 polymerase chewback reaction in the presence of dTTP creates free 5' overhangs. Annealing of short universal reverse-strand and target-specific oligonucleotides leave a 19 bp sequence single-stranded. After transformation in *E. coli*, bacteria repair and amplification the circular plasmid, containing the desired hybrid sgRNA sequence (method and figure adapted from Schmidt *et al.*, 2015).

2.11 CRISPR/Cas9 transfection

MitoEagI HEK 293 T-REx cells were plated at a density of 1×10^4 cells per 96-well, in 100 μ L culture medium. On the next day, cells were transfected with 200 ng of CRISPR/Cas9 plasmids using GeneJuice transfection reagent (Novagen) according to the manufacturers protocol. For creating the POLG knockin, an additional 148 bp single-stranded oligonucleotide (POLG_HDRF) was co-transfected.

This oligo represented the target region of the POLG gene, but carried the desired missense point mutation as well as silent point mutations for disrupting the protospacer adjacent motif (PAM) and a restriction endonuclease site (PstI).

2.12 Single cell cloning

Transfected cells were monitored each day by optical and fluorescence light microscopy for up to 48 hours post transfection. Transfection efficiency was assessed by DsRed quantification, expressed by CRISPR/Cas9 plasmids. Usually, efficiency increased with passing days, however, correlated Cas9 activity is prognosed to last only for up to 48 hours. For single cell cloning, transfection medium was carefully removed and replaced by 100 μ L fresh culture medium, which was used to wash the well in order to detach the cells. Cell suspension was collected in an 1.5 mL Eppendorf tube. Half of its volume (50 μ L) was used for cell counting and diluted only with 50 μ L Erythrosine B staining solution. 5 cells/mL were set as a final concentration for single cell cloning, using 100 μ L final volume per 96-well. If the required volume of cells was below 1 μ L, a predilution was performed. 50 μ L of cell suspension were diluted in 5 mL culture medium (new dilution factor 100). The required volume of cells is then also multiplied by the new dilution factor (x100). 96-well plates were incubated at 37°C with 10% CO₂ for 2 weeks.

2.13 CRISPR/Cas9 clone screening

After 2 weeks incubation from single cell cloning, wells can be analysed under a light microscope and screened for the formation of colonies. Only singular colonies per well were pursued for screening. Medium was carefully removed and replaced by 200 μ L fresh culture medium, which was used to wash and detach cells from the well. 100 μ L were transferred to a new 96-well plate and filled up to 200 μ L for further growth. The other 100 μ L were transferred to a PCR microtube and spun down at 2000 g for 1 min. The cellular pellet was resuspended in 20 μ L lysis buffer (1 mM CaCl₂, 3 mM MgCl₂, 1 mM EDTA, 1% Triton X-100, 10 mM Tris pH 7.5) containing proteinase K (0.2 mg/mL, Qiagen). The reaction was incubated at 65°C for 10 min, followed by heat inactivation at 95°C for 15 min. Lysates were directly used for PCR amplification and subsequent Sanger sequencing. As for knockin clones, PCR amplification products were screened for the loss of the PstI restriction sites, prior screening (digested at 37°C for 1h).

2.14 PCR detection

PCRs performed used the AccuTaq polymerase with 20 ng of total DNA in a 12.5 μ L reaction mix (see conditions below). Primer specific annealing temperatures were optimized before, for each primer pair.

PCR conditions (annealing temperature changed between primer pairs).

95°C 2.5 min

95°C 15s
50–68°C 2 min } 42 cycles

72°C 10 min

Reagent	Volume (μ L)
10x AccuTaq buffer	1.25
dNTPs (2.5 mM)	1.25
PrimerF (50 pmol / μ L)	0.1
PrimerR(50 pmol / μ L)	0.1
Jumpstart AccuTaq	0.125
DNA (20 ng / μ L)	1

2.15 Agarose gel electrophoresis

5 μ L of PCR product was mixed with 5 μ L loading buffer (5x) and loaded on an agarose gel (1–2%). Percentage changed, depending on the expected PCR product size. A 1 kb DNA or 2-log DNA ladder was used as reference for band identification. Voltage and duration were kept constant at 180 V for 60 min. Images were captured with the camera of the UV-illuminator GelDoc™ XR at excitatory wavelengths between 254 and 365 nm.

2.16 Polyacrylamide gel electrophoresis (PAGE)

PCR products smaller than 300 bp were separated on 10% polyacrylamide gels at 30 mA for 40 min.

Reagent	Volume (mL)
H ₂ O	5.4
TBE	2
Acrylamide/Bis, 40%	2.5
APS, 10%	0.1
TEMED	0.01

Afterwards, gels were stained in 35 mL TBE buffer + 5 μ L SYBR Green for 15 min, while shaking. Visualization was exactly as for agarose gel electrophoresis.

2.17 Sanger sequencing

PCR amplification products were purified, using the ExoSAP PCR product cleanup reagent (Thermo Scientific) according to the manufacturer's protocol and subsequently diluted in H₂O. Sanger sequencing of the purified PCR products was performed by a commercial sequencing service (Eurofins).

2.18 Quantitative PCR (Real-time)

Total DNA was diluted 2-fold, starting from 20 ng and was used in triplets per concentration for quantitative real-time PCR. DNA was mixed with a SYBR Green Supermix, from the SYBR Green RT-PCR Kit (BIO-RAD), containing also a primer mix (12.5 pmol) for either the mitochondrial *EagI* gene (MITOEAGIF+R) or the nuclear *Kir* gene (KIR835F+Kir903R).

PCR reactions were performed on an iQ5 qPCR system (BIO-RAD) under the following conditions:

95 °C for 5 min
95 °C for 15 sec } 45 cycles
62,5 °C for 30 sec }

CT values were analysed by SigmaPlot and defined at the inflection points of fitted sigmoidal regression curves (4-parameters Chapman curves, Zhao and Fernald, 2005). The sigmoidal regression curve had four parameters $-y_0$, a , b and c , which determined the shape and degree of the exponential function. The parameters were gained from the software using this formula:

$$y = y_0 + a (1 - e^{-bx})^c$$

The CT value, calculated at the inflection point of the sigmoidal curve were calculated with the following formula:

$$CT = \ln(c) / b$$

Mean and standard deviation was calculated for each sample triplet and per serial dilution. Next, cycle number differences were calculated by subtracting the CT values of the mtDNA fragment (CT_{mito}) from the CT values of the nuclear reference gene (CT_{nuc}). To determine mitochondrial copynumbers (CN_{mt}), the ratio between the diploid single nuclear gene and the mitochondrial sequence was calculated.

2.19 Protein purification

Pelleted cells were resuspended in Lysis buffer (~100 μ L/mio cell) on ice, before sonicated 2 times for 15 s with ultrasonic processor GEX-600 (8% Amplitude), followed by 30 min shaking at 4°C. After centrifugation (20 min, 10.000 g) supernatant (lysate) was taken for analysis and protein concentration measurement (Peterson's modification of the micro-Lowry method).

For SDS-PAGE lysate (15 μ g protein per lane) was diluted in 4xLaemmli buffer. After addition of small amount of β -mercaptoethanol (1 μ L in 20 μ L total volume) lysate/Laemmli solution was heated at 95°C for 5 min.

2.20 Glycine SDS-PAGE

Glycine sodium dodecyl sulfate-polyacrylamide gel electrophoresis (SDS-PAGE) was performed to separate proteins according to their molecular weight. 1x SDS-running-buffer (25 mM Tris, 1.92 M Glycine, 0.1% [w/v] SDS) was used for conducting electrophoresis at 100 V for 30 min, and 130 V for 1–1.5 h.

Reagent	Volume (mL)	
	Resolving gel (10%)	Stacking gel
Acrylamide/bis (30/0.8)	5.7	0.83
1.875 M Tris pH 8.8	3.5	-
0.8 M Tris pH 6.8	-	0.5
10 % [w/v] SDS	0.17	0.05
ddH ₂ O	7.5	3.55
10 % [w/v] APS	0.1	0.05
TEMED	0.01	0.01

2.21 Western blot

Proteins separated by SDS-Page were transferred to a polyvinylidene fluoride (PVDF) membrane using semi-dry Western blot technique. PVDF membranes were activated in 70% ethanol for 5 min and washed in blotting buffer (20 mM Tris, 150 mM glycine, 0.02% SDS). Filter papers were soaked in blotting buffer and put above and below gel with PVDF membrane. Blotting was performed at max. 100 mA for 1.5 h (while not exceeding 25 V). Membranes were stained with

Coomassie Brilliant Blue R-250 Staining Solution (BIO-RAD) followed by destaining solution (30% methanol, 10% acetic acid) for visualization of total proteins. For complete destaining, the membranes were treated with methanol. After washing in water 3 times in PBST solution (PBS, 0.1% Tween 20), the blocking (5% dry milk in PBS) was performed for 1h. After washing twice in PBS and then in PBST, primary antibodies were diluted in PBST containing 2% dry milk and used for O/N incubation at 4 °C. On the next day, membranes were washed three times in PBST, containing 1% Triton X-100, followed by incubation with anti-rabbit antibody coupled to horseradish peroxidase (1:20.000, diluted in PBST containing 2% dry milk) 1 h at room temperature. After washing three times in PBST and once in PBS, the membranes were treated with SuperSignal West Pico Chemiluminescent Substrate (Thermo Scientific) according to the manufacturer manual. Detection of western blot signals was recorded on a ChemiDoc Imaging System (Bio-Rad) at different exposure times (10–60 s).

2.22 Nucleic acid quantitation

Concentration of isolated total DNA was calculated by measuring optical density (OD) with spectrophotometer. Absorption of ultraviolet light shows maximum for double-stranded DNA at wavelength $\lambda = 260$ nm, for proteins at $\lambda = 280$ nm. DNA concentration (C) in ng/ μ L is calculated by the following formula:

$$C = [-36.0(\text{OD } 280\text{nm} - \text{OD } 320\text{nm}) + 62.9(\text{OD } 260\text{nm} - \text{OD } 320\text{nm})] \times \text{dilution factor}$$

Multiplying DNA concentration C by the purified sample volume (mL) gives the total yield of isolated DNA (μ g). Purity of DNA is provided by the OD ratio of 260nm/280nm.

DNA ratios between 1.8 and 2 were considered of suitable quality. DNA impurities can be detected at $\lambda = 320$ nm, OD 320nm, using the following formula:

$$\text{DNA purity} = (\text{OD } 260 \text{ nm} - \text{OD } 320 \text{ nm}) / (\text{OD } 280 \text{ nm} - \text{OD } 320 \text{ nm}).$$

2.23 DNA quantitation using PicoGreen®

1 μ L DNA sample was diluted in 180 μ L of TBE. Lambda calibration curve was established through a 5x serial dilution in 180 μ L TBE. DNA and Lambda samples were mixed with 180 μ L of PicoGreen + 1x TBE (1:200). Emission range was set between 500–600 nm, with expected peak of emission at 520 nm. Each sample was read in a Lambda-2 Spectrophotometer with a quartz cuvette against a TE blank plus calibration curve.

2.24 Southern blot

1 μ g of total DNA was digested for 2 hours at 37°C with 1 μ L BamHI (restriction endonuclease, 20.000 U/mL, New England Biolabs), loaded on an 0.6% agarose gel and separated over night at 40 V, using the 1 kb extended DNA ladder (New England Biolabs) and DIG-labeled DNA Molecular Weight Marker II or III (Roche). On the next day, gels were treated with 250 mM HCl for 30 min, rinsed with ddH₂O and washed twice with denaturation buffer for 20 min each, rinsed again with ddH₂O and washed twice with neutralization buffer for 20 min each, before blotted to Zeta-Probe membranes (Bio-Rad) in 2xSSC buffer overnight. On the next day, membranes were washed in 1xSSC buffer to remove agarose traces. Afterwards, DNA was immobilized on membranes by baking at 80°C for 30 min. Blots were put into hybridization tubes (DNA facing inward and upwards) and tubes put into rotating oven. Pre-hybridization of membranes was performed for 3 hours in DIG Easy Hyb buffer (Sigma) at 48°C. Two different PCR-generated digoxigenin-labelled mtDNA probes (PCR DIG Probe Synthesis Kit, Roche) were used, located on either of the BamHI cutting site (1st probe at region 12602–12690; 2nd probe at region 14588–14695). A nuclear ribosomal DNA (18S) probe served as quantification reference. 20 ng/mL DIG-probe was hybridized per blot in hybridization buffer overnight, at 48°C. On the next day, washing and blocking steps were performed according to the manufacturers protocol (Roche), using anti-DIG-AP antibody F_{ab} fragments (Roche). For chemiluminescent detection, blots were treated with CSPD (Roche) and incubated 10 min at room temperature followed by 15 min at 37°C. Signal was recorded on a ChemiDoc Imaging System (Bio-Rad) at different exposure times (50–300 s).

To remove DIG-probes, blots were treated twice with stripping buffer at 37°C (0.2 M NaOH + 0.1% SDS), for 15 min each, followed by a quick rinse in 2xSSC, before continuing pre-hybridization for 3 hrs and probe hybridization over night at 48°C.

2.25 Southern blot quantification

Semiquantitative analysis on southern blot fragments was performed using the image processing program ImageJ. The region of interest (ROI) was marked per fragment and analysed by the program for area (A) and mean signal intensity (MSI), on a 255-bit image. A background triplet was also marked per lane, to calculate a background mean (BG), which was subtracted from its corresponding lanes ROI.

To determine the signal intensity, the following formula was used:

$$\text{signal} = (\text{MSI}_{\text{ROI}} - \text{MSI}_{\text{BG}}) * A_{\text{ROI}}$$

To quantify degrees of mtDNA degradation, a ratio was formed between the mitochondrial signal ($\text{signal}_{\text{mito}}$) and its 18s ribosomal DNA signal ($\text{signal}_{18\text{s}}$), to calculate a normalized signal ($\text{signal}_{\text{norm}}$) for each lane. For relative quantification, 0 h values were used as reference value (1) against each individual $\text{signal}_{\text{norm}}$.

3. Results

3.1. Effects of mitochondrial nuclease activity on linear mtDNA

Exonuclease activity of mitochondrial nucleases is most often described in the context of flap intermediate processing and proofreading during mtDNA replication as well as in mtDNA repair (Copeland *et al.*, 2008) while mtDNA degradation is still hypothesized to be performed by an uncharacterized pathway and not by known mitochondrial nucleases (Moretton *et al.*, 2017). To address these questions, if and how mitochondrial nucleases are involved in the degradation of linear mtDNA, the CRISPR/Cas9-system was used to alter the genes of known mitochondrially-targeted exonucleases in the mitoEagI HEK 293 cell line.

3.1.1 Monitoring degradation of linearized mtDNA in human cells

The modified HEK 293 T-REx cell line, expressing the mitochondria-targeted restriction endonuclease EagI under the control of a tet-on system was used in this study (created by Dr. M. Minczuk and colleges). Upon induction with doxycycline, mitoEagI cleaved the mitochondrial genome at a single position within the minor arc (position 2566/2570), creating a double-strand break with 5'-overhangs. These overhangs serve as starting points for mitochondrial exonucleases, which will degrade the now linearized mtDNA over time, resulting in a steady decrease of mitochondrial copy numbers. This makes the mitoEagI HEK cell line a useful tool for studying kinetics of linear mtDNA degradation. It is noteworthy, that even in the absence of doxycycline, there is a small baseline expression of the mitoEagI protein (termed leaky expression) which cuts mtDNA.

Linearized mtDNA was monitored over the first twenty-four hours, with samples taken each second hour. Total DNA was used for RT-PCR with primers spanning the mitoEagI cutting site, inside the mitochondrial genome (Figure 15). Data showed, about 80 % of mtDNA was linearized four hours after mitoEagI induction. The remaining proportion of circular mtDNA continued to decrease over the time-course and reached below 5 % after twenty-four hours.

This confirmed the nuclease activity of mitoEagI, which lead to the successful cleavage and linearization of circular mtDNA followed by its subsequent degradation.

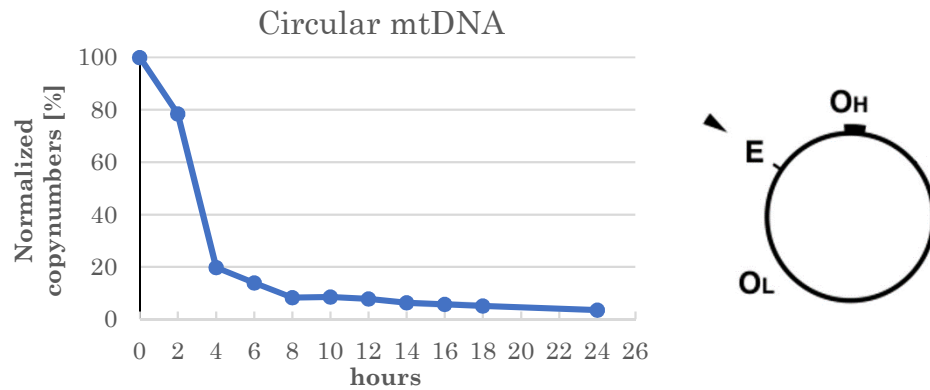


Figure 15: Inducible mitoEagI model for linearizing mtDNA. Time curve showing mitoEagI restriction efficiency over time in induced mitoEagI HEK cells, through RT-PCR kinetics, spanning the cutting site (E), over the first 24 h. Copy numbers were normalized to zero-hour data.

3.2 Generation of CRISPR/Cas9-edited knockout and knockin cell lines, with targeted mitochondrial exonucleases

Having the mitoEagI model established to linearize mtDNA, now the mitochondrial nucleases had to be investigated separately in their effect on linear mtDNA degradation. Genome editing was performed on the following members with known mitochondrial nuclease function: MGME1, POLG, EXOG and APEX2. Using the CRISPR/Cas9 system on mitoEagI expressing HEK 293 T-REx cells, knockouts (ko) were created for MGME1, EXOG and APEX2, respectively (Figure 16). Only clones with homozygous frameshift indels (insertions or deletions) were used for subsequent experiments. A complete knockout of polymerase γ would result in the loss of mtDNA over time, since mtDNA replication can no longer be performed and was therefore not applicable with the intention to analyse linear mtDNA degradation in this work.

Hence, the p.D274A point mutation was introduced in the POLG gene, which had been reported to selectively silence the 3'–5' exonuclease activity of POLG in yeast and mouse (Vanderstraeten *et al.*, 1998; Trifunovic *et al.*, 2004). Two additional silent mutations were introduced as well, one to alter the gRNAs PAM site, preventing Cas9 from further endonuclease activity and one to remove a PstI restriction site, allowing for easier screening later on.

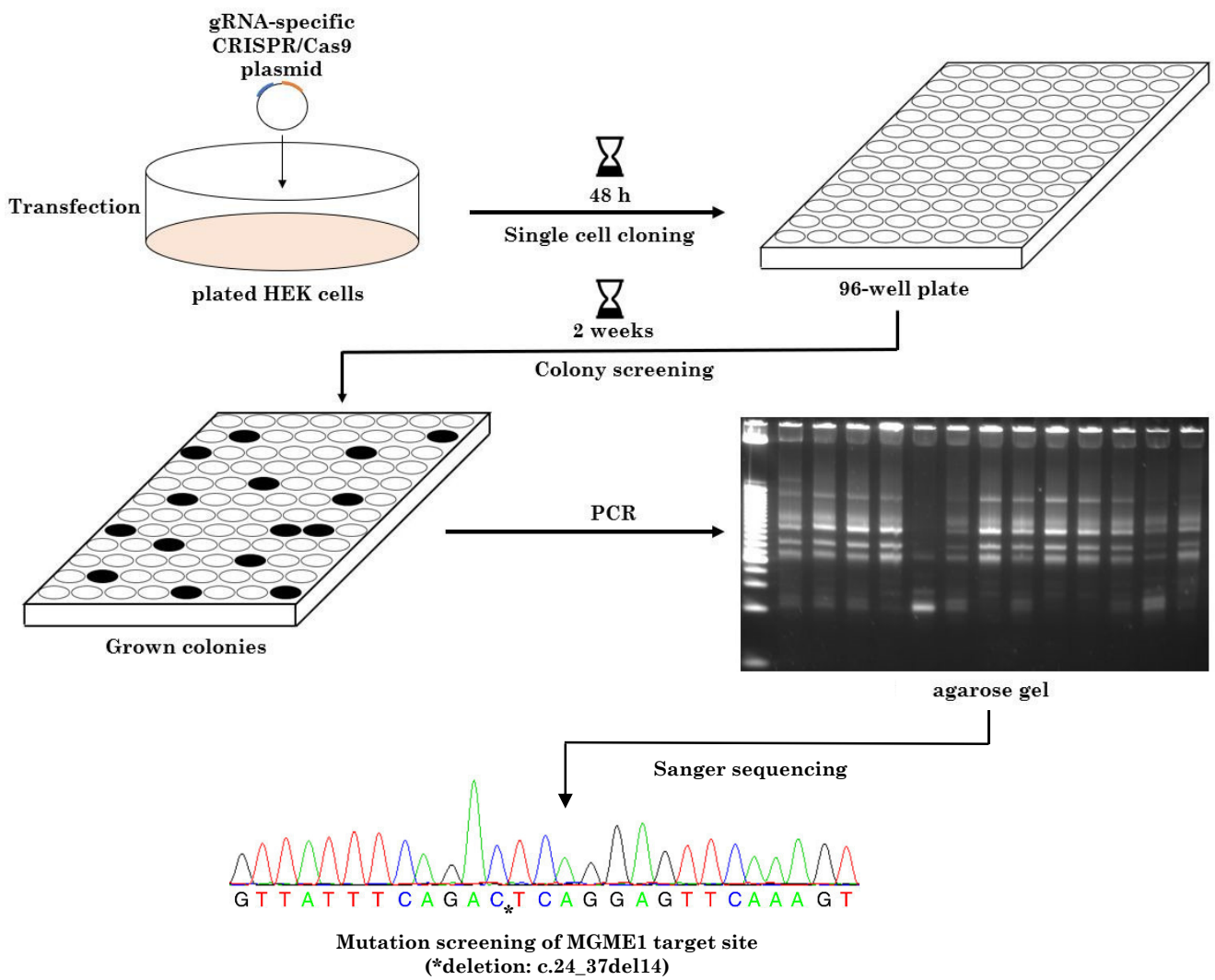


Figure 16: Schematic process of the generation of CRISPR/Cas9-edited HEK cell lines. Transfection with CRISPR/Cas9-plasmids, bearing an additional gene-specific target sequence (gRNA) was performed on HEK cells. After single cell cloning on 96-well plates with subsequent incubation time, DNA samples were taken from grown colonies for PCR amplification of the targeted gene. Following agarose gel screening, prominent indels were sent for Sanger sequencing for genotyping.

Detailed cloning information per targeted gene can be taken from Table 13 below.

Table 13: Cloning statistics per CRISPR/Cas9-targeted gene in HEK cells. Total number of individual mitoEagI HEK colonies listed against the number of screened clones with a successful knockout / knockin and the corresponding CRISPR/Cas9-editing efficiency.

Gene target	Total number of colonies	Number of successful knockouts / knockins	Efficiency %
MGME1	288	2	0,7
POLG	460	1	0,2
EXOG	18	2	11
MGME1 + EXOG	19	2	10,5
APEX2	34	2	6

One of the greater challenges in creating CRISPR/Cas9-edited HEK cell lines with altered mitochondrial nucleases was establishing a streamlined work-pipeline, which allowed for a high throughput of culture plates (and clones) with a reliable, but fast screening technique. Differences between the commercially acquired vector against MGME1 and the custom generated BGH-pA-CMV-gRNA-Cas9 vector (used for all other targeted genes) were not investigated. For the double-knockout of MGME1+EXOG, the MGME1 knockout cell line was used, in which EXOG was targeted second. The POLG p.D274A point mutation showed a very low efficiency, which was expected, because homologous recombination with the co-transfected oligonucleotide template was much less likely to occur than NHEJ (Mao *et al.*, 2008). Except for POLG, all other clones were directly screened for indels by Sanger sequencing. POLG clones were digested by PstI prior sequencing and only undigested PCR bands, bearing the mutated knockin represented clones of interest.

Results

The screening results (Figure 17) presented two knockout clones for *MGME1*, both having frameshift deletions (14 bp and 8 bp, respectively), one *POLG* knockin with the desired p.D274A point mutation, one knockout clone for *EXO* (T duplication) and one knockout clone for *APEX2* (C duplication). Two double-knockout clones for *MGME1* + *EXO* were created as well (data not shown). The *POLG* knockin clone first appeared to be a polyclonal mixture. Therefore, a second round of single cell cloning was performed from that clone, producing 30 sub-clones in total, with 6 bearing the homozygous, monoclonal knockin.

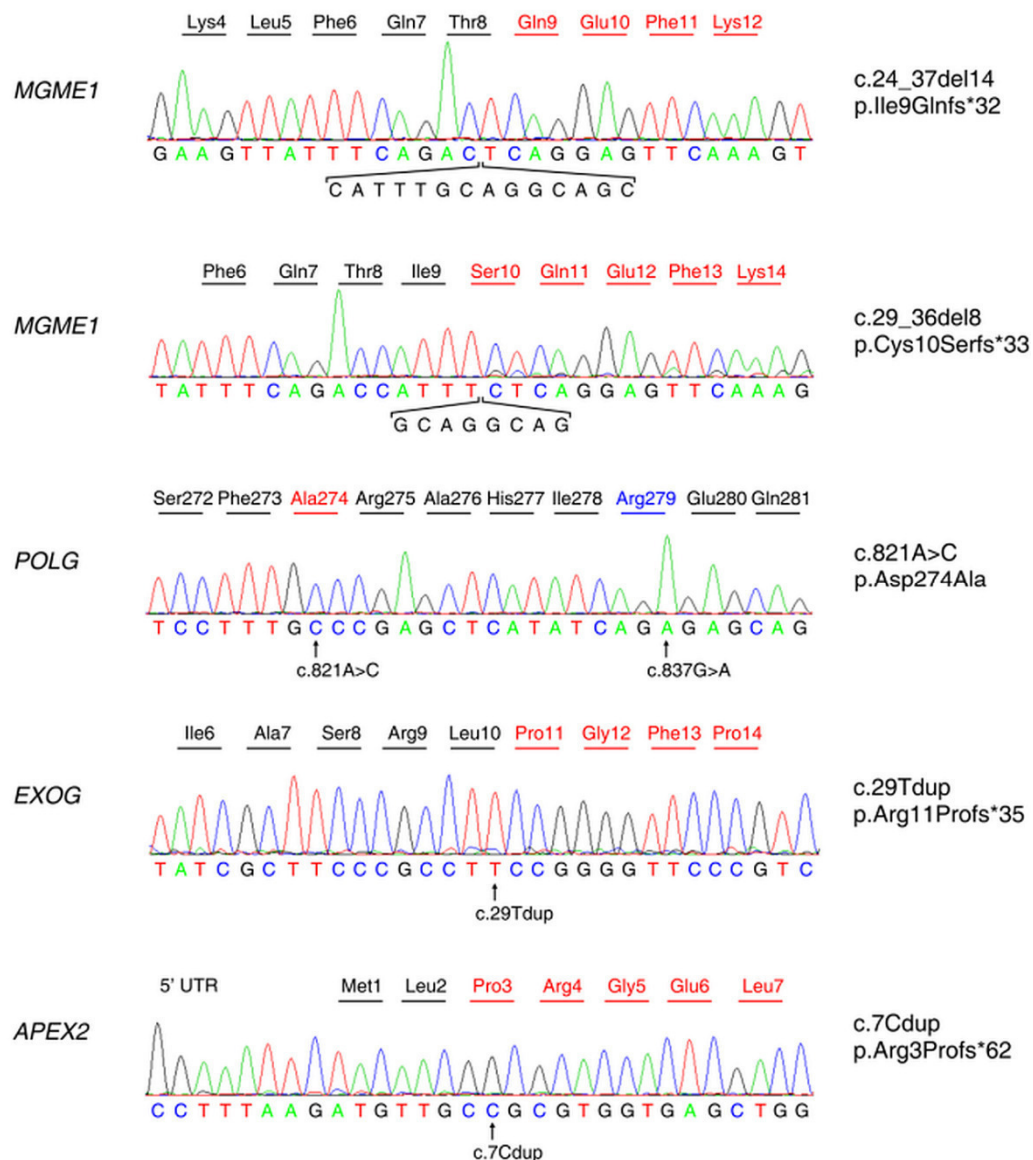


Figure 17: CRISPR/Cas9-edited genes in mitoEagI HEK cells. Sanger sequencing data showing knockouts for *MGME1*, *EXO* and *APEX2* as well as p.D274A knockin of *POLG* in mitoEagI expressing HEK cells. Corresponding amino acids are shown on top of each sequence (black colour: wild type sequence; red colour: mutated sequence), indels or point mutations are shown below the sequences (figure adapted from Peeva and Blei *et al.*, 2018).

Results

The mutator cell lines had to be examined for their expression of the mitoEagI protein, which was crucial in order to study linear mtDNA degradation. Through Western blotting, the hemagglutinin epitope of the restriction endonuclease was targeted in an uninduced (zero hour) and induced (twenty-four hour) state (Figure 18).

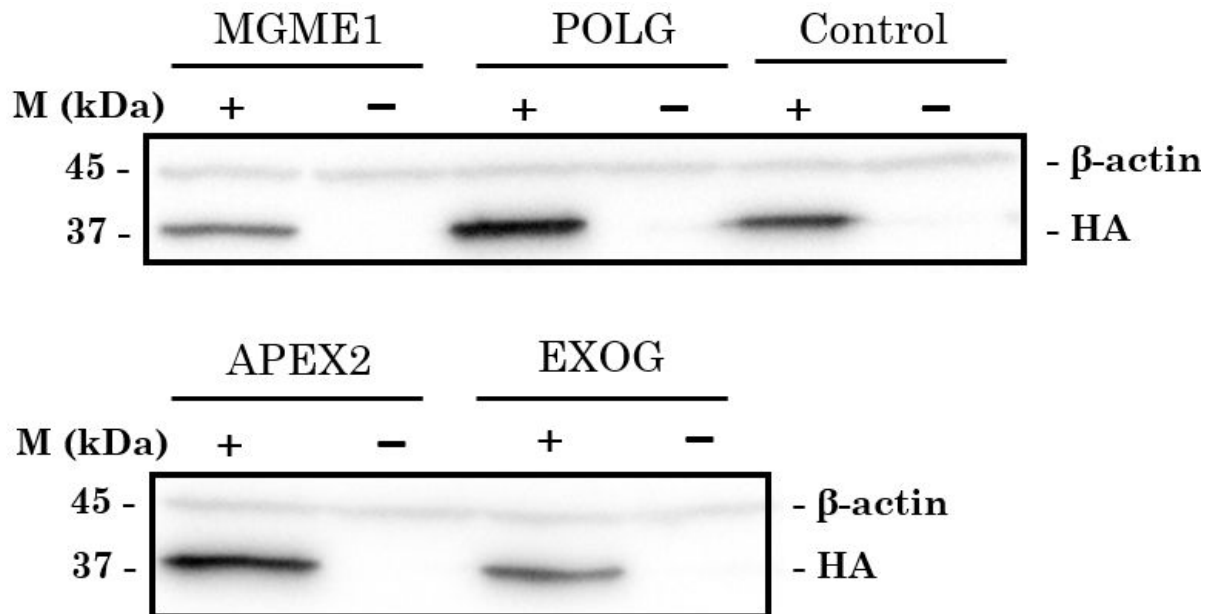


Figure 18: Western blot analysis of mitoEagI protein expression in CRISPR/Cas9-modified mitoEagI HEK cells. Whole cell protein extracts were used for mitoEagI protein detection, through targeting the hemagglutinin epitope (HA). Blot shows samples of the induced (+) and uninduced (-) state from MGME1, POLG, control, APEX2 and EXOG clones. β -actin was used as reference control.

The comparison between uninduced state at zero hour and induced state after twenty-four hours showed a strong signal for mitoEagI in all induced cell lines. The control itself was a non-mutated wild-type single-cell clone, originating from CRISPR/Cas9 editing to check whether off-target effects from Cas9 would influence the doxycycline induction.

This showed, that mitoEagI was stably expressed upon induction and that this induced expression did not decay over the chosen time frame of twenty-four hours, used for the experiments performed in this work. Notably, the previously mentioned leaky expression of mitoEagI in the uninduced state was not strong enough to create a signal, which could be detected by Western blotting.

Results

After mitoEagI protein expression was confirmed in HEK clones, endonuclease activity of mitoEagI on circular mtDNA was analysed six hours after induction (Figure 19). Induction efficiency of mitoEagI on mtDNA was checked, as before, with RT-PCR spanning the cutting site in all clones.

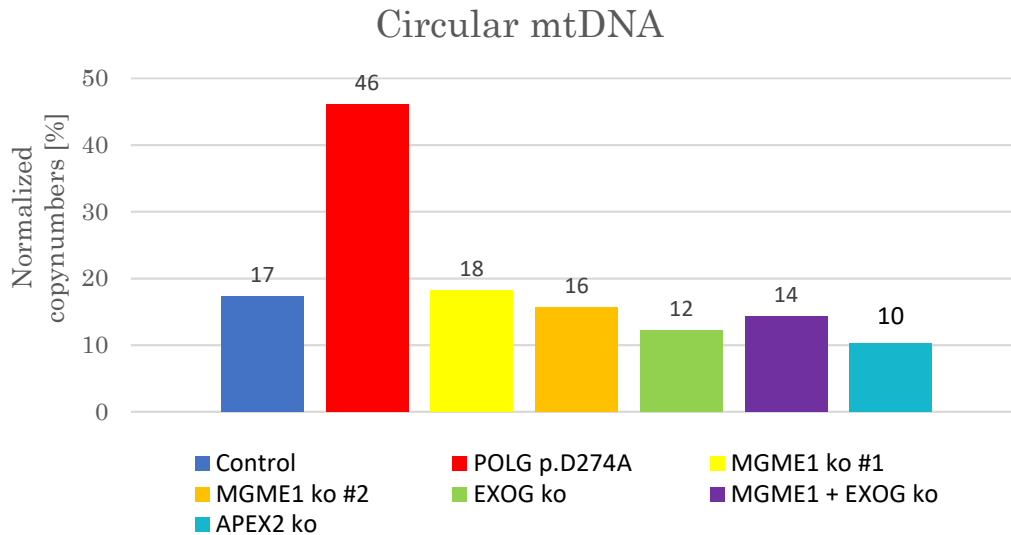


Figure 19: Induced mitoEagI endonuclease activity on circular mtDNA in CRISPR/Cas9-edited HEK cells. The bar graph shows the amount (%) of remaining circular mtDNA 6 h after mitoEagI induction, per HEK cell line. The data were normalized to their respective 0 h value.

The control showed no significant difference in mitoEagI cutting efficiency six hours after induction, compared to previous results (Figure 15). As mentioned before, the control originated from CRISPR/Cas9-treated single-cell clones, failing to show genome-editing effects for the targeted gene. Knockout clones (MGME1, EXOG, MGME1 + EXOG, APEX2) also showed similar cutting efficiency as control (10-22 % of remaining circular mtDNA). POLG knockin clone still had 46 % of circular mtDNA remaining, six hours after induction, which can be explained by the high passage number, resulting from the required second single cell dilution. Additionally, at later timepoints (8 h and more) this clone showed similar, comparable numbers of cleaved circular mtDNA (data not shown).

Together, this data showed that CRISPR/Cas9-edited mitoEagI HEK cells were still able to inducibly express the mitoEagI protein and that its endonuclease activity was comparable in its cutting efficiency to controls. Only the POLG clone showing lower cutting efficiency than the other clones, but it was still

enough to address the question of interest, namely whether or not POLG is involved in the degradation of linear mtDNA. Testing for the expression of the mitoEagI protein and its cutting efficiency on circular mtDNA also showed, that CRISPR/Cas9-editing did not alter the ability of mitoEagI to linearize circular mtDNA.

3.3 Effects of mitochondrial exonuclease activity on linear mtDNA in induced CRISPR/Cas9-modified human cells

MitoEagI HEK cell lines with altered genes of mitochondrial nucleases were examined together with controls for effects on degradation of linear mtDNA.

Control showed, through Southern blotting of total DNA (Figure 20 a), full-length mtDNA at zero hour (uninduced state). Leaky expression was not detectable via Southern blotting, probably due to the fast degradation of the linearized molecules. After induction, full-length fragment was still present after two hours, but with decreased band intensity (Figure 20 b) and Southern blot showed the additional formation of a smaller-sized fragment. Rapid degradation of the full-length fragment was observed after that time point, reaching 75–90 % of mtDNA being cleaved and linearized. At two hours, the fragment with ends originating from the original mitoEagI cutting site was detectable (Figure 20 c). After four hours, this fragment turned into a mixture of smaller-sized mtDNA fragments, with prominent bands ranging from a few hundred to up to several thousand base pairs downstream the mitoEagI cutting site. Another prominent band in this mix corresponded to a fragment spanning from oriL to mitoBamHI cutting site, which started showing signs of decay at eighteen hours. In summary, induction of the mitoEagI protein in control showed rapid linearization of circular mtDNA as well as strong degradation effects of linear mtDNA, performed by mitochondrial exonucleases starting from free ends.

3.3.1 Rapid degradation of linear mtDNA fragments is absent in *POLG* knockin and *MGME1* knockout during the first 24 hours

Southern blotting of total DNA showed for *POLG* p.D274A clone a clearly visible full-length fragment at zero hour, too. Linearization of full-length mtDNA was slightly delayed, when compared to control (Figure 20 b), but reached comparable levels at later time points. The mitoEagI fragment showed increased intensity over time and almost no signs of degradation (loss of signal), over the first eighteen hours (Figure 20 c). Also the smaller-sized mix, formed due to degradation from the ends, was not detectable in *POLG* p.D274A clone. Notably, degradation of the bands, produced by mitoEagIs leaky expression resulted in the formation of some smaller sized fragments as well, including the mitoEagI and oriL bands.

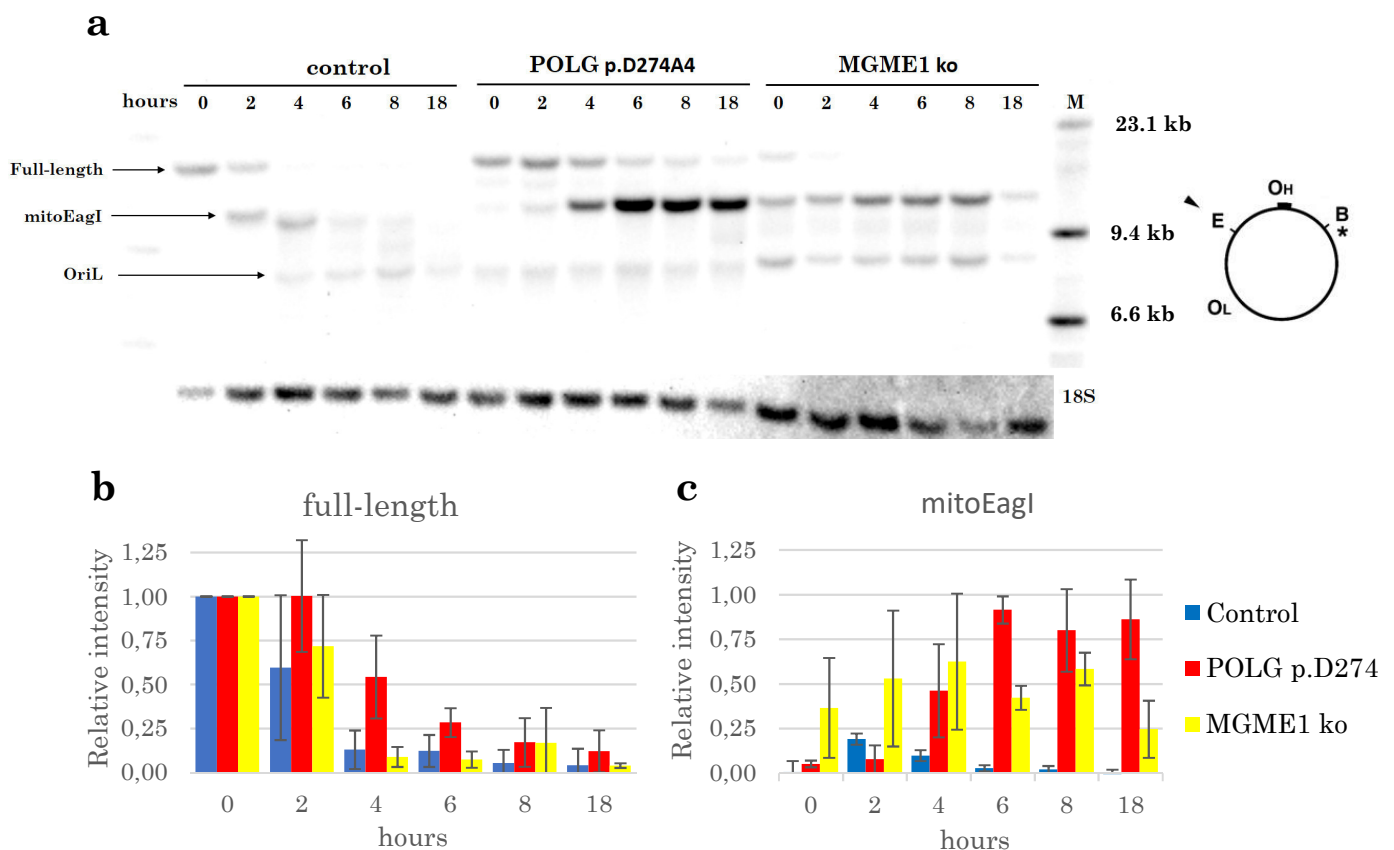


Figure 20: Degradation of the linearized mtDNA fragment in control, *POLG*- and *MGME1*-mutant mitoEagI expressing HEK cells, showing the large digested fragment. **a)** Southern blot showing degradation of the large linear mtDNA fragment, spanning from mitoEagI cutting site (E) till BamHI cutting site (B) in control, *POLG* p.D274A and *MGME1* ko cells within the first 18 hours of induced mitoEagI expression. BamHI endonuclease was used to linearize circular, full-length mtDNA. Position of probe 1 is indicated by a black asterisk (*) on the simplified mitochondrial genome (right), close to the BamHI cutting site. Note that the most prominent bands in control hour 4–8 are slightly smaller than the non-degraded linearized

Results

mitoEagI fragment visible at 2 h. Southern blot quantification of **b**) full-length fragment shows efficient linearization of mtDNA and **c**) persistency of the mitoEagI fragment in POLG and MGME1 mutant cells. Relative intensity was calculated with a probe against a nuclear ribosomal DNA (18S). Existing mitoEagI and oriL bands in POLG and MGME1 mutator cells at zero hour formed due to leaky expression of mitoEagI. Data represents the mean of three independent experiments. Error bars indicate the standard error of the mean (SEM).

MGME1 knockout cells also showed a clear full-length fragment at zero hour and a comparable degradation of this fragment over time in comparison to control. An additional oriL fragment was detectable at zero and two hours (Figure 20 a). The mitoEagI fragment persisted in MGME1 ko clone as well, but appeared with sharper bands compared to the POLG knockin. The persistence of the mitoEagI fragment in MGME1 ko over the first eight hours was also similar to POLG clones (Figure 20 b) and indicated the absence of rapid degradation of linear mtDNA in this clone. Only after eighteen hours, the mitoEagI fragment started to lose intensity.

Using the small fragment probe (⊗) allowed for the evaluation of the smaller mtDNA fragment produced by mitoEagI and BamHI cutting (Figure 21 a). Linearization of full-length mtDNA showed a comparable pattern as with probe 1 in all clones (Figure 21 b). The mitoEagI fragment in control showed again rapid signs of degradation—after four hours it was very weak, but still detectable (Figure 21 c) and its smaller fragments were completely degraded after eight hours. The persistence of the mitoEagI fragment in MGME1 ko was slightly higher than in POLG p.D274A and also showed sharper bands for MGME1 ko, which could indicate partial degradation for POLG might start sooner than in MGME1 ko. Leaky expression of mitoEagI at zero hour was visible in MGME1 ko cells.

Results

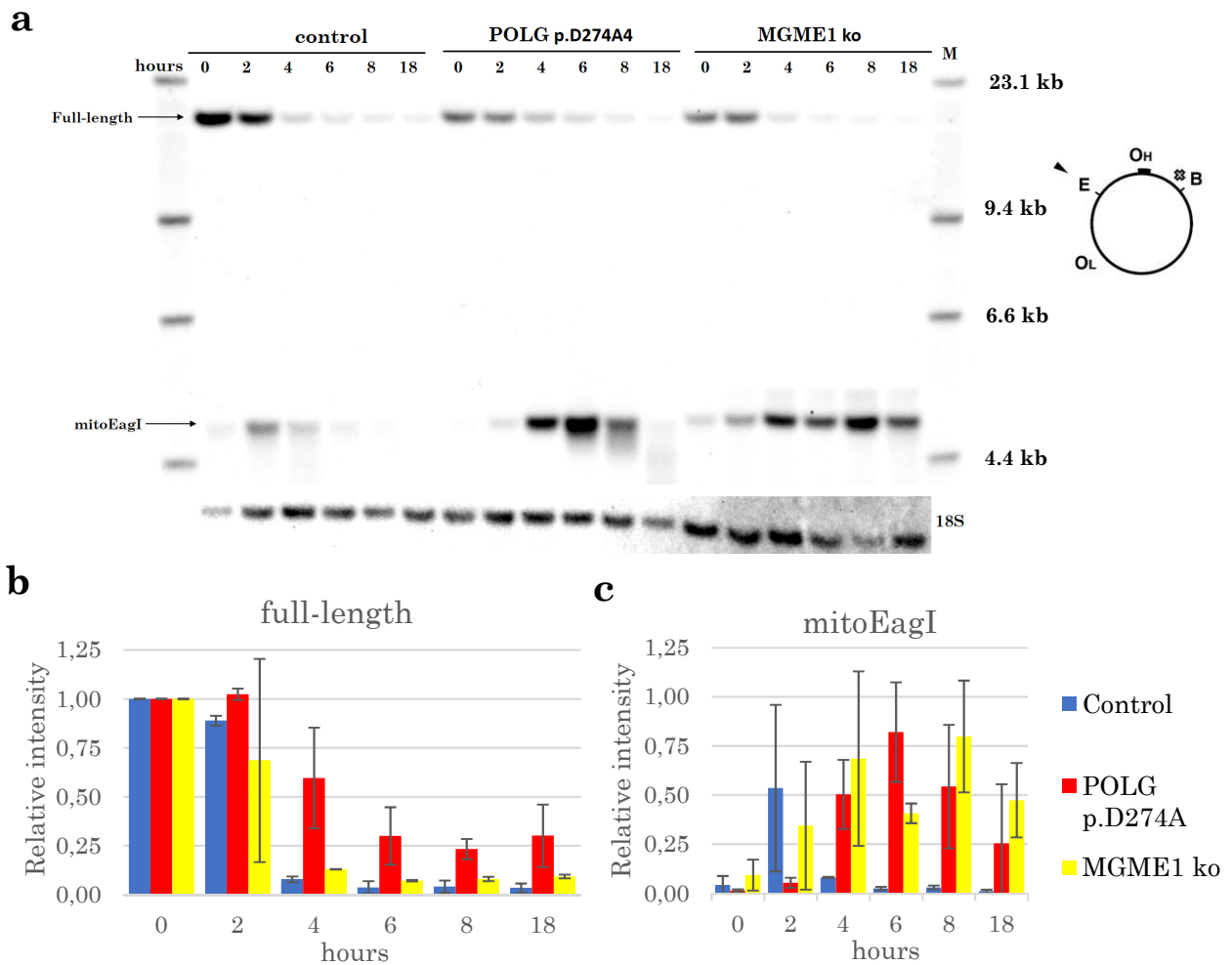


Figure 21: Degradation of the linearized mtDNA fragment in control, POLG- and MGME1-mutant mitoEagI expressing HEK cells, showing the small digested fragment. **a)** Southern blot showing degradation of the small mtDNA fragment, produced by mitoEagI (E) and BamHI (B) endonuclease activity in control, POLG p.D274A and MGME1 ko cells within the first 18 hours of induced mitoEagI expression. BamHI endonuclease was used to linearize circular, full-length mtDNA. Position of probe 2 is indicated by a white X on the simplified mitochondrial genome (right), close to the BamHI cutting site. Southern blot quantification of **b)** full-length fragment shows efficient linearization of mtDNA and **c)** persistency of the mitoEagI fragment in POLG and MGME1 mutant cells. Relative intensity was calculated with a probe against a nuclear ribosomal DNA (18S). Existing mitoEagI and oriL bands in POLG and MGME1 mutator cells at zero hour formed due to leaky expression of mitoEagI. Data represents the mean of two independent experiments. Error bars indicate the standard error of the mean (SEM).

Overall, both probes detected a successful linearization of circular mtDNA by mitoEagI in control and mutated HEK cells. Even though the POLG p.D274A clone showed the lowest cutting efficiency of mitoEagI, it was still enough to produce strong signals for the mitoEagI fragment, which was required to study degradation of linear mtDNA. Both clones showed persistence of the mitoEagI fragment during the first eight hours, compared to the control. Interestingly, mitoEagI bands on Southern blot appeared sharper for MGME1 ko and slightly lower and blurred or POLG knockin, indicating at least partial degradation.

Also, the detectable mitoEagI ends of the large mtDNA fragment showed higher persistence in the POLG clone, after six hours of induction (Figure 20c), compared to the MGME ko clone. When comparing mitoEagI ends in the small mtDNA fragment, their persistence was higher in MGME1 ko clone, which remained over eighteen hours. POLG knockin clone showed strong persistence only until six hours past induction for the smaller fragment with decreasing intensity at eight hours and beyond, with only a mixture of smaller sized fragment remaining after eighteen hours. Leaky expression (zero-hour intensity) of mitoEagI bands was higher in MGME1 clone, which would explain differences to POLG at early hours after induction.

Results

(18S). Data represents the mean of two independent experiments. Error bars indicate the standard error of the mean (SEM).

Two hours after induction, the DNA fragment belonging to the original mitoEagI cutting site was formed in EXOG^{-/-} and APEX2^{-/-} cells, but got rapidly degraded into a composition of complex smaller-sized fragments (Figure 22 a, c). Leaky expression and lack of degradation seemed to be not as prominent as in the other mutant cell lines and resembled more the control, too.

Visualizing the small mtDNA fragment between mitoEagI and BamHI cutting sites (Figure 23 a), using probe 2 revealed similar linearization patterns on full-length fragments during the first eighteen hours (Figure 23 b). Detection of the mitoEagI fragment showed a strong signal at two hours, with weak, but still detectable bands at later time points (Figure 23 c).

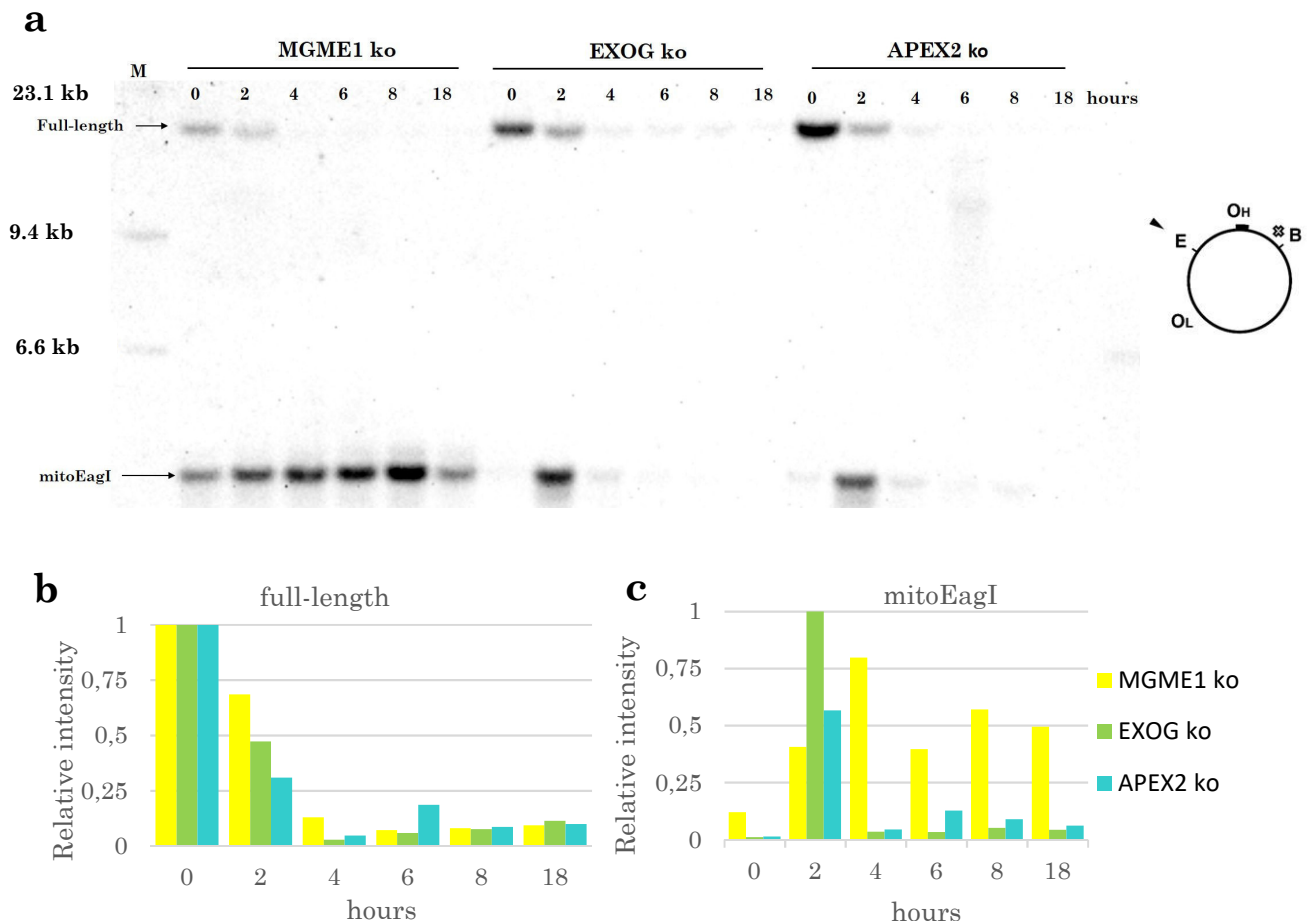


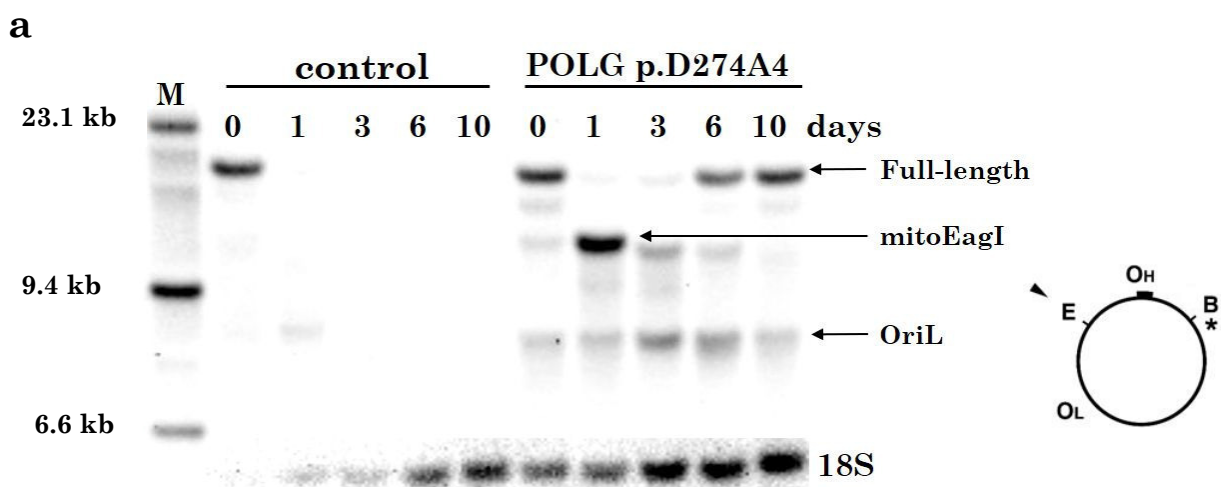
Figure 23: Degradation of the linearized mtDNA fragment in MGME1-, EXOG- and APEX2-knockout mitoEagI expressing HEK 293 cell lines, showing the small digested fragment. a) Southern blot, showing degradation of the small mtDNA fragment between mitoEagI (E) and BamHI (B) cutting site, within the first eighteen hours after mitoEagI induction. Total DNA was treated with BamHI endonuclease to linearize circular, full-length mtDNA. Position of prob 2 is indicated by a white X on the simplified mitochondrial genome (right), close to the BamHI cutting site. Quantification shows degradation of b) full-length and c) mitoEagI fragment during the first 18 hours, after induction, with no persistency of the

mitoEagI fragment. Relative intensity was calculated with a probe against a nuclear ribosomal DNA (18S).

3.3.3 Long term effects of linear mtDNA degradation in mitochondrial nuclease-deficient mitoEagI HEK clones

Following the investigation of linear mtDNA degradation in mitochondrial nuclease-deficient mitoEagI HEK cell lines, degradation effects after prolonged mitoEagI induction were studied. For this purpose, doxycycline was removed from the medium after twenty-four hours, with clones being monitored over ten days total. Total DNA was again treated with BamHI to linearize circular mtDNA and visualized by Southern blotting (Figure 24 a-c).

Circular mtDNA was again almost completely linearized by mitoEagI after twenty-four hours of induction in all clones (Figure 24 d). Presence of the mitoEagI fragment was detectable between zero hour (due to leaky expression of mitoEagI) and one day after induction in POLG p.D274A, MGME1 ko and MGME1 + EXOG double ko cells (Figure 24 e). POLG knockin showed on day three a slightly smaller-sized mitoEagI fragment, with an additional mix of smaller fragments below. This mixture was previously detectable in control, EXOG ko and APEX2 ko cells, but after a much shorter time point (four hours after doxycycline induction). Interestingly, while the full-length fragment seemed to recover in POLG knockin starting at day six (Figure 24 a, d), the mitoEagI fragment got further degraded and reduced in size.



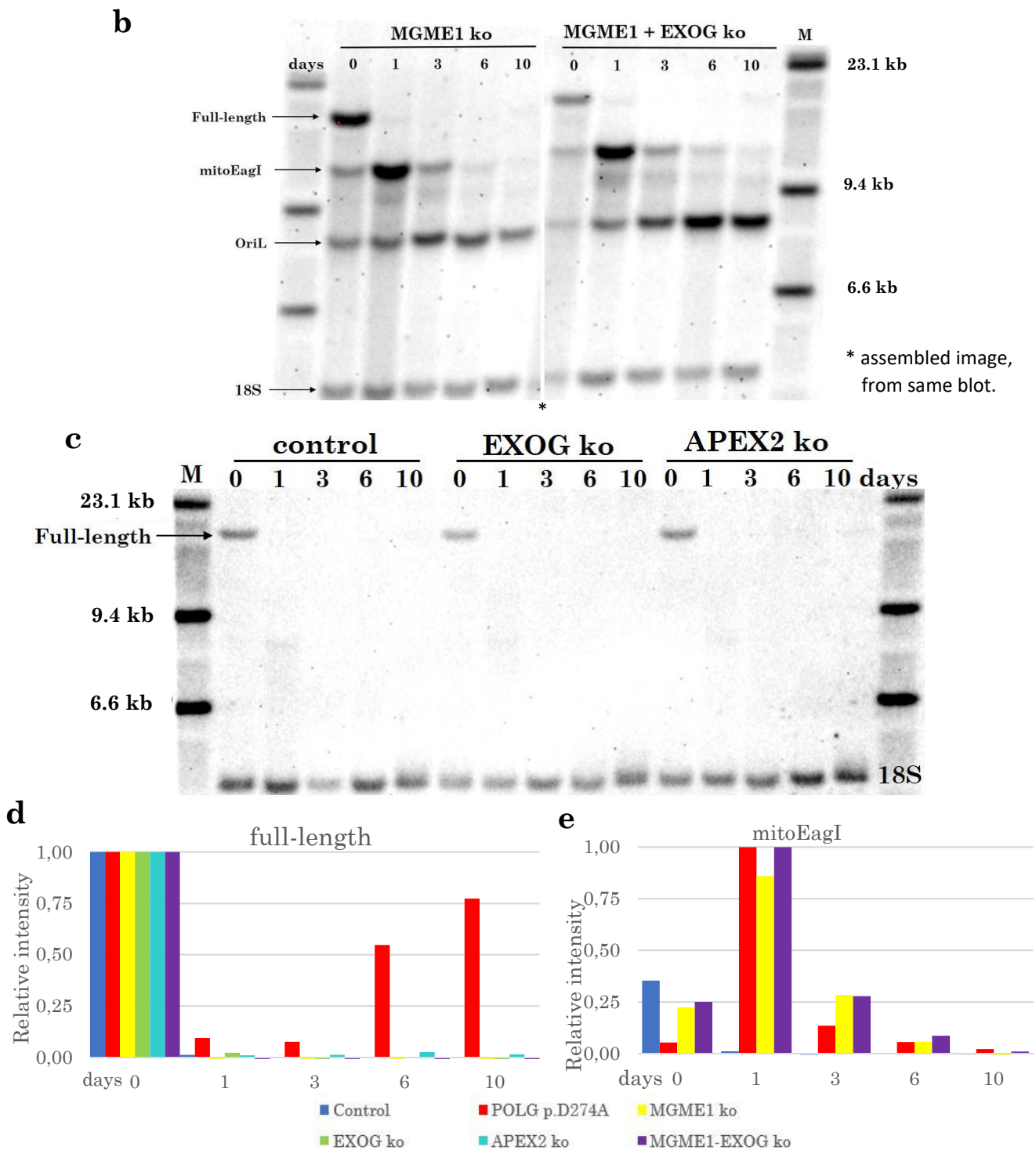


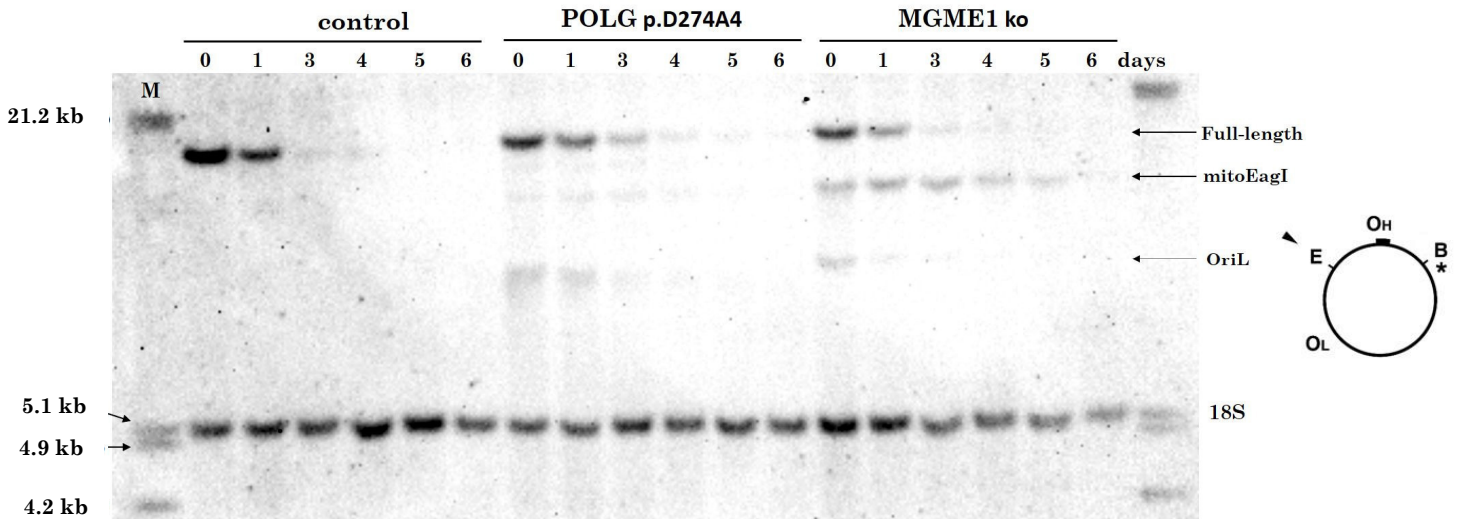
Figure 24: Long term degradation effects on the linearized mtDNA fragment in mitoEagI expressing HEK clones, showing the large digested fragment. Cells were incubated over the first 24 hours in the presence of doxycycline, then doxycycline was removed from the media and incubation continued over 10 days. Southern blots showing degradation of the larger mtDNA fragment, spanning from the mitoEagI (E) and BamHI (B) cutting site. Total DNA was treated with BamHI endonuclease to linearize circular, full-length mtDNA. Position of probe is indicated by a black asterisk (*) on the simplified mitochondrial genome, close to the BamHI cutting site. Linear mtDNA degradation of **a)** control and POLG p.D274A, **b)** MGME1 ko plus MGME1-EXOG double ko and **c)** EXOG ko plus APEX2 ko clones shows rapid degradation in control and knockout clones. Note that Figure b shows the same Southern blot, with only the middle part removed. POLG knockin clone shows the complex mixture of smaller-sized fragments of the original mitoEagI fragment 3 days after induction started. Quantification of **d)** full-length and **e)** mitoEagI fragments in selected clones was calculated, using a nuclear 18S ribosomal DNA probe as reference.

Double knockout of MGME1 and EXOG showed an almost identical degradation pattern as the MGME1 knockout alone (Figure 24 b, d, e), indicating no additional participation of EXOG to degradation of linear mtDNA during the chosen time frame. The smaller-sized oriL fragment also got rapidly degraded, already after twenty-four hours in control, EXOG and APEX2 knockout cells. Persistence of the oriL fragment was detectable in POLG knockin, MGME1 knockout and MGME1 + EXOG double knockout cells, with a notable increase in intensity in the double knockout at later days (day 6-10, Figure 24 b).

3.4 Depletion effect of mitochondrial DNA by ddC in mitochondrial nuclease-deficient POLG and MGME1 clones

Another way of inducing mtDNA depletion in human cells is the application of 2',3'-dideoxycytidine (ddC), which is a competitive inhibitor of POL γ as well as a terminator of the nascent strand during replication (Mancini *et al.*, 1988, Steward *et al.*, 2011). Optimized ddC concentration was determined prior this experiment through a killing curve, performed over one week on mitoEagI HEK cells (data not shown). POLG knockin and MGME1 knockout mitoEagI HEK cells were therefore incubated in the presence of 400 μ M ddC over six days. Each second day, medium was exchanged to refresh the ddC concentration. Total DNA was again treated with BamHI to linearize circular mtDNA and used for Southern blotting (Figure 25 a). Incubation with ddC showed over 90% depletion of mtDNA in control at day three (Figure 25 b). Depletion in POLG knockin and MGME1 knockout clones was delayed and reached similar 90% depletion levels only after four days. Smaller-sized mitoEagI and oriL fragments were visible in mutant clones due to the leaky mitoEagI expression, even without doxycycline induction (visible at zero hour and in the absence of ddC; not detectable in control, probably due to degradation effects) and showed similar persistency as the full-length fragment.

a



b

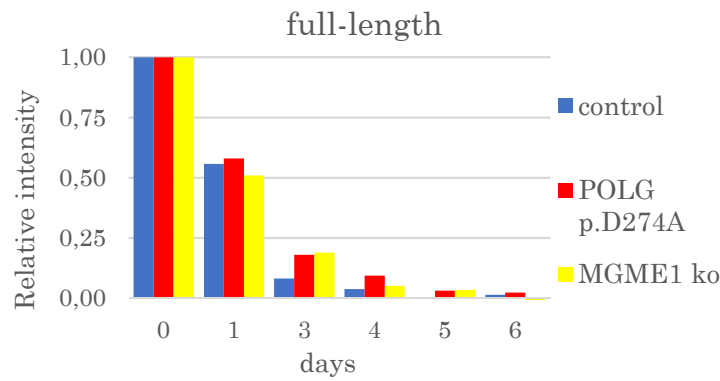


Figure 25: Depletion of mtDNA in POLG and MGME1 mutant HEK cells. a) Southern blot shows depletion of the mtDNA in control, POLG p.D274A and MGME1 ko cell lines over six days. Total DNA was treated with BamHI endonuclease to linearize circular, full-length mtDNA. Position of probe 1 is indicated by a black asterisk (*) on the simplified mitochondrial genome (right), close to the BamHI (B) cutting site. MitoEagI (E) and oriL fragments appear due to leaky expression of mitoEagI. **b)** Quantification of full-length fragment. Band intensity was compared to a nuclear ribosomal DNA (18S).

4. Discussion

The degradation of linear mitochondrial DNA is presumably performed by mitochondrial exonucleases. The size evaluation of free ends from linearized mtDNA over time indicated a gradual degradation, starting from the free ends and then progressing over several thousand nucleotides, which is characteristic for the activity of exonucleases (Peeva and Blei *et al.*, 2018). Still, the precise molecular machinery behind this mechanism is unknown. This work was dedicated to study the function of mitochondrial nucleases on mtDNA and to answer the question how linear mtDNA degradation, which is unique for the mitochondrial genome, is performed. My results give insights on the composition of the mtDNA degradation machinery, or ‘degradosome’, and show that POLG and MGME1 both perform pivotal tasks in this process. Other evaluated mitochondrial nucleases (APEX2 and EXOG) displayed no direct effect and are therefore not involved in this function, suggesting that enzymes, which are part of the mtDNA replication machinery, might be responsible not only for synthesis of mtDNA but for degradation of linear mtDNA as well.

4.1 CRISPR/Cas9-editing creates stable human cell lines with altered mitochondrial nucleases

Up to date it is not possible to directly modify the mitochondrial genome, using CRISPR/Cas9, to study effects of mitochondrial nucleases, as mitochondria apparently lack an endogenous mechanism of nucleic acid import, which is a prerequisite for CRISPR/Cas9 gene-editing (Gammage *et al.*, 2017). Therefore, mitochondrial nucleases were used, which can also perform precise targeting of mtDNA, and introduce DSB’s to study linear degradation of mtDNA. However, the recognition site of mitochondrial endonucleases can not be designed as it is given on the mitochondrial genome sequence.

CRISPR/Cas9-editing of mitochondrial exonucleases was performed in a human mitoEagI expressing cell line, which is usable for inducing mtDNA DSB’s and afterwards analysing the possible effects of dysfunctional mtDNA degradation. The CRISPR/Cas9-system proved to be an effective tool for permanently gene-editing of mitochondrial nucleases in mitoEagI HEK 293 cells.

The method by Schmidt *et al.* (2015) allowed to create custom-built CRISPR/Cas9-vectors containing specific gRNA sequences against any nuclear gene of interest. It was reported that the Cas9 protein binds to the sgRNA and the protospacer region in a largely sequence-independent manner, but favouring protospacer regions with G/C rich regions at positions 17/18 (Schmidt *et al.*, 2015). Furthermore, sequences with A/T regions at positions 14/15 should display higher genomic editing activity (Schmidt *et al.*, 2015). Although all knockout sequences (against MGME1, APEX2, EXOG) met the G/C condition (Table 10), only APEX2 fulfilled the A/T condition, but did not display a higher editing efficiency (Table 13). The importance of specific nucleotides at these positions is still elusive, as higher genome-editing activity was reported for sequences with G/C rich regions at positions 17/18, but not 14/15 (Wang *et al.*, 2014). Doench *et al.* (2014) showed similar results for positions 14/15, while presenting different findings for other positions. Schmidt *et al.*, suspect that Cas9 activity chooses a favourable thermodynamic profile of either the protospacer region, the sgRNA:protospacer complex or the sgRNA molecule itself. To ensure that CRISPR/Cas9-editing successfully renders the targeted gene dysfunctional at the level of protein expression, the position of each sgRNA was chosen within the earliest possible exons and at least within the first half of the coding region of the gene. In consistency with previous reports from the literature (Wang *et al.*, 2014, Doench *et al.* 2014, Schmidt *et al.* 2015), indel mutations by sgRNAs, targeting early exons, increase the efficiency of functional knockouts as they result in clear loss-of-function mutations. The targeted mitochondrial nucleases MGME1, EXOG and APEX2 showed frameshift indels (Figure 17) through exploitation of the NHEJ repair pathway in mitoEagI HEK cells. The 3'–5' exonuclease activity of POLG was selectively silenced by introducing the p.D274A point mutation, by using a co-transfected oligonucleotide as template for homologous-directed repair. This mutation previously led to an elimination of the 3'–5' exonuclease activity of POLG in yeast (Foury and Vanderstraeten, 1992), mice (Trifunovic *et al.*, 2004) and flies (Bratic *et al.*, 2015). The additional silent mutation for the PstI endonuclease restriction site greatly accelerated the pre-screening phase of the vast number of POLG clones. After Cas9 introduced the DSB, its repair through NHEJ is

usually performed within the first thirty minutes; HR on the other hand, takes over seven hours to complete the DSB repair (Mao *et al.*, 2008). The large discrepancy in efficiency between both methods can be explained through the presence or absence of the co-transfected oligonucleotide, which serves as a repair template for homologous recombination. In its absence, no HR can be performed to introduce the desired p.D274A point mutation for POLG. It was crucial for studying linear mtDNA degradation, that occurring off-target effects produced by Cas9 did not interfere with the artificial expression of the mitoEagI protein in mutant HEK 293 cell lines. Recent studies, analysing CRISPR/Cas9-mediated off-target effects on a genome-wide level in single cell clone revealed deviating number of incidences for this event, depending on the cell line: In human pluripotent stem cell (hPSC) clones, the risk for off-target mutations were very low and posed no significant concern for applications like disease research (Veres *et al.*, 2014, Smith *et al.*, 2014). However, in cancer cell lines, like K562 cells (human myelogenous leukemia cells) or HEK 293 cells, off-target effects have been reported to occur at much higher incidences (Fu *et al.*, 2013, Hsu *et al.*, 2013). The assessments in this study, regarding Cas9 off-target effects in HEK 293 cells, focused on potential harmful effects to the mitoEagI protein expression, since mitoEagI is required to linearize the mitochondrial DNA upon induction. No deficiencies were observed in any mutant HEK 293 cell line, neither in protein expression (Western blot, Figure 18) during the first twenty-four hours, nor in doxycycline-induced endonuclease activity on circular mtDNA (qPCR data, Figure 19). CRISPR/Cas9 engineering on MGME1 produced two knockout clones with different indels, showing the same deficiencies of linear mtDNA degradation, which minimizes the chances that off-target effects can be made responsible for this result. In the POLG knockin mutant, mitoEagI endonuclease activity was reduced due to genomic instability, but still sufficient enough to study linear mtDNA degradation, as Southern blots later showed the clear formation of smaller-sized fragments and the absence of their rapid degradation (Figure 20).

This demonstrates, that the CRISPR/Cas9-system proved to be a powerful technique for creating mutant mitoEagI HEK cell lines with permanently altered expression of mitochondrial nucleases, without damaging the mitoEagI endonuclease gene through off-target effects. The established mutant cell lines have to be re-evaluated over time for their efficient induction of mitoEagI, given the genomic instability of the HEK 293 cells, which increases especially in high-passage lines.

4.2 POLG and MGME1 perform linear mtDNA degradation

Both, POLG and MGME1 are key enzymes responsible for mtDNA maintenance. Previously it was reported, that POLG and MGME1 are in physical contact (Nicholls *et al.*, 2014) and MGME1 is known to cleave 5'-flaps for POLG during replication, while POLG processes 3'-flaps on its own to create ligatable ends (Uhler *et al.*, 2015). Later it was shown, that MGME1 alone is poor at generating these ligatable ends, but exerts a very strong flap-processing activity, when in combination with POLG (Uhler *et al.*, 2016). Uhler *et al.* argued, that interaction between Pol γ and MGME1 is dependent on the 3'-5' exonuclease activity of POLG and that MGME1 is the sole nuclease in removing mtDNA flaps in coordination with Pol γ (Uhler *et al.*, 2016). Therefore we chose POLG and MGME1 as prime targets in the search for participants of the mitochondrial degradation machinery.

By studying the effects of deficient mitochondrial nucleases in the context of linear mtDNA degradation, I could show that POLG and MGME1 both play a major role in rapid linear mtDNA degradation. MGME1 possesses 5'-3' exonuclease activity on single-stranded mtDNA and pathogenic mutations in MGME1 have been described to cause disturbances in mtDNA maintenance leading to multisystemic mitochondrial diseases (Kornblum *et al.*, 2013, Nicholls *et al.*, 2014). The mitochondrial polymerase γ possesses an exonuclease domain (POLG) with an additional 3'-5' exonuclease activity, which is most often mentioned for its proof-reading activity, performing base excision repair, during replication (Foury *et al.*, 1992). Under normal circumstances, damage to mtDNA, which is due to the formation of DNA double-strand breaks, results in the degradation of this particular, damaged mtDNA molecule. Since

mitochondria are unique in their multicopy genomic nature, degrading and thus losing a small percentage of its genome imposes no threat to the total mitochondrial genome of the cell. My data could show that linearized mtDNA remained largely intact during the first six hours after mitoEagI induction in MGME1 knockout and POLG knockin clones (Figure 20 and 18). The results between both mutant cell lines, displaying differences corresponding to the mitoEagI fragments raised the question whether this ‘degradosome’ can operate in both strand-directions simultaneously.

In our recent publication, we could show, with ultra-deep sequencing of linker-ligated mtDNA in MGME1 knockout and POLG knockin cells, six hours after inducing double-strand breaks, that MGME1 showed unaltered persistency of the non-degraded ends and POLG displayed over 80% of detectable ends within a distance of 600 base pairs from the cutting site (Peeva and Blei *et al.*, 2018, Figure 3a). A one-side-blunt double-stranded linker ligation to either native or T4-polymerase-blunted mtDNA showed similar quantities of detectable ends through ultra-deep sequencing (Peeva and Blei *et al.*, 2018, Figure 3d-e). We therefore concluded, that the majority of non-degraded and partially-degraded mtDNA ends exist *in vivo* as blunt double-strands, as pre-treatment with T4 polymerase would otherwise have drastically increased the number of ligatable ends. This suggested that bulk degradation of linear mtDNA occurs from the free ends and is performed by exonucleases (Peeva and Blei *et al.*, 2018).

It is interesting to speculate about the reasons for the different mtDNA ends between MGME1 and POLG mutants. The complete knockout in MGME1 prevents 5'-flap processing and MGME1 mutant showed no signs of degradation on the ends, after linearization (Peeva and Blei *et al.*, 2018, Figure 3a). Silencing the 3'-5' exonuclease domain (POLG) from mitochondrial polymerase γ still prevents rapid degradation but displayed a slightly progressed degradation from the cutting site. Maybe the p.D274A point mutation of POLG does not completely inhibit the 3'-5' exonuclease activity. It was reported, that MGME1 cannot rescue ligation in POLG^{-/-} cells and that coordination between Pol γ and MGME1 depends on POLG's functional 3'-5' exonuclease activity (Uhler *et al.*, 2016). Alternatively, mitochondrial nucleases like APEX2 or MRE11, both

possessing single-strand DNA 3'–5' exonuclease activity, might compensate for the loss of POLG's exonuclease activity. APEX2 predominantly localizes in the nucleus and only to some extent in mitochondria (Tsuchimoto *et al.*, 2003) and its BER activity has not been demonstrated yet in mitochondria (Bruni *et al.*, 2016). Mitochondrial DNA repair pathways still raise several unanswered questions, especially on topics like mismatch repair and double-strand break repair. While NHEJ is undetectable in mitochondria (Tadi *et al.*, 2016), an alternative pathway to NHEJ, known as microhomology-mediated end joining (MMEJ) utilizes microhomology regions for recombination, but also results in larger deletions in mitochondria (Tadi *et al.*, 2016, Dahal *et al.*, 2017). Dahal and colleagues compared the difference between MMEJ and homologous-directed repair (HDR) in mitochondria and found a localization of the MRN complex (MRE11, RAD50, NBS1), RAD51 and Ligase III (LIG3) in mitochondria (Dahal *et al.*, 2017). HDR results in an error-free repair without loss of sequences, while the error-prone MMEJ is performed, if the DSB is close to the direct repeat, used for HDR (Dahal *et al.*, 2017). However, evaluation of our ultra-deep sequencing data revealed only break points caused by NHEJ, which were predominantly present as blunted ends after mitoEagI cleavage (Peeva and Blei *et al.*, 2018). Yet, it was shown that MRE11 nuclease activity can be modulated in several ways, like through the presence of RAD50 or NBS1, but also through stimulation by ATP or sequence homology in the DNA substrate (D'Amours and Jackson, 2002). It remains a task for further studies to shed light on this topic how the mitochondrial maintenance machinery changes its mode of action during impaired mitochondrial nuclease activities.

In 2015, Bratic *et al.* already showed that recombinant human POLG proteins, expressed in insect cells can degrade small linear DNA fragments, *in vitro*, through exonuclease activity in the absence of deoxynucleotides (Bratic *et al.*, 2015). In recent results, knockdown of POLG in *Drosophila* prevented the elimination of the paternal mitochondrial genome during spermatogenesis (Yu *et al.*, 2017), suggesting an additional function of the exonuclease domain for mtDNA maintenance. It is known, that T4 DNA polymerase can use its 3'–5' exonuclease activity in the absence of deoxyribonucleotide triphosphate (dNTP) substrates to remove single-stranded DNA stretches (Huang and Lehman, 1972).

Very recent findings by Moretton *et al.* (2017) questioned the idea that known mitochondrial nucleases are involved in linear mtDNA degradation and instead suggest an undiscovered mtDNA degradation pathway performed by currently unknown mitochondrial nucleases (Moretton *et al.* 2017). After conducting knockdown studies on selected mitochondrial nucleases (ENDOG, EXOG, DNA2, FEN1, MGME1) in an inducible mitoPstI HEK 293 cellular model (similar to mitoEagI, but has two cutting sites inside the mitochondrial genome, removing a fragment of ~2110bp), Moretton and colleagues found no deficiencies in linearized mitochondrial DNA degradation. Our knockdown results on MGME1, POLG and TWNK in the mitoPstI model showed the formation of a prominent fragment after four hours of induction (Peeva and Blei *et al.*, 2018 Figure 2) – Moretton *et al.* evaluated the degradation effects after two hours, which might be another reason for the differences between both results. Before we used the CRISPR/Cas9 tool in mitoEagI HEK 293 cells to target mitochondrial nucleases, we also tried to perform knockdown studies with MGME1 in mitoEagI HEK 293 cells. Efficient knockdown of MGME1 was already achieved after three days at the mRNA level, but prolonged siRNA treatment over a total period of six days showed an additional depletion at the protein level. Still, evaluations on mtDNA depletion and accumulations of 7S levels still differed from the original findings by Kornblum *et al.* (2013). Western blot analysis on the selected mitochondrial nucleases performed by Moretton *et al.* also showed small levels of protein expression after three-day siRNA treatment (Moretton *et al.* 2017, Supplementary Figure 1), which likely explains

why no direct effects of MGME1 knockdown on linear mtDNA degradation were observed. Of note is, that doxycycline induction of HEK 293 cells did not influence the protein expression of neither the selected mitochondrial nucleases nor other mitochondrial proteins, like Twinkle or POLG (Moretton *et al.* 2017, Figure 1-2).

Apart from our findings that POLG and MGME1 participate in linear degradation of mtDNA (Peeva and Blei *et al.*, 2018), Medeiros *et al.* (2018) also showed very recently in starving cells of *Saccharomyces cerevisiae*, that POLG also displayed a strong 3'–5' exonuclease-dependent mode of mtDNA degradation to adjust increasing mtDNA copy numbers during nucleotide limitations (Medeiros *et al.*, 2018). Medeiros *et al.* proposed a central role for POLG in mtDNA copy number regulation in response to physiological changes by switching between the two opposing modes of replication and degradation (Medeiros *et al.*, 2018).

4.3 No additional mitochondrial nucleases, besides MGME1, influence rapid linear mtDNA degradation

With POLG and MGME1 being the first identified candidates involved in linear mtDNA degradation, the question occurred if other mitochondrial nucleases with 3'–5' or 5'–3' exonuclease-activity could perform or support this task. Most mitochondrial nucleases have been described to perform flap-processing functions for mtDNA maintenance, including MGME1 (Kornblum *et al.*, 2013). One set of possible nuclease candidates consists of FEN1 and DNA2, which showed increased flap processing efficiency in conjunction (Zheng *et al.*, 2008, Uhler *et al.*, 2015). Knockdown experiments on FEN1 and DNA2 however, showed no deficiencies on linear mtDNA degradation (Peeva and Blei *et al.*, 2018) and mitochondrial localization of FEN1 is even still debated (Bruni *et al.*, 2017). Holt and colleagues have reported a shorter isoform of FEN1, named FENMIT, that can bind, but not cleave RNA flaps (Kazak *et al.*, 2013), which might substitute FEN1s activity in mitochondria. Three other nucleases are known, besides DNA2 and FEN1, which localize in mitochondria: ENDOG, EXOG and MGME1. EXOG can also exert a 5'–3' exonuclease activity, just like MGME1, on ssDNA during SSB repair (Cymerman *et al.*, 2008) and depletion

of EXOG was reported to cause persistent SSBs in mtDNA, enhanced ROS levels and apoptosis (Tann *et al.*, 2011). This bears the question if EXOG can support or even substitute MGMGE1s task during linear mtDNA degradation. Likewise, it was shown that mtDNA elimination during spermatogenesis is dependent on ENDOG and POLG (DeLuca and O'Farrel, 2012). We demonstrated that neither the knockout of EXOG, nor the knockdown of ENDOG showed any effect on rapid degradation of linearized mtDNA (Supplementary Figure 4, Peeva and Blei *et al.*, 2018).

In the past, it was suggested that EXOG and ENDOG influence mtDNA depletion, initiated by Herpes Simplex Virus (HSV) 1-mediated mtDNA depletion, through its viral alkaline nuclease UL12.5 (Duguay and Smiley, 2013), however HSV infection already causes major damage to the mitochondrial genome within a few days (Saffran *et al.*, 2007) and therefore the additionally performed knockdown and overexpressing experiments on EXOG and ENDOG, by Duguay and Smiley might have shown only smaller depletion effects to the already greatly disturbed mtDNA maintenance machinery. Monitoring the 5'–3' exonuclease activity of EXOG in a cellular model provided additional insights on EXOGs participation in linear mtDNA degradation.

When looking for other nucleases with 3'–5' exonuclease activity, like POLG (and besides MRE11), one finds APEX2, which predominantly localizes in the nucleus, but also in mitochondria (Tsuchimoto *et al.*, 2001). APEX2 uses its 3'–5' exonuclease activity preferentially during mismatched base repairs (Burkovics *et al.*, 2006) and is presumed to be involved in nuclear BER – even though mitochondrial activity has not been demonstrated yet (Bruni *et al.*, 2016). Together with EXOG, APEX2 both provide an additional set of nucleases which can perform 3'–5' or 5'–3' exonuclease activity and might therefore play a role in the degradation process of linear mitochondrial DNA.

My experiments performed on APEX2 and EXOG knockout cell lines showed no signs of altered degradation on linearized mtDNA (Figure 22-21). Even the double-knockout of MGMGE1+EXOG showed no significant increased persistency of the linear fragment, resulting from the original mitoEagI ends in the prolonged time course experiments (Figure 24), compared to MGMGE1 knockout alone. Furthermore, knockdown experiments performed on ENDOG and MRE11

also showed no changes to regular linear mtDNA degradation (Peeva and Blei *et al.*, 2018, Supplementary Figure 4), which altogether point towards POLG and MGME1 being the prime nucleases involved in mtDNA degradation.

4.4 Linearized mtDNA fragments show signs of degradation in POLG and MGME1 mutants after the first 24 hours

In order to gain a better understanding of mitochondrial DNAs degradosome, I performed long term degradation experiments, which put the scope beyond the first twenty-four hours of induced mitoEagI expression. Without doxycycline induction, mitoEagI expression should cease, apart from the leaky expression and only already expressed mitoEagI endonucleases would perform their DSB on the mitochondrial genome. This might give the cells the chance to replicate and recover their lost mtDNA. However, after one day, mitoEagI endonuclease activity linearized nearly the complete mitochondrial genome in all knockout clones and most of it in the POLG knockin mutant. Furthermore, half-life time of the mitoEagI protein after doxycycline induction stopped was not assessed, but could be performed through Western blotting. EXOG and APEX2 mutants had no mtDNA molecules left, to be utilized for mtDNA repair and replication. Yet it also seems that both exonucleases don't have additional functions on linear mtDNA degradation. This would also explain why no additional effects were observable in the MGME1+EXOG double-knockout and suggest, that EXOG provides no compensatory mechanisms, in case of incapacitated MGME1 exonuclease activity. The free ends in MGME1 and POLG mutants on the other hand could have been available, in theory, for mitochondrial DSB-repair, due to the absence of rapid degradation and in absence of induced mitoEagI endonuclease. The observed recurrence of the full-length fragment in POLG knockin at late days, could stem from the fact that a subcellular population lost the mitoEagI-expressing plasmid and overgrew the remaining cells. Alternatively, since induced mitoEagI expression was stopped through the medium change at day one, mtDNA maintenance was indeed able to repair the full-length fragment through HDR. Another possibility could be, that due to the loss of the exonuclease (and proof-reading) activity, mitochondrial polymerase γ might display an accelerated polymerase activity, resulting in faster

synthesized mtDNA, which now bears a lot of mistakes. A recent study, assessing the speed of mitochondrial DNA replication however, found no effect in mice with a deficient POLG^{D275A} variant, that resulted in a lack of proofreading activity (Forslund *et al.*, 2018).

Another approach of eliminating the mitochondrial genome used the incorporation of dideoxycytidine (ddC), which inhibits mtDNA replication, either through acting as a terminator of nascent strand elongation or by being a competitive inhibitor of mitochondrial polymerase γ (Brown *et al.*, 2002). Being unable to finish mtDNA replication leaves the terminated single-stranded mtDNA strand prone to linear mtDNA degradation, or strand-breaks, which ultimately results in a depletion of mitochondrial copy numbers, without being dependent on the expression of the mitoEagI endonuclease. Dideoxycytidine must be phosphorylated to its active triphosphate form by cytoplasmic kinases, before being transported into the mitochondria, to inhibit mtDNA replication (Brown *et al.*, 2002). In my previous experiments, circular mtDNA was cleaved by mitoEagI endonuclease and showed a complete linearization of mtDNA during the first twenty-four hours in all tested cell lines. Here, depletion of circular mtDNA progressed at a much slower pace, as incorporation of ddC and subsequently terminated strand synthesis can only occur during replication of intact mtDNA, which takes between one and two hours to complete an entire cycle of replication (Clayton, 1982). There was a small effect observable on linear degradation of mtDNA between day three and day four, delaying the depletion of mitochondrial copy numbers in both POLG and MGME1 mutants compared to control (Figure 25). The inhibition of POLGs exonuclease domain by ddC has not been demonstrated yet, only for other chain-terminating dideoxynucleoside analogues (Bridges *et al.*, 1993, Gray *et al.*, 1995). A previously reported slower depletion rate of mitochondrial copy numbers in MGME1^{-/-} fibroblasts (Kornblum *et al.*, 2013), suggesting an impaired mtDNA breakdown, could not be replicated in mitoEagI HEK cells. Perhaps the major difference in ddC concentration (20-times higher than in fibroblasts) or the genomic instability of the HEK 293 cell line influenced the possibility of discovering this finding.

4.5 TWNK, POLG and MGME1 compose the mitochondrial ‘degradosome’

Overall, these findings present strong evidence for the involvement of POLG and MGME1 in linear mtDNA degradation. Since both enzymes are part of the mtDNA replication and maintenance machinery, the question occurs if other members from it might play a role in degradation, too. In order to expand single-stranded mtDNA and allow continuous replication or degradation, first, double-stranded mtDNA must be unwound by the mitochondrial helicase Twinkle. Without TWNK, only overhangs resulting from DSB, could be processed. We addressed this question in our recent publication and performed knockdown experiments on TWNK in mitoPstI HEK 293 cells, which showed severe impairment of rapid degradation on linearized mitochondrial DNA (Peeva and Blei *et al.* 2018 Figure 5b), even with a small fraction of protein expression for Twinkle remaining (15% expression after TWNK knockdown, Peeva and Blei *et al.* 2018 Supplementary Figure 6). Together these findings strongly suggest that rapid linear degradation of linearized mitochondrial DNA is performed by the same enzymes, which are involved in replication of mtDNA. This implies novel additional roles for the enzymes TWNK, POLG and MGME1, which are normally part of the mtDNA replication and maintenance machinery (Figure 26).

Future studies could investigate factors, which are relevant to switch the mtDNA maintenance machinery from performing replication towards degradation. Different types of template mtDNA (free double-stranded ends being degraded versus single-stranded 3' ends initiating replication) or protein factors could be among these factors. The accessory subunit POLG2 does not seem to be required for POLG to perform degradation (Peeva and Blei *et al.* 2018 Supplementary Figure 4), despite the fact that it is necessary for replication, indicating that the interaction between POLG and POLG2 could be another regulatory element.

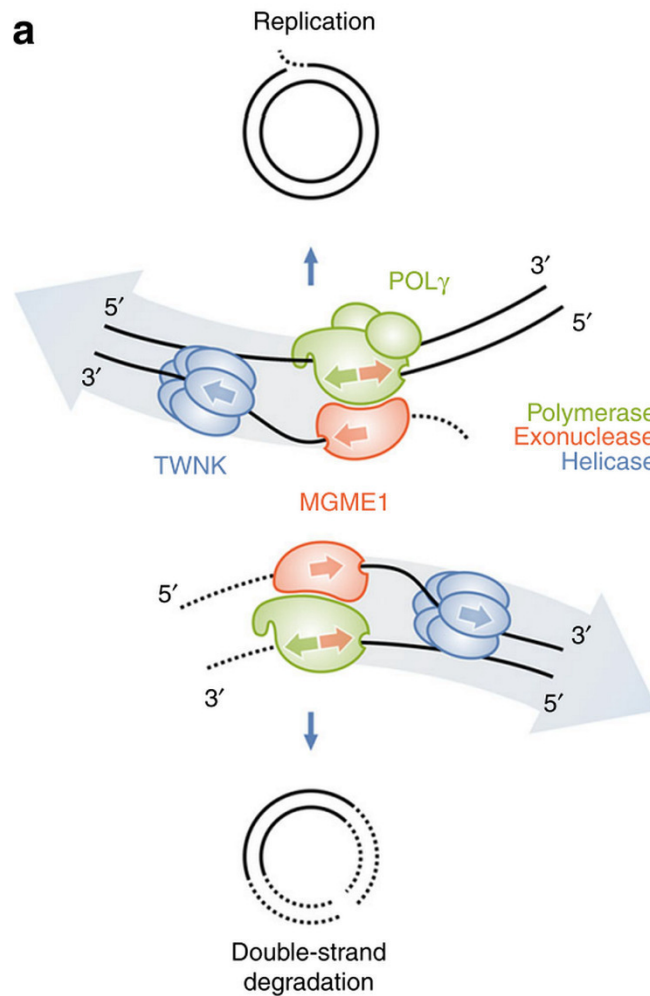


Figure 26: Models of replication and double-strand degradation of mtDNA by the same machinery. TWNK, POLG and MGME1 play a role in replication (upper panel) and degradation (lower panel) of mitochondrial DNA. During replication, the polymerase activity of POLG determines the overall movement speed of the machinery. Here, MGME1 removes flap structures and creates ligatable ends. Upon degradation, net movement is reversed and correlates to the exonuclease activity of POLG (Figure adapted from Peeva and Blei *et al.*, 2018).

Concluding, this thesis in conjunction with our recent publication (Peeva and Blei *et al.*, 2018) presented strong evidence for a novel mechanism in mitochondrial DNA maintenance, which expands our knowledge on linear mtDNA degradation and the formation of mtDNA rearrangements.

References

Alani E, Reenan RAG, Kolodner RD, Interaction between mismatch repair and genetic recombination in *Saccharomyces cerevisiae*, Genetics, 1994.

Alexevey M, Shokolenko I, Wilson G, LeDoux S, The Maintenance of Mitochondrial DNA Integrity - Critical Analysis and Update, Cold Spring Harbor Perspectives in Biology, 2013.

Anders C, Niewoehner O, Duerst A, Jinek M, Structural basis of PAM-dependent target DNA recognition by the Cas9 endonuclease. Nature, 2014.

Anderson S, Bankier AT, Barrell BG, de Bruijn MHL, Coulson AR, Drouin J, Eperon IC, Nierlich DP, Roe BA, Sanger F, Schreier PH, Smith AJH, Staden R, Young IG, Sequence and organization of the human mitochondrial genome, nature, 1981.

Asin-Cayuela, Gustafsson CM, Mitochondrial transcription and its regulation in mammalian cells. Trends Biochem Sci, 2007.

Bacman SR, Williams SL, Moraes CT, Intra- and inter-molecular recombination of mitochondrial DNA after in vivo induction of multiple double-strand breaks. Nucleic Acids Res, 2009.

Bannwarth S, Procaccio V, Lebre AS, Jardel C, Chaussonot A, Hoarau C, Maoulida H, Charrier N, Gai X, Xie HM, Ferre M, Fragaki K, Hardy G, Mousson de Camaret B, Marlin S, Dhaenens CM, Slama A, Rocher C, Paul Bonnefont J, Rötig A, Aoutil N, Gileron M, Desquiret-Dumas V, Reynier P, Ceresuela J, Jonard L, Devos A, Espil-Taris C, Martinez D, Gaignard P, Le Quan Sang KH, Amati-Bonneau P, Falk MJ, Florentz C, Chabrol B, Durand-Zaleski I, Paquis.Flucklinger V, Prevalence of rare mitochondrial DNA mutations in mitochondrial disorders. J Med Genet, 2013.

Bogenhagen DF, Rousseau D, Burke S, The Layered Structure of Human Mitochondrial DNA Nucleoids, J Biol Chem, 2008.

Bolotin A, Quinquis B, Sorokin A, Ehrlich SD, Clustered regularly interspaced short palindrome repeats (CRISPRs) have spacers of extrachromosomal origin. Microbiology, 2005.

Bratic A, Kauppila TE, Macao B, Grönke S, Siibak T, Stewart JB, Baggio F, Dols J, Patridge L, Falkenberg M, Wredenberg A, Larsson NG, Complementation between polymerase- and exonuclease-deficient mitochondrial DNA polymerase mutants in genomically engineered flies, Nature Communications, 2015.

Bridges EG, Faraj A, Sommadossi JP, Inhibition of mammalian DNA polymerase-associated 3' to 5' exonuclease activity by 5'-monophosphates of 3'-azido-3'-deoxythymidine and 3'-amino-3'-deoxythymidine, Biochem Pharmacol., 1993.

References

- Brown GG, Gadaleta G, Pepe G, Saccone C, Sbisá E, Structural conservation and variation in the D-loop-containing region of vertebrate mitochondrial DNA, J Mol Biol, 1986.
- Brown TA, Clayton DA, Release of replication termination controls mitochondrial DNA copy number after depletion with 2',3'-dideoxycytidine, Nucleic Acids Research, 2002.
- Brown TA, Ceccino C, Tkachuk AN, Bustamante C, Clayton DA, Replication of mitochondrial DNA occurs by strand displacement with alternative light-strand origins, not via a strand-coupled mechanism. Genes & Development, 2005.
- Bruni F, Lightowlers RN, Chrzanowska-Lightowlers ZM, Human mitochondrial nucleases, FEBS Journal, 2017.
- Bua E, Johnson J, Herbst A, DeLong B, McKenzie D, Salamat S, Aiken JM, Mitochondrial DNA-deletion mutations accumulate intracellularly to detrimental levels in aged human skeletal muscle fibers. J Hum Gene, 2006.
- Buis J, Wu Y, Leddon J, Westfield G, Eckersdorff M, Sekiguchi JM, Chang S, Ferguson DO, Mre11 nuclease activity has essential roles in DNA repair and genomic stability distinct from ATM activation. Cell, 2008.
- Burkovics P, Szukacsov V, Unk I, Haracska L, Human Ape2 protein has a 30-50 exonuclease activity that acts preferentially on mismatched base pairs, Nucleic Acids Research, 2006.
- Cairns SS, Bogenhagen DF, Mapping of the Displacement Loop within the Nucleotide Sequence of Xenopus laevis Mitochondrial DNA, J Biol Chemistry, 1986.
- Carrodegua JA, Theis K, Bogenhagen DF, Kisker C, Crystal structure and deletion analysis show that the accessory subunit of mammalian DNA polymerase gamma, Pol gamma B, functions as a homodimer. Mol Cell, 2001.
- Cerritelli SM, Frolova EG, Feng C, Grinberg A, Love PE, Crouch RJ, Failure to produce mitochondrial DNA results in embryonic lethality in Rnaseh1 null mice. Mol Cell 2003.
- Chabi B, Mousson de Camaret B, Duborjal H, Issartel JP, Stepien G, Quantification of mitochondrial DNA deletion, depletion, and overreplication: application to diagnosis. Clin Chem, 2003.
- Chen L, Nievera CJ, Lee AY, Wu X, Cell cycle-dependent complex formation of BRCA1.CtIP.MRN is important for DNA double-strand break repair. J Biol Chem, 2008.
- Clayton DA, Doda JN, Friedberg EC, Absence of a pyrimidine dimer repair mechanism for mitochondrial DNA in mouse and human cells. Basic Life Sci., 1975.
- Clayton DA, Replication of Animal Mitochondrial DNA, Cell, 1982.

References

Cline SD, Mitochondrial DNA Damage and its Consequences for Mitochondrial Gene Expression, *Biochim Biophys Acta*, 2012.

Cogliati S, Frezza C, Sorianno ME, Varianta T, Quantana-Cabrera R, Corrado M, Cipolat S, Costa V, Casarin A, Gomes LC, Perales-Celemnte E, Salviati L, Fernandez-Silvia P, Enriquez JA, Scoranno L, Mitochondrial cristae shape determines respiratory chain supercomplexes assembly and respiratory efficiency, *Cell*, 2013.

Cong L, Ran FA, Cox D, Lin S, Barretto R, Habib N, Hsu PD, Wu X, Jiang W, Marraffini LA, Zhang F, Multiplex genome engineering using CRISPR/Cas systems. *Science*, 2013.

Copeland WC, Longley MJ, DNA2 Resolves Expanding Flap in Mitochondrial Base Excision Repair, *Molecular Cell*, 2008.

Copeland WC, Longley M, Mitochondrial genome maintenance in health and disease, *DNA Repair*, 2014.

Costa-Guda J, Tokura T, Roth, SI, Arnold A, Mitochondrial DNA mutations in oxyphilic and chief cell parathyroid adenoma, *BMC Endocrine Disorders*, 2007.

Crews S, Ojala D, Posakony J, Nishiguchi J, Attardi G, Nucleotide sequence of a region of human mitochondrial DNA containing the precisely identified origin of replication, *Nature*, 1979.

Croteau DL, Bohr VA, Repair of oxidative damage to nuclear and mitochondrial DNA in mammalian cells, *J Biol Chem*, 1997.

Cymerman IA, Chung I, Beckmann BM, Bujinicki JM, Meiss G, EXOG, a novel paralog of Endonuclease G in higher eukaryotes, *J Biol Chem*, 2008.

Dai WJ, Zhu LY, Yan ZY, Xu Y, Wang QL, Lu XJ, CRISPR-Cas9 for in vivo Gene Therapy: Promise and Hurdles, *Molecular Therapy - Nucleic Acids*, 2016

D'Aurelio M, Gajewski CD, Lin MT, Mauck WM, Shao LZ, Lenaz G, Moraes CT, Mafredi G, Heterologous mitochondrial DNA recombination in human cells. *Hum Mol Genet*, 2004.

Davis AF, Clayton DA, In Situ Localization of Mitochondrial DNA Replication in Intract Mammalian Cells, *J Cell Biology*, 1996.

DeBalsi KL, Hoff KE, Copeland WC, Role of the mitochondrial DNA replication machinery in mitochondrial DNA mutagenesis, aging and age-related diseases, *Ageing Res Rev.*, 2017.

DeBrosse S, Parikh S, Neurologic Disorders Due to Mitochondrial DNA Mutations, *Semin Pediatr Neurol*, 2012.

DeLuca SZ, O'Farrell PH, Barriers to Male Transmission of Mitochondrial DNA in Sperm Development, *Dev Cell.*, 2012.

References

- Deltcheva E, Chylinski K, Sharma CM, Gonzales K, Chao Y, Pirzada ZA, Eckert MR, Vogel J, Charpentier E, CRISPR RNA maturation by *trans*-encoded small RNA and host factor RNase III. Nature, 2011.
- Doench JG, Hartenian E, Graham DB, Tothova Z, Hedge M, Smith I, Sullender M, Ebert BL, Xavier RJ, Root DE, Rational design of highly active sgRNAs for CRISPR-Cas9-mediated gene inactivation, Nat. Biotechnol., 2014.
- Duguay BA, Smiley JR, Mitochondrial Nucleases ENDOG and EXOG Participate in Mitochondrial DNA Depletion Initiated by Herpes Simplex Viurs 1 UL12.5, J Virol., 2013.
- Falkenberg M, Gaspari M, Rantanen A, Trifunovic A, Larsson LG, Gustafsson CM, Mitochondrial transcription factors B1 and B2 activate transcription of human mtDNA, Nature, 2002.
- Farr CL, Wang Y, Kaguni LS, Functional interactions of mitochondrial DNA polymerase and single-stranded DNA-binding protein. Template-primer DNA binding and initiation and elongation of DNA strand synthesis. J Biol Chem, 1999.
- Fish J, Raule N, Attardi G, Discovery of a major D-loop replication origin reveals two modes of human mtDNA synthesis. Science, 2004.
- Fisher RP, Lisowsky T, Parisi MA, Clayton DA, DNA wrapping and bending by a mitochondrial high mobility group-like transcriptional activator protein. J Biol Chem, 1992.
- Forslund JME, Pfeiffer A, Stojkovic G, Wanrooij PH, Wanrooij S, The presence of rNTPs decreases the speed of mitochondrial DNA replication, PLoS Genet., 2018.
- Foury F, Vanderstraeten S, Yeast mitochondrial DNA mutators with deficient proofreading exonucleolytic activity. EMBO, 1992.
- Franssons A, Ruusala A, Aspenström P, Atypical Rho GTPases have roles in mitochondrial homeostasis and apoptosis. J Biol Chem, 2003.
- Fu Y, Foden JA, Khayter C, Maeder ML, Reyon D, Joung JK, Sander JD, High frequency off-target mutagenesis induced by CRISPR-Cas nucleases in human cells, Nat Biotechnol., 2013.
- Fusté JM, Wanrooik S, Jemt E, Granycome CE, Cluett TJ, Shi Y, Atanassova N, Holt IJ, Gustafsson CM, Falkenberg M, Mitochondrial RNA polymerase is needed for activation of the origin of light-strand DNA replication, Mol Cell, 2010.
- Gammage PA, Morae CT, Minczuk M, Mitochondrial Genome Engineering: The Revolution May Not Be CRSIRP-Ized. Trend Genet., 2017.

References

- Garneau JE, Dupuis MÈ, Villion M, Romero DA, Barrangou R, Boyaval P, Fremaux C, Horvath P, Magadán AH, Moineau S, The CRISPR/Cas bacterial immune system cleaves bacteriophage and plasmid DNA. *Nature*, 2010.
- Gilkerson RW, Schon EA, Hernandez E, Davidson MM, Mitochondrial nucleoids maintain genetic autonomy but allow for functional complementation. *J Cell Biol*, 2008.
- Gilkerson RW, Bravo L, Garcia I, Gaytan N, Herrera A, Maldonado A, Quintanilla B, The Mitochondrial Nucleoid: Integrating Mitochondrial DNA into Cellular Homeostasis, Cold Spring Harbor Perspectives in Biology, 2013.
- Gorman GS, Chinnery PF, DiMauro S, Hirano M, Koga Y, McFarland R, Suomalainen A, Thorburn DR, Zeviani M, Turnbull DM, Mitochondrial Diseases, *Nature Reviews Disease Primers*, 2016.
- Gray NM, Marr CL, Penn CR, Cameron JM, Bethell RC, The intracellular phosphorylation of (-)-2'-deoxy-3'-thiacytidine (3TC) and the incorporation of 3TC 5'-monophosphate into DNA by HIV-1 reverse transcriptase and human DNA polymerase gamma, *Biochem Pharmacol.*, 1995.
- Gredilla R, Garm C, Stevnsner T, Nuclear and Mitochondrial DNA Repair in Selected Eukaryotic Aging Model Systems, *Oxid Med Cell Longev*, 2012.
- Greenleaf AL, Kelly JL, Lehman IR, Yeast *RP041* gene product is required for transcription and maintenance of the mitochondrial genome, *Genetics*, 1986.
- He J, Mao CC, Reyes A, Sembongi H, Di Re M, Granycome C, Clippingdale AB, Fearnley IM, Harbor M, Robinson AJ, Reichelt S, Spelbrink JN, Walker JE, Holt IJ, The AAA+ protein ATAD3 has displacement loop binding properties and is involved in mitochondrial nucleoid organization. *J Cell Biol*, 2007.
- Hedge ML, Izumi T, Mitra S, Oxidized Base Damage and Single-Strand Break Repair in Mammalian Genomes: Role of Disordered Regions and Posttranslational Modifications in Early Enzymes, *Prog Mol Biol Transl Sci*, 2012.
- Hiraoka LR, Harrington JJ, Gerhard DS, Lieber MR, Hsieh CL, Sequence of human FEN-1, a structure-specific endonuclease, and chromosomal localization of the gene (FEN1) in mouse and human. *Genomics*, 1995.
- Holt IJ, Lorimer HE, Jacobs HT, Coupled leading-and lagging-strand synthesis of mammalian mitochondrial DNA. *Cell*, 2000.
- Holt IJ, Reyes A, Human Mitochondrial DNA Replication, *Cold Spring Harb Perspect Biol*. 2012.
- Hsu P, Scott DA, Weinstein JA, Ran FA, Konermann S, Agarwala V, Li Y, Fine EJ, Wu X, Shalem O, Cradick TJ, Marraffini LA, Bao G, Zhang F, DNA targeting specificity of RNA-guided Cas9 nucleases, *Nat Biotechnol.*, 2013.

References

Huang WM, Lehman IR, On the Exonuclease Activity of Phage T4 Deoxyribonucleic Acid Polymerase, J Biol. Chem., 1972).

Jansen R, Embden JD, Gaastra W, Schouls LM, Identification of genes that are associated with DNA repeats in prokaryotes. Mol Microbiol, 2002.

Jinek M, Chylinski K, Fonfara I, Hauer M, Doudna JA, Charpentier E, A programmable dual-RNA-guided DNA endonuclease in adaptive bacterial immunity. Science 2012.

Kazak L, Reyes A, He J, Wood SR, Brea-Calvo G, Holen TT, Holt IJ, A cryptic targeting signal creates a mitochondrial FEN1 isoform with tailed R-Loop binding properties, PLoS ONE, 2013.

Krishnan N, Davis AJ, Giebultowics JM, Circadian regulation of response to oxidative stress in *Drosophila melanogaster*, Biochem Biophys Res Comm, 2008.

Koike K, Wolstenholme DR, Evidence for discontinuous replication of circular mitochondrial DNA molecules from Nivokoff rat ascites hepatoma cells. J Cell Biol., 1974.

Korhonen Jenny A, Pham XH, Pellegrini M, Falkenberg M, Reconstitution of a minimal mtDNA replisome *in vitro*, EMBO Journal, 2004.

Kornblum C, Nicholls TJ, Haack TB, Schöler S, Peeva V, Danhauser K, Hallmann K, Zsurka G, Rorbach J, Iuso A, Wieland T, Sciacco M, Ronchi D, Comi GP, Moggio M, Quinzii CM, DiMauro S, Calvo SE, Mootha VK, Klopstock T, Strom TM, Meitinger T, Minczuk M, Kunz WS, Prokisch H, Loss-of-function mutations in *MGME1* impair mtDNA replication and cause multi-systemic mitochondrial disease, Nature Genetics, 2013.

Labun K, Montague TG, Gagnon JA, Thyme SB, Valen E, CHOPCHOP v2: a web tool for the next generation of CRISPR genome engineering, Nucleic Acids Res, 2016.

Lakshmanan LN, Gruber J, Halliwell B, Gunawan R, Role of Direct Repeat and Stem-Loop Motifs in mtDNA Deletions: Cause or Coincidence? PLoS One, 2012.

Lange H, Kispal G, Lill R, Mechanism of Iron Transport to the Site of Heme Synthesis inside Yeast Mitochondria, J Biol. Chemistry, 1999.

Leffler II AT, Creskoff E, Luborsky SW, McFarland V, Mora PT, Isolation and characterization of rat liver mitochondrial DNA, J Mol Biol, 1970.

Lenaz G, The Mitochondrial Production of Reactive Oxygen Species: Mechanisms and Implications in Human Pathology, Life, 2001.

Longley MJ, Prasad R, Srivastava DK, Wilson SH, Copeland WC, Identification of 5'-deoxyribose phosphate lyase activity in human DNA polymerase gamma and its role in mitochondrial base excision repair *in vitro*, Proc Natl Acad Sci, 1998.

References

- Makarova KS, Grishin NV, Shabalina SA, Wolf YI, Koonin EV, A putative RNA-interference-based immune system in prokaryotes: computational analysis of the predicted enzymatic machinery, functional analogies with eukaryotic RNAi, and hypothetical mechanisms of action. Biol Direct, 2006.
- Mancini WR, Williams WS, Lin TS, Specific inhibition of DNA biosynthesis induced by 3'-amino-2',3'-dideoxycytidine, Biochemistry, 1988.
- Mao Z, Bozzella M, Seluanov A, Gorbunova V, Comparison of nonhomologous end joining and homologous recombination in human cells, DNA Repair, 2008.
- Masuda-Sasa T, Imamura O, Campbell JL, Biochemical analysis of human Dna2, Nucleic Acids Res, 2006.
- Medeiros TC, Thomas RL, Ghillebert R, Graef M, Autophagy balances mtDNA synthesis and degradation by DNA polymerase POLG during starvation. J Cell Biol, 2018.
- Meyer RR, Simpson MV, DNA biosynthesis in mitochondria: Partial purification of a distinct DNA polymerase from isolated rat liver mitochondria. Proc. Nat. Acad. Sci., 1968.
- Miller FJ, Rosenfeldt FL, Zhang C, Linnane AW, Nagley P, Precise determination of mitochondrial DNA copy number in human skeletal and cardiac muscle by a PCR-based assay: lack of change of copy number with age, Nucleic Acids Research, 2003.
- Miller WL, Steroid hormone synthesis in mitochondria, Molecular and Cellular Endocrinology, 2013.
- Moretton A, Morel F, Macao B, Lachaume P, Ishak L, Lefebvre M, Garreau-Balandier I, Vernet P, Falkenberg M, Farge G, Selective mitochondrial DNA degradation following double-strand breaks, PLoS ONE, 2017.
- Nass S, Nass MMK, Intramitochondrial Fibers with DNA Characteristics, J Cell Biol, 1963.
- Nicholls TJ, Zsurka G, Peeva V, Schöler S, Szczesny RJ, Cysewski D, Reyes A, Kornblum C, Sciacco M, Moggio M, Dziembowski A, Kunz WS, Minczuk M, Linear mtDNA fragments and unusual mtDNA rearrangements associated with pathological deficiency of MGME1 exonuclease. Hum Mol Genet, 2014.
- Nishimasu H, Ran FA, Hsu PD, Konermann S, Shehata SI, Dohmae N, Ishitani R, Zhang F, Nureki O, Crystal structure of Cas9 in complex with guide RNA and target DNA. Cell, 2014.
- Norenberg MD, Oxidative and Nitrosative Stress in Ammonia Neurotoxicity, Hepatology, 2003.
- Pascucci B, Versteegh A, van Hoffen A, van Zeeland AA, Mullenders LHF, Dogliotti E, DNA Repair of UV photoproducts and mutagenesis in human mitochondrial DNA, J Mol Biol, 1997.

- Peeva V, Blei D, Trombly G, Corsi S, Szukszto M, Kudib AP, Becker C, Altmüller J, Munczuk M, Zsurka G, Kunz WS, Linear mitochondrial DNA is rapidly degraded by components of the replication machinery, Nature Communications, 2018.
- Pikó L, Bulpitt KJ, Meyer R, Structural and replicative forms of mitochondrial DNA in tissues from adult and senescent BALB/c mice and Fisher 344 rats. Mech Ageing Dev., 1984.
- Pitceathly RD, Rahman S, Hanna MG, Single deletions in mitochondrial DNA-molecular mechanisms and disease phenotypes in clinical practice. Neuromuscul Disord, 2012.
- Prakash A, Doublie S, Base Excision Repair in the Mitochondria, J Cell Biochem, 2015.
- Ramakrishna S, Kwaku Dad AB, Beloor J, Gopalappa R, Lee SK, Kim H, Gene disruption by cell-penetrating peptide-mediated delivery of Cas9 protein and guide RNA. Genome Res, 2014.
- Reyes A, Kazak L, Wood SR, Yasukawa T, Jacobs HT, Holt IJ, Mitochondrial DNA replication proceeds via a 'bootlace' mechanism involving the incorporation of processed transcripts, Nucleic Acids Res, 2013.
- Richter C, Park JW, Ames BN, Normal oxidative damage to mitochondrial and nuclear DNA is extensive, Genomics, 1988.
- Robberson DL, Kasamatsu H, Vinograd J, Replication of mitochondrial DNA. Circular replicative intermediates in mouse L cells. Proc. Natl. Acad., 1972.
- Ropp PA, Copeland WC, Cloning and characterization of the human mitochondrial DNA polymerase, DNA polymerase gamma. Genomics, 1996.
- Rosignol R, Faustin B, Rocher C, Malgat M, Mazat JP, Letellier T, Mitochondrial threshold effects, Biochem J, 2003.
- Rötig A, Poulton J, Genetic causes of mitochondrial DNA depletion in humans, Biochim Biophys Acta, 2009.
- Saffran HA, Pare JM, Corcoran JA, Weller SK, Smiley JR, Herpes simplex virus eliminates host mitochondrial DNA. EMBO Rep., 2007.
- Schmidt T, Schmid-Burgk JL, Hornung V, Synthesis of an arrayed sgRNA library targeting the human genome, Nature Scientific Reports, 2015.
- Sen D, Nandakumar D, Tang GQ, Patel SS, Human mitochondrial DNA helicase TWINKLE is both an unwinding and annealing helicase. J Biol Chem, 2012.
- Shoffner JM, Lott MT, Voljavec AS, Soueidan SA, Costigan DA, Wallace DC, Spontaneous Kearns-Sayre/chronic external ophthalmoplegia plus syndrome associated with a mitochondrial DNA deletion: a slip-replication model and metabolic therapy. Genetics, 1989.

- Smith C, Gore A, Yan W, Abalde-Atristain L, Li Z, He C, Wang Y, Brodsky RA, Zhang K, Cheng L, Ye Z, Whole-Genome Sequencing Analysis Reveals High Specificity of CRISPR/Cas9 and TALEN-Based Genome Editing in Human iPSCs, Cell Stem Cell, 2014.
- Sparks JL, Chon H, Cerritelli SM, Kunkel TA, Johansson E, Crouch RJ, Burgers PM, RNase H2-initiated Ribonucleotide Excision Repair, Mol Cell, 2012.
- Spelbrink JN, Li FY, Tiranti V, Nikali K, Yuan QP, Tariq M, Wanrooik S, Garrido N, Comi G, Morandi L, Santoro L, Toscano A, Fabrizi GM, Somer H, Croxen R, Beeson D, Poulton J, Suomalainen A, Jacobs HT, Zeviani M, Larsson C, Human mitochondrial DNA deletions associated with mutations in the gene encoding Twinkle, a phage T7 gene 4-like protein localized in mitochondria, Nature Genetics, 2001.
- Steward JD, Schoeler S, Sitarz KS, Horvath R, Hallmann K, Pyle A, Yu-Wai-Man P, Taylor RW, Samuels DC, Kunz WS, Chinnery PF, POLG mutations cause decreased mitochondrial DNA repopulation rates following induced depletion in human fibroblasts, Biochim Biophys Acta, 2011.
- Tadi SK, Sebastian R, Dahal S, Babu RK, Choudhary B, Raghavan SC, Microhomology-mediated end joining is the principal mediator of double-strand break repair during mitochondrial DNA lesions, MBoC, 2015).
- Takamatsu C, Umeda S, Ohsato T, Ohno T, Abe Y, Fukuoh A, Shinagawa H, Hamasaki N, Kang D, Regulation of mitochondrial D-loops by transcription factor A and single-stranded DNA-binding protein, EMBO reports, 2002.
- Tann AW, Boldogh I, Meiss G, Qian W, Van Houten B, Mitra S, Szczesny B, Apoptosis Induced by Persistent Single-strand Breaks in Mitochondrial Genome, J Biol Chemistry, 2011.
- Thömmes P, Marton RF, Cotterill S, Isolation and characterisation of dhel II, a DNA helicase from *Drosophila melanogaster* embryos stimulated by *Escherichia coli*-type single-stranded-DNA-binding proteins, Eur J Biochem, 1996.
- Trifunovic A, Wredenberg A, Falkenberg M, Spelbrink JN, Rovio AT, Bruder CE, Bohlooly-Y M, Gidlöf S, Oldfors A, Wiborm R, Törnell J, Jacobs HT, Larsson NG, Premature ageing in mice expressing defective mitochondrial DNA polymerase. Nature, 2004.
- Tsuchimoto D, Sakai Y, Sakumi K, Nishioka K, Sasaki M, Fujiwara T, Nakabeppu Y, Human APE2 protein is mostly localized in the nuclei and to some extent in the mitochondria, while nuclear APE2 is partly associated with proliferating cell nuclear antigen. Nucleic Acids Res, 2001.
- Uhler JP, Falkenberg M, Primer removal during mammalian mitochondrial DNA replication. DNA Repair, 2015.

References

- Vafai S, Mootha VK, Mitochondrial disorders as windows into an ancient organelle, Nature, 2012.
- Vandecasteele G, Szabadkai G, Rizzuto R, Mitochondrial calcium homeostasis: mechanisms and molecules, IUBMB Life, 2001.
- Vanderstraeten S, Van den Brûle S, Hu J, Foury F, The role of 3'–5' exonucleolytic proofreading and mismatch repair in yeast mitochondrial DNA error avoidance. J Biol Chem, 1998.
- Veres A, Gosis BS, Ding Q, Collins R, Ragavendran A, Brand H, Erdin S, Talkowski ME, Musunuru K, Low incidence of off-target mutations in individual CRISPR-Cas9 and TALEN targeted human stem cell clone detected by whole-genome sequencing, Cell Stem Cell, 2014.
- Viscomi C, Zeviani M, mtDNA-maintenance defects: syndromes and genes, J Inherit Metab Dis, 2017.
- Walther DM, Rapaport D, Biogenesis of mitochondrial outer membrane proteins, Biochimica et Biophysica Acta (BBA) - Molecular Cell Research, 2009.
- Wang T, Wei JJ, Sabatini DM, Lander ES, Genetic screens in human cells using the CRISPR-Cas9 system. Science, 2014.
- Wanrooij S, Falkenberg M, The human mitochondrial replication fork in health and disease, Biochimica et Biophysica Acta, 2010.
- Wiesner RJ, Zsurka G, Kunz WS, Mitochondrial DNA damage and the aging process: facts and imaginations, Free Radic Res, 2006.
- Yakubivskaya E, Chen Z, Carrodegua JA, Kisker C, Bogenhagen DF, Functional Human Mitochondrial DNA Polymerase γ Forms a Heterotrimer, J Biol Chem, 2006.
- Yang MY, Bowmaker M, Reyes A, Vergani L, Angeli P, Gringeri E, Jacobs HW, Holt IJ, Biased Incorporation of Ribonucleotides on the Mitochondrial L-Strand Accounts for Apparent Strand-Asymmetric DNA Replication, Cell, 2002.
- Yang C, Curth U, Urbanke C, Kang C, Crystal structure of human mitochondrial single-stranded DNA binding protein at 2.4 Å resolution. Nat Struct Biol, 1997.
- Yasukawa T, Reyes A, Cluett TJ, Yang MY, Bowmaker M, Jacobs HW, Holt IJ, Replication of vertebrate mitochondrial DNA entails transient ribonucleotide incorporation throughout the lagging strand, EMBO Journal, 2006.
- Young MJ, Copeland WC, Human mitochondrial DNA replication machinery and disease. Curr Opin Genet Dev, 2016.
- Yu Z, O'Farrell PH, Yakubovich N, DeLuca SZ, The Mitochondrial DNA Polymerase Promotes Elimination of Paternal Mitochondrial Genomes, Curr Biol., 2017.

References

Zhao S, Fernald RD, Comprehensve algorithm for quantitative real-time polymerase chain reaction, J Comput Biol, 2005.

Zheng L, Zhou M, Guo Z, Lu H, Qian L, Dai H, Qiu J, Yakubovskaya E, Bogenhagen DF, Demple B, Shen B, Human DNA2 is a mitochondrial nuclease/helicase for efficient processing of DNA replication and repair intermediates, Mol Cell, 2008.

Zsurka G, Peeva V, Kotlyar A, Kunz WS, Is There Still Any Role for Oxidative Stress in Mitochondrial DNA-Dependent Aging? Genes, 2018

Bibliography

Alberts, Johnson, Raff, Roberts, Walter, Molecular Biology of the Cell, Fifth Edition, 2011.

List of Publications:

Peeva V*, Blei D*, Trombly G, Corsi S, Szukszto M, Kudib AP, Becker C, Altmüller J, Munczuk M, Zsurka G, Kunz WS, Linear mitochondrial DNA is rapidly degraded by components of the replication machinery, Nature Communications, 2018. * equal contribution.

Declaration

I, hereby confirm that this work is my own. This thesis has been written independently and with no other sources and aids than stated. The presented thesis has not been submitted to another university and I have not applied for a doctorate procedure so far.

Hiermit versichere ich, dass die vorgelegte Arbeit - abgesehen von den ausdrücklich bezeichneten Hilfsmitteln - persönlich, selbständig und ohne Benutzung anderer als der angegebenen Hilfsmittel angefertigt wurde. Aus anderen Quelle direkt oder indirekt übernommenen Daten und Konzepte sind unter Angabe der Quelle kenntlich gemacht worden. Die vorliegende Arbeit wurde an keiner anderen Hochschule als Dissertation eingereicht. Ich habe früher noch keinen Promotionsversuch unternommen.

Ort, Datum

Unterschrift